Towards improving predictions of non-Newtonian settling slurries with Delft3D: theoretical development and validation in 1DV

Final report – Jill L.J. Hanssen

May 12 2016

DELFT UNIVERSITY OF TECHNOLOGY
Faculty of Civil Engineering and Geosciences
Department of Hydraulic Engineering

Towards improving predictions of non-Newtonian settling slurries with Delft3D: theoretical development and validation in 1DV

by

Jill L.J. Hanssen

in partial fulfilment of the requirements for the degree of

Master of Science in Hydraulic Engineering

at the Delft University of Technology

Student name:	Jill Hanssen
Student number:	4240162

Graduation committee:

Prof. dr. ir. C. v. Rhee	Delft University of Technology, chairman
Prof. dr. ir. J.C. Winterwerp	Deltares & Delft University of Technology
Dr. ir. A. M. Talmon	Deltares & Delft University of Technology
Dr. ir. C. J. Sloff	Deltares & Delft University of Technology
Ir. L. Sittoni	Deltares

Under the authority of: Deltares

Preface

This report is the final product of my thesis. The thesis concludes my Master study of Hydraulic engineering of the faculty Civil Engineering at Delft University of Technology.

I would like to thank the graduation committee for their complicity and enthusiasm during the past months. In particular to prof. Cees v. Rhee who was chairman of the committee and his independent advise. Han Winterwerp and Arno Talmon, for sharing their expertise and knowledge on soft sediments and hydrodynamics resulting in numerous valuable dialogs. Luca Sittoni and Kees Sloff, who counseled me in the process management of the thesis.

Adjacent to the committee, Deltares, colleagues and other people were (closely) involved.
I would like to express my gratitude to Deltares who provided this thesis subject, accommodated my workspace and supplied the required resources. The colleagues of Deltares for their support and interest. Especially to R. Uittenbogaard and J. v. Kester who assisted me during the numerical study.
I would like to acknowledge A.D. Thomas who offered additional rheological data to perform the theoretical study.

Life is a flow driven by your own curiosity, ambitions and family and friends. Lastly, I wish to offer a special word of thanks to them who gave their moral support and encouragement throughout my life.

Abstract

To date there is limited knowledge about the flow behaviour of non-Newtonian slurry and tailings flows. In hydraulic engineering and the mining industry numerous questions and uncertainties still exist. Different numerical and analytical models have been developed attempting to meet this demand. For the larger part they describe the rheological properties of the flow and are commonly developed for the mining industry. Delft3D is a widely used and proven numerical modelling suite to predict flow behaviour of different water bodies including physical processes e.g. the transport of sediments and stratifications. This thesis contributes to embedding the rheological characterizations for mud-sand-water mixtures and settling of granular material in Delft3D. This thesis includes:

- An analysis of three different formulas that describe the rheological properties of mud-sand flows.
- A theoretical description of a settling model that accounts for shear induced hindered settling of granular material in a Non-Newtonian flow.
- The implementation of the three rheological models and the segregation model into Delft3D, completed by model verification on theoretical relations, and simple validation.

The present model is able to simulate non-Newtonian laminar flows and the segregation of granular material in the carrier fluid in 1DV.

Executive Summary

Many examples of mud-sand mixtures flows can be found in nature and engineering applications, especially as many industrial activities are moving towards thicker and fines based material.. These include for example natural debris flows, dredge sediment or main tailings management or land reclamation project.

This drives the demand to improve the understanding and the modelling of the behaviour of the mud-sand. Throughout the past years a lot of research, mainly constituted by physical experiments, is done towards closing these gaps. Nonetheless still many challenges are left in understanding the flow and coarse particles settling behaviour of sand-mud mixtures, as well as beach geometry and slope. More recent is the exploration of modelling these flows numerically. A numerical model expands the possibility to investigate large scale flows on short and long time scales, and to evaluate different operational and management scenarios, reducing (but not eliminating) the need for costly large field trials.

This study aims to improving predicting capabilities of thick sand-mud flows. Specifically, it includes a theoretical investigation to describe the rheology and segregation of laminar non-Newtonian mud-sand flows and to implement this theory in a numerical 1DV model analogous to Delft3D. Delft3D is a widely used open source process based numerical model for hydrodynamic and sediment transport simulations, developed and maintained by Deltares.

Rheology

Mud-sand mixtures consist of various amounts of water, clay, silt and sand. Clay and fine silt constitute the mud (or fines) fraction. Mud and water constitute the carrier fluid. Clay particles are electrical charged and able to bind with other particles. Mixtures consisting of a moderate to large amount of clay particles tend to express viscous Non-Newtonian behaviour and yield stress. These are important features which affect the flow behaviour compared to Newtonian flows e.g. water.

Granular material (sand and coarse silt) does not have a cohesive behaviour, nor yield stress. Nevertheless, the particles enhance the viscosity of a mud-sand mixture. These particles can build a granular skeleton if the volume concentration is large enough.

The yield stress and viscosity determine the shear stress of a fluid. A rheological function describes the relation between the shear rate and the shear stress. The function provides information on the resistance to flowing of a mixture if it is deformed. Many different rheological functions are found in literature. In this study we consider three of them, which are traditionally separately derived for different fields of expertise of mud-sand flows. An overview is presented in Table 1. The rheological section of this study targets at comparing these three rheological formulations, and to include them in the same numerical model.

Table 1 Three rheological models; origin and fluid type

Model	Specialism	Established from	Fluid type
1	Fluid mud and soft sediment dynamics	Fractal dimension theory	Power law behaviour incl. yield stress
2	Mine tailings	Relative water content	Bingham
3	Industrial concentrates	Viscosity enhancement and empirical fit	Bingham

The presence of sand in sand-mud mixture increases the internal friction, contributing to the viscosity. At the same time, it also reduces the mud amount, decreasing its cohesiveness or strength decreases. Experimental data of A.D. Thomas shows this behaviour. All three models predict this as well. The three models predicted similar behaviour up to xx% solids, and then deviated. In general, the accuracy of prediction differs for different in total volume concentrations and sand to solid ratios. At high sand to solid ratio (above 60%) the accuracy decreases. This is caused by three features: 1) the mixture shifts into the granular regime for high sand to solid ratios and a sand skeleton is formed, with the behaviour of the mixture being beyond the validity range of the formulas; 2) the particles size distribution and shape of the grains has an influence on the internal friction; and 3) the accuracy of the measurements may decrease for high sand concentrations, with the particles that tend to segregate during the measurement procedure. The latter emphasizes the importance of the precise measurement of the physical parameters and empirical parameters within the models.

Segregation or Settling of Coarse Particles

A concentrated static non-Newtonian fluid with shear strength above few Pascals is able to keep coarser silt or sand solid particles in suspension thanks to the yield stress. This bearing capacity is acquired from the force balance between weight of the particle weight and the buoyancy. In a sheared fluid the strength of the fluid is described by the apparent viscosity, which decreases for increasing shear rates, causing the coarse particle to settle. This phenomenon is expressed in the shear induced settling formula. The presence of many coarse particles within the carrier fluid hinders to settling of each single particle. Therefor the settling formula is expanded to a shear induced hindered settling formula.

Flow Behaviour

In a sheared mud-sand mixture the hydrodynamics of the flow, rheology of the mixture and the segregation are coupled. The rheology of the mixture determines the flow velocity profile. Velocity variations over the vertical introduce a shear. Shear rate influence coarse particles segregation or settling. The sand concentration (at each layer) and the shear rate influences the apparent viscosity, which influences the rheology, and so on.

In the plug of the flow the yield stress is larger than the shear stress and particles segregation will not be enhanced. In the sheared zone the shear stress exceeds the yield stress and segregation of particles is enhanced by the shear rate. The segregation rate depends on the particle concentration, diameter, density and shear rate. In laminar flow, therefor without turbulent

upward mixing, the fluid will not reach an equilibrium state until all the granular material settled. This behaviour of the mud-sand flows is observed by different physical experiments.

Numerical model

Delft3D is an open source numerical flow model developed and maintained by Deltares. The model is used for various scientific and engineering applications world-wide. The model is generally implemented for (Newtonian) flows in hydrodynamic, sediment transport and water quality studies.

In this study a first step is made to extend the model to account for segregating (sand settling) non-Newtonian thick sand-mud mixtures flow. As a first step, and main effort of this thesis, the three rheological models and segregation model are implemented in a 1DV model which includes the 1DV formulations of Delft3D. This ensures best control on embedding into the model and relative validation.

The calculation sequence of the critical rheology and sand settling processes, as embedded in the 1DV model is presented in Figure 1.
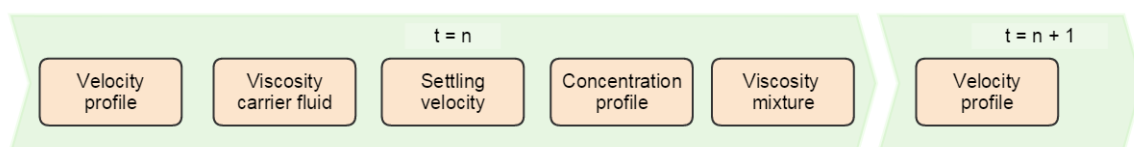

Figure 1 Calculation sequence of 1DV model

This thesis focuses on laminar non-Newtonian flows including and excluding segregation. Two different configurations have been tested with the 1DV model.
- Horizontal bed; flow is driven by a prescribed mean flow velocity and prescribed flow depth.
- Sloping bed (e.g. long beach); flow is driven by the gravitational acceleration with a prescribed slope, with prescription of the specific discharge.

For optimum and structured implementation and testing, the model was first tested for non-segregating (uniform) conditions only, focussing on the three different rheological models. In a second phase, the sand settling segregation behaviour was included and analysed.

The model is able to represent the non-segregating flow on a horizontal bed and along a slope for all three rheological models. An analytical model is used to verify the coupling between the rheology and hydrodynamics. The simulated interaction between the hydrodynamics and rheology corresponds with the observations and theory described in literature. All three models performed similarly and in agreement with the theory, with larger deviation between the Bingham and the power law model, which was expected given the different formulation.

Instabilities are noticed in the numerical domain if segregating flows on a horizontal bed are modelled. This behaviour is initiated when the shear stress and yield stress have similar values, causing large gradients in the apparent viscosity, which is passed to the behaviour of the flow. The boundary conditions force the fluid to a specified mean velocity and water depth. Therefor the velocity and shear rate profile are artificially modified compared to a natural open channel flow situation. These processes are stiffly coupled in the system, with no artificial numerical

diffusion. Therefor variations in the apparent viscosity have large and immediate effects on the other variables.

The simulations of the segregating flows along a slope behave consistently with the theory. In the plug of the flow the velocity profile is nearly constant accompanied by a relative small shear rate and settling velocity, and high apparent viscosity. In the sheared zone the velocity profile follows a power function (Model 1) or a parabolic shape (Model 2 and 3). The shear rate increases drastically in proximity of the top of the sheared zone, where the apparent viscosity reduces strongly and the segregation rate increases. Near the bed the concentration of settling granular material increases and a gelled layer is formed. The velocity is reduced by the high concentration and the shear stress increases resulting in a higher apparent viscosity and a decrease of the segregation rate. The reduction in sand concentration profiles differ between Model 1 and Models 2 and 3. The former induces a more pronounced reduction in absolute value, but thinner layer of sand depletion, with the sand segregating front moving upward slower. Also, Model 1 produces a smoother transition in sand concentration profile near the gelled layer. Models 2 and 3 show similar behaviour, with thicker sand depletion layer, and with lower segregation rates.

In these simulations a small single wiggle was visible in all three models. This wiggle is the result of a sharp gradient in the concentration profile which is likely not physical. The wiggle may grow due to the positive feedback mechanism that connects the various processes in the system. In longer simulations (up to 6 to 9 hours of continuous flow) additional disturbances entered the domain of Model 3. Again the cause is an alternation between a high and a low apparent viscosity. However these large differences are not likely in the gelled bed layer and are a numerical artefact. The occurring (single) wiggle(s) can be diminished by diminishing time step or grid size, or by adding numerical diffusion, i.e. averaging the apparent viscosity over multiple layers or introducing, making it less sensitive to sudden changes in the concentration or changes in the yield stress and shear stress profile.

Conclusion and recommendations

This thesis integrated and compared different rheological models traditionally applied in different engineering field. This thesis also optimized the derivation of a sand settling formula for thick non-Newtonian mixtures. These two fundamental processes were embedded and tested in the 1DV version of Delft3D, together with minor improvement to the code to handle these processes effectively.

The 1DV model is able to capture the main rheological and sand settling processes for laminar thick sand-mud mixtures, in line with theoretical predictions. This model was able to reproduce plug flow behaviour, sand settling and consequent modification of the sand concentration profile, and gelled bed layer with reduction of flow velocity proportional to increase in sand concentration. As it generally occurs in numerical models, this 1DV model tends to show instabilities when pushed near critical limits, being this shear stress near yield stress values. This is especially the case if the yield stress and shear stress approach each other due to relatively rapid sand settling.

As in all (successful) developments, new challenges have been uncovered. In addition of what described above, these are:
- Further examine stratification (due to segregation), which involve instabilities in the sheared region;

- Continue the sensitivity analysis on all parameters and comparisons with experiments to enhance the understanding of the numerical model;
- Validate thoroughly the segregation model with experimental data, if available;
- Modelling the transition between non-Newtonian and Newtonian flows and the alternation between laminar and turbulent flows, based on the Re and gradient in solids concentration;
- Extend the validity of the rheological models and segregation model into the granular regime to model the whole range of mud-sand compositions;
- Implement the rheological formulas and segregation formula of the 1DV model into Delft3D to model the three dimensional features which occur in nature.

Table of Contents

1. Introduction

1.1. Tailings

In nature and in the field of engineering many examples exist of tailings or slurries. The flows consist of water, mud and sand. In the dredging industry often a mixture of sand and mud is used for land reclamation. To guarantee the bearing capacity of the artificial land it is essential to keep the fractions mixed (e.g. non-segregating) while depositing. In the mine industry the mud-sand flow is a residue which is deposited in tailings basins. The behaviour of the material determines strongly the operational processes. Debris flows occur in mountain areas as a result of heavy rainfall (Haldenwang et al., 2010). Their impact on the surroundings is devastating.

The common property of these examples is the high solid content of the slurries influencing the rheology and behaviour of the flow.

Due to the high clay fractions the rheological properties alter and the flows become non-Newtonian. The flow structure differs from Newtonian streams like water. The sand particles influence the rheology of the (non-Newtonian) flow. A fluid in motion generates a shear stress affecting the settlement of the sand particles. Due to segregation an inhomogeneous concentration profile over depth develops with an increase of particles towards the bottom. The mutated solids fraction results in a modified rheology and as a result the flow field is influenced (P. Slatter, 2011). The settled sand forms a gelled bed and, if time allows, the settled particles and bed are able to consolidate. The understanding of the coupled physics of these mud-sand flows is still limited (Haldenwang & Slatter, 2006; Haldenwang et al., 2010; Slatter & Williams, 2013; Spelay, 2007)

In the mining industry different analytical models, empirical models and numerical models are developed to predict the non-Newtonian flow behaviour including segregation (e.g.(Fitton et al., 2007; Sittoni et al., 2015; Spelay, 2007)). These models are especially used in mine tailings management applications.
Deltares developed a 3D numerical open source model, Delft3D. It has the ability to simulate all different kinds of water bodies and includes physical processes such as multi-fraction sediment transport and the development of deltas. Due to the variety in utilizations it is able to serve a large number of users with a different background. Until now the considered flows are mainly Newtonian. Deltares objective is to evolve the model in a way that it is also suitable to model high concentrated non-Newtonian flows including the feedback processes as discussed above. To prevent that every new development becomes a separate application, unanimity is of high importance. A first towards this objective is made in 2015 with Delft3D-Slurry, which includes a qualitative 2D simulation of different tailings (Sittoni et al., 2015). This thesis intends to continue along this path, with rigorous validation of the main rheological and sand settling processes.

1.2. Problem definition

Engineers come across different kinds of tailings and debris flows in various settings. In time several formulations are developed to describe the rheological properties of these flows. Numerical simulations allow predicting the flows and related channel formations.

"How to define and incorporate the rheological properties of a laminar non-Newtonian flow, segregation and the coupling to the hydrodynamics in an existing 3D numerical model?"

To answer this question a stepwise approach is used which is explained in Section 1.4.

1.3. Research objective

The related research objective of this thesis is:

"A theoretical study to three different rheological models and a segregation model and implementation of these in a numerical 1DV model analogous to Delft3D".

1.4. Research approach

The thesis consists of the two main parts. First a literature study was done to have a general understanding of the subject matter and related questions. Secondly the formulations are implemented in a 1DV model analogous to Delft3D, which is subsequently tested and validated

Part I - Literature study

A Literature study was carried out to describe laminar non-Newtonian homogeneous flow as well as segregating flows and related formulations. This includes:

1. Elaboration on the composition of the fluid and the rheological properties.
2. Comparison and alignment of three different rheological formulas originating from three different fields of expertise:
   - Power law model (Kranenburg & Winterwerp),
   - Bingham model (Jacobs et al., 2011)
   - Bingham model (A. D. Thomas, 1999).
3. Derivation of a hindered settling-function of coarse particles in a non-Newtonian flow which includes the time dependent behaviour of the rheology.
4. Understanding of the coupled processes: hydrodynamics, rheology and segregation.
5. Conclusion and recommendation

Part II – Model development and validation

Modelling of the settling behaviour of coarse material in a laminar Non-Newtonian flow in a 1DV-model similar to Delft3D was conducted. This concerns:

1. Investigation on the current state of the 1DV model.
   - Used theory and formulas of physical process and how they are implemented in the model.
   - Deficiency of the application in formulation and script.
   - Conclusion and recommendations to improve the model.
2. Non-segregating flow
   - Implementation of the theory of the literature study (Part I-1and I-2) and possible changes in the model.
   - Model simulation with different input parameters.
   - Validations of the results against analytical solutions.
   - Grid size independency test
   - Calibration and evaluation of the model results based on experimental data.
3. Segregating flow
   - Implementation of the theory of the literature study (part I-3
   - Model simulations varying different parameters.
   - Validations of the results against analytical solutions.
   - Grid size and time step independency test
   - Evaluation of the model results based on experimental data.
4. Conclusion and recommendation

1.5. Thesis structure

The structure of this report is in line with the research approach presented above. An overview of the literature study is given in Chapter 2. Chapter 3 presents the three investigated rheological formulas, their analytical comparison with data and the segregation formula. An in depth elucidation of the 1DV model and the adjustments made for this thesis are included in Chapter 4. Chapter 5 presents the numerical simulations and verifications of the adapted model. The conclusions and recommendations conclude this report in Chapter 6.

2. Literature survey

The literature study provides a general overview of the relevant physics within slurries, tailings and debris flows. The material properties and rheological properties are described in Section 2.1 and Section 2.2 respectively. Section 2.3 treats the hydrodynamics Section 2.4 explains the concept of segregation. An elaboration on the coupling of these processes is given in 2.5. The second part, i.e. Section 2.6, is an overview on the related research towards numerical modelling of non-Newtonian flows: the state-of-the-art and the relative knowledge gaps.

2.1. Physical properties

2.1.1. Material properties

The fluids under concern in this thesis are mostly mixtures of water, sand and / or mud. Depending on the type and amount of particles, the mixture is Newtonian or non-Newtonian.

Sediment grains can be divided in different classes depending on their size and physical properties. Currently there is not a single international standard for this classification. A common used division in three classes is presented in Table 2-1. *d* is the (equivalent) diameter of the material. Mud consists of clay, silt and water.

Table 2-1 Anorganic material; representative nominal diameter and properties

Type	Size	Properties
Sand	d > 63 μm	Euclidian (Spherical) particles. Able to build a structure (skeleton).
Silt	2 < d < 63 μm	Euclidian (Spherical) particles. Able to build a structure (skeleton).
Clay	d <2 μm	Non-Euclidian (Flat) particles Electrical charged, therefore cohesive. Contains more than 90% water.

Figure 2-1 is a visualization of the relations between volume concentration solids fraction of the sediments and water. Ψ is the solids fraction, φ ia the volume concentration. n is the porosity of the soil. When the soil is saturated – which is assumed in this thesis – the pores are filled with water. The subscript *s* refers to solids, the superscripts *cl, sa* and *si* are used for clay, sand and silt respectively.

In natural mud-sand samples also other material will be present e.g. organic material, metal etc. Research to these elements is beyond the scope of this thesis.
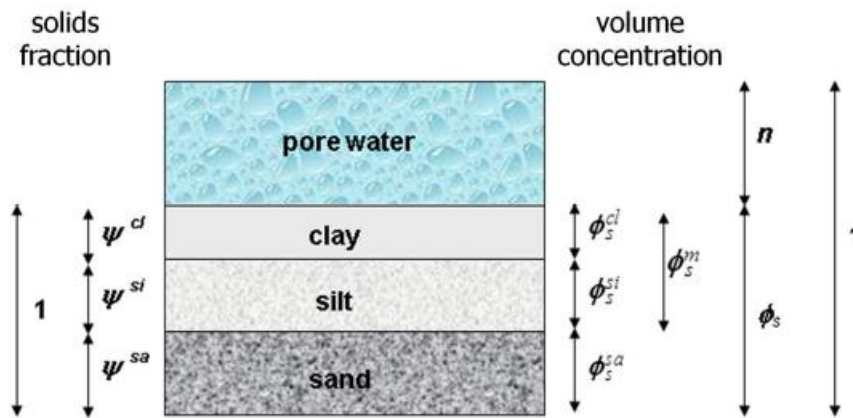
Figure 2-1 Schematization of soil sample including relations between solids fraction and volume concentration. Figure by (J C Winterwerp & van Kesteren, 2004)

Clay

Clays have a plate-like shape and a relative high specific surface. The particles are silicate minerals built up from chlorite, kaolinite, illite and smectite. They are electrical negatively charged and able to attract or repel other charged elements. In the first case clay elements will repel each other. Positively charged cations like $H+$ or $Na+$, coupled to molecules in the fluid, will be attracted. A 'positive' layer is formed around the particle. This layer can attract another clay particle by the molecular van der Waals force. To do so the particles have to be close enough and overcome an energy barrier formed by repulsive forces at long distance and the born repulsive force. If the van der Waals force is strong enough, the particles collide and form aggregates from which flocs are built. Shear rates as a result of velocity differences induce the formation and break-up of flocs. This flocculation process leads to the cohesive properties and is reversible. The clays are able to bind with different materials e.g. water, contaminants and polymers. A floc grows according to the concept of self-similarity.

Self-similarity

The concept of self-similarity is based on the assumption that the formation of a larger floc has an identical structure as the primary aggregate. Therefore the structure is independent on the size of the aggregate. The growth of an aggregate is defined by the fractal dimension, which is the ratio between the amount of particles that are connected within the primary aggregate (*m1*) and the rate of increase of the size of the evolved aggregate (*m2*) if the build-up of this structure is repeated. The growth of an aggregate is schematised in Figure 2-2.
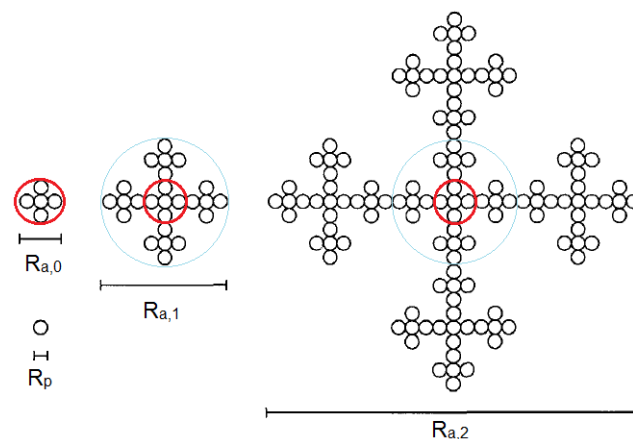

Figure 2-2 Schematization of aggregation by self-similarity. Figure by (L. Merckelbach, 2000)

The rate of increase of the size of an aggregate is a function of the aggregate size R_a and the size of the primary particle R_p.

$$m_2 = \frac{R_a}{R_p} \tag{2.1}$$

The fractal dimension n_f reads:

$$n_f = \frac{\ln(m1)}{\ln(m2)} \tag{2.2}$$

The mass of the floc is related to the length scale of the aggregate and the fractal dimension. Depending on the clay composition the value of n_f varies between 1-3. The lower bound holds for dilute samples. Within higher concentrations, higher values of n_f are found. For estuarine and coastal waters the value ranges between 1.7-2.2. Bed material obtains a value between 2.6-2.8. (Dyer & Manning, 1999; Winterwerp & van Kesteren, 2004) The ability of forming these structures gives the clay a certain yield strength. This will be explained more in-depth in paragraph 2.1.2.

Mud is formed by clay and silt. Due to the flocculation the clay particles can trap the silt. The enclosure of silt particles depends on the salinity of the mixture. In fresh water clay particles are able to capture the silt particles. The silt will not settle unless the entire clay floc settles. In a saline environment, more ions (positive charged cations) are presented and the pH (slightly) higher. The resulting effect is twofold. The ions form a bridge between the clay particles. Due to the presents of the ions the double layer becomes closer to the particle. This increases the clogging denstity. Secondly due to the (slightly) higher pH the bounds between clay particles are more vulnerable (Mietta et al., 2009). At higher shear rates the flocs break-up more easily. If the bounds break-up, the silt particles are able to settle as well.

The ratio of silt to clay is constant for specific locations in many estuaries (Flemming, 2000). If the amount of sand is known, the other two quantities can be determined from the Ternary diagram.

Granular material

Silt and sand particles are Euclidean (spherical). If the concentration is high enough, the particles touch and form a granular skeleton by their angle of internal friction. In between are voids present. The porosity is the ratio between the volume of pores and total volume. Its value depends on the properties of the sand/silt mixture, e.g. particle diameter, volume concentrations and grain size distribution. The most dense packing of the particles is $n = 25\%$. If $n > 48\%$ it is not possible to form a skeleton and soil becomes quick sand.

A mixture of sand and silt particles results in a combined value for the porosity. Figure 2-3, presents the maximum and minimum value. The concentration by weight of sand and silt is presented at the bottom axis and top axis respectively. For sand it increases from left to right for silt from right to left. For zero silt $n_{sand} = 48\%$. The minimum value can be found for a concentration of 78% and 22% of sand and silt respectively (i.e. silt will fill the sand pares). The sand and/ or silt concentration is one minus the porosity. The parameter determines different physical aspects, e.g. the maximum packing density.
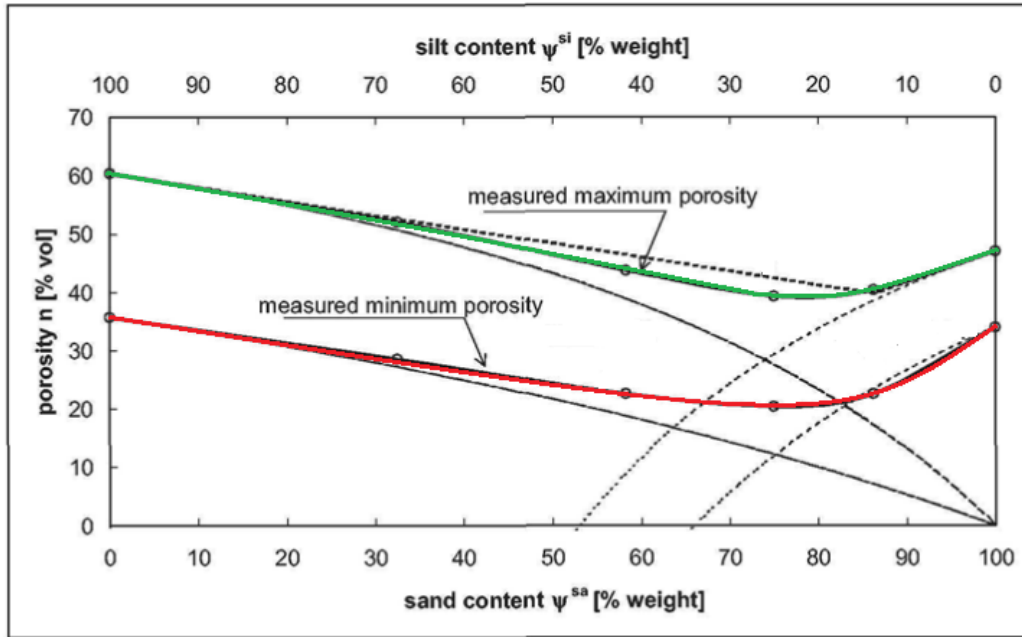
Figure 2-3 Minimum and maximum porosity related to silt and sand. Figure by (J C Winterwerp & van Kesteren, 2004)

2.1.2. Rheology

Rheology defines the strength of a certain fluid by the rheological properties yield strength and the viscosity.

Yield stress

Yield stress is the ability of a fluid to withstand a certain stress before it starts flowing. A lot of research has been performed to quantify the yield stress and viscosity of slurries by different measurements (e.g. rotoviscometer tests). Fundamental is the work of C. Kranenburg (Kranenburg, 1994) who described the rheological properties of the clay particles in relation to the self-similar fractal model of the clay. Although this concept is very useful, one should keep in mind that the formation of flocs is more complicated and not exactly self-similar. Biological processes are not taken into account. For the determination of the rheological properties it is assumed that the formation and break-up of aggregates is in dynamic equilibrium. The empirical factors in the exponents have to be derived from measurements of the considered samples.

The yield stress of a floc depends on the number of bonds between the particles and is not related to the floc size due to self-similarity. An increase of concentration improves the flocculation leading to a higher yield strength. σ_y is the yield pressure, R_a is the size of the aggregate and ρ_a the excess density.

$$\sigma_y \sim R_a^{-2} \sim \Delta\rho_a^{\frac{2}{3-n_f}} \tag{2.3}$$

Viscosity

The viscosity is the stickiness of the fluid. By deformation of a fluid, particles move relative to each other (on a microscopic scale). With this movement transfer of momentum is involved which acts as a forcing on the particles. Viscosity is the ability of a fluid to resist this forcing by internal friction within the fluid. It delays an applied stress resulting in a constant rate of deformation. Because these features occur on a microscopic scale, the exact viscous behaviour of

10

the fluid is difficult to predict or determine. For civil engineering the macroscopic scale behaviour is of interest. The dynamic viscosity of water is 10E-3 Pa s whereas the dynamic viscosity of clay is easily one to three orders of magnitude larger. If a fluid has a high viscosity it is more difficult to stretch or separate it. A high viscous mixture will flow less fast downstream a slope and more energy is needed to keep it in motion. The viscosity of a mixture can be influenced by several aspects summed below. This should be kept in mind when measuring and/ or modelling a certain fluid.

- A decrease of the particle concentration decreases the colloidal interaction, the fluid will behave less or non-cohesive. The shift of the flow curve of a mixture is called Flow curve similarity. (Concept of the Flow curve is explained in Subsection Flow curve).
- A difference in temperature can increase or decrease the viscosity. Many relations for different fluids exist in literature. Generally the viscosity decreases for increasing temperature.
- The increase in positively charged molecules increases the flocculation process therefore the viscosity.
- A lower pH-value of the fluid improves flocculation.
- Clay particles and flocs are not spherical and can have different shapes. The change of shape due to flocculation influences the viscosity.
- The type of clay may influence the viscosity due to a different shape for every clay type.

C. Kranenburg (Kranenburg, 1994) defined the amount of collisions by the amount of particles, the distance between them and the differential velocity between the particles. This is a rough estimate. Due to external factors and the shape of the aggregates the amount of collisions is larger and increases with the size of an aggregate. The momentum transferred is a function of the viscous force acting on the particles times the time needed to collide. For steady state conditions (no change of the conditions in time) the apparent viscosity is the ratio between the shear stress and shear rate.

$$\mu_a = \frac{\tau_y}{\dot{\gamma}} \sim \mu_w \varphi_p^{\frac{2(1+a)}{3}} \left[\frac{\dot{\gamma}_c}{\dot{\gamma}} \right]^{\frac{(1+a)(3-n_f)}{3}} \tag{2.4}$$

τ_y is the yield strength, μ_w and μ_a are the viscosity of water and the clay respectively. a is an anisometric parameter that indicates the influence of the particle geometry, $\dot{\gamma}$ the shear rate and $\dot{\gamma}_c$ the critical shear rate. If this value is exeeded particles breakdown to their primary particles. The equation shows that for an increasing shear rate, the viscosity will decrease and the shear stress will increase.

Flow curves

A rheogram or flow curve visualizes the yield strength and/ or viscosity of the remoulded state of a fluid as a function of the shear rate. In Table 2-2 four categories of fluids are presented, defined by their rheological properties. For every fluid a rheological model (mathematical function) can be defined, expressing the relation between the shear stress and the share rate. The most common are included in Table 2-2. τ is the shear stress, τ_y the yield stress, μ is the *dynamic viscosity* (Newtonian fluid) or *plastic viscosity* (Bingham fluid) or *viscosity* (other non-Newtonian fluids), n is the flow index. In a Herschel-Bulkley model the viscosity is often presented by K and called the consistency index. Depending on the flow rate the strength of a mixture may increase or decrease if it is sheared. There are several methods and devices to measure the properties. Examples are a vane test (to measure the yield stress), tube viscometer and a rational viscometer.

Type of fluid	Explanation	Rheological model
Newtonian (e.g. water)	A constant line through the origin. (The viscosity is for visibility high.)	Constant $$\tau = \mu\dot{\gamma} \qquad (2.5)$$
Pseudo plastic	$\tau_y = 0$ $\dot{\gamma}$ increase ; $\mu_{apparent}$ decreases The fluid gets thinner due to the lower viscosity.	Ostwald-deWaele Power law $$\tau = \mu\dot{\gamma}^n; \qquad 0 < n < 1 \qquad (2.6)$$
Dilatant	$\tau_y = 0$ $\dot{\gamma}$ increase ; $\mu_{apparent}$ increases The increasing viscosity results in a thicker fluid.	Ostwald-deWaele Power law $$\tau = \mu\dot{\gamma}^n; \qquad n > 1 \qquad (2.7)$$
Pseudo plastic with yield point or plastic liquid.	$\tau_y > 0$ $\dot{\gamma}$ increase ; $\mu_{apparent}$ decreases (if $0 < n < 1$) $\dot{\gamma}$ increase ; $\mu_{apparent}$ increases (if $n > 1$)	Bingham and Green $$\tau = \tau_y + \mu\dot{\gamma} \qquad (2.8)$$ Herschel and Bulkley $$\tau = \tau_y + K\dot{\gamma}^n; \qquad 0 < n > 1 \qquad (2.9)$$ Casson $$\sqrt{\tau} = \sqrt{\tau_y} + \sqrt{\mu\dot{\gamma}} \qquad (2.10)$$

Figure 2-4 (left) the different models are presented. The viscosity is the tangent of the flow curve (or plastic viscosity for Bingham fluids). The apparent viscosity is the slope of the line from the origin to a certain shear stress on the flow curve. Figure 2-4 (right) presents both for a Herschel Bulkley model.
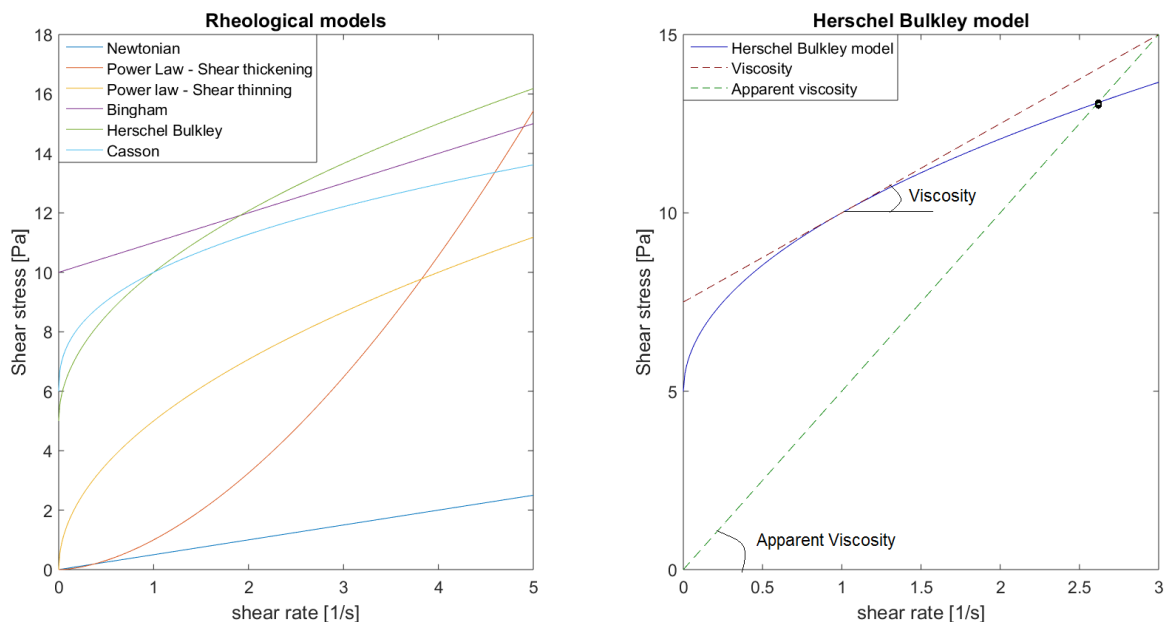

Figure 2-4 Left: six rheological models. Right: Herschel Bulkley model and dynamic viscosity and apparent viscosity. Source: (Litzenberger, 2003).

Clay - Water content

For cohesive sediments the shear strength of the material can be measured by penetrometer tests or vane tests. For mixtures containing a high amount of water it is possible to determine the undrained shear strength as a function of the water content and the clay properties. This approach is based on the Atterberg-Limits, defined in geotechnical water content (W). W is the mass of water over the mass of solids. These are:

- Liquid-Limit (*LL*): the maximum W at which the mixture is not fluidized. This corresponds to an undrained shear strength, $c_u \approx 100$ Pa
- Plastic-Limit (*PL*): the minimum W at which the mixture does not crumble if it is remoulded. This corresponds to an undrained shear strength, $c_u \approx 100$ kPa

The range of water content between the two limits is the plasticity index (*PI*). By relating the properties to the water content W it is possible to estimate the undrained shear strength. The Liquidity Index (LI) is a relation between W, PL and PI:

$$LI = \frac{W - PL}{PI} = \frac{W - PL}{LL - PL} \tag{2.11}$$

The *LI* represents the amount of water in the mixture relative to the amount of water captured by the clay. The amount of captured water is related to the clay fraction. The *LI* increases with increasing permeability of the material. Therefore the undrained shear strength as a function of the relative water content W_{rel} gives more insight for dilute mixtures. It is the ratio between the water content and clay concentration.

$$W_{rel} = \frac{W}{PI} \tag{2.12}$$

Figure 2-5 presents a decreasing strength for increasing water content or decreasing clay content of the total mixture of different mud samples. The undrained shear strength of exclusively clay is a function of W_{rel} to a certain power. (Jacobs et al., 2011; Jacobs, van Kesteren, & Winterwerp, 2008; J C Winterwerp & van Kesteren, 2004). Other experiments prove an equal relation between the plastic viscosity and the W_{rel}.
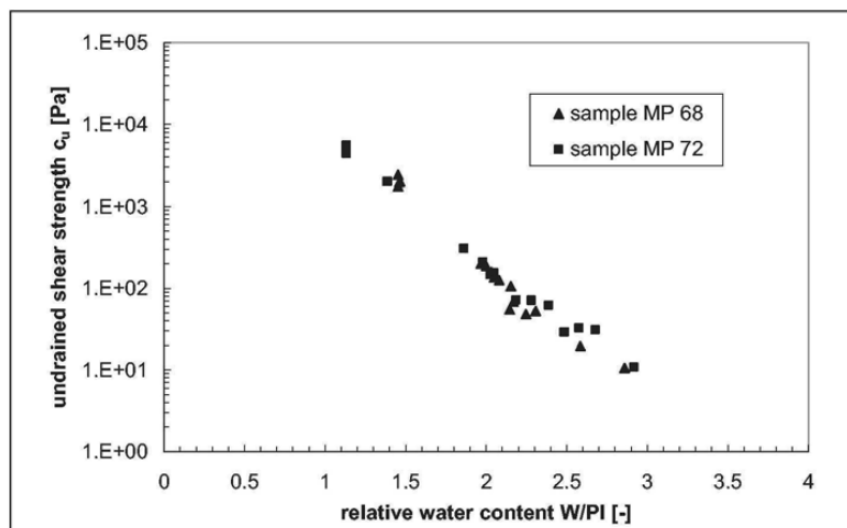

Figure 2-5 Relation of the undrained shear strength and relative water content. Figure by (J C Winterwerp & van Kesteren, 2004) Data Ijmuiden mud.

Different material properties can be derived from the Atterberg-Limits. In an Activity-plot the *PI* is plotted against the clay content of the soil. At a certain amount of clay the soil behaves cohesively. The cohesiveness of a sample is determined by the available clay content minus the minimum content for cohesive behaviour. The clay activity A_{clay} is the ratio between the *PI* and the content contributing actively to the cohesiveness of the clay.

$$A_{clay} = \frac{PI}{(\xi_{cl} - \xi_0)} \tag{2.13}$$

A_{clay} is a constant value for a certain type of clay. ξ is the mass of solids divided by the total solids mass. The subscripts *cl* and *0* refer to the present amount of clay and minimum amount of clay for cohesive behaviour respectively. The value of ξ_0 is (roughly) 7%. For lower values the mixture is non-cohesive (J C Winterwerp & van Kesteren, 2004). The mixture has a yield stress and is able to with stand some forcing if stirred. Possibly it is non-Newtonian.

Influence of sand and silt

The effect of the granular material on the behaviour of a mixture is twofold: on one side it increases internal friction; on the other side it introduces non-cohesive particles. The resulting effect is that at equal volume concentration or density, yield stress and viscosity decreases with increasing sand content. Yet, adding sand to a specific sample increases its density, thus generally its yield stress and viscosity. This behaviour has been demonstrated in numerous experimental studies and can mathematically be described in different ways. If silt particles are captured by the clay, they do not contribute to the internal friction.

For Newtonian fluids (e.g. water), Einstein found that sand increases the viscosity of the fluid (eq.(2.14)). If the fluid is sheared it has to flow around and in between the present sand particles. Therefore the shear resistance increases compared to a fluid without suspended material. The increase is related to the increase in volume concentration of sand particles. Many others used this classic equation as a starting point to include particle effects in rheological formulations (e.g. (Bagnold, 1954), (D. G. Thomas, 1965)). Important to notice is that this equation does not limit the maximum concentration of sand, i.e. the concentration can approach one which is physical impossible (Mueller, Llewellin, & Mader, 2010).

$$\frac{\mu_{mixture}}{\mu_{carrier-fluid}} = 1 - B\phi_{sa} \tag{2.14}$$

Bagnold performed experiments on the neutrally buoyant solids influence with Newtonian fluids having two different viscosities (Bagnold, 1954). He derived a mathematical expression for the effect of the grain stresses based on the linear concentration λ. λ is the ratio of the particle diameter and the spacing between the particles. This can be rewritten in terms of the maximum sand concentration $\phi_{sa,max}$ and the present sand concentration ϕ_{sa}.

$$\lambda = \frac{1}{\left(\phi_{sa,max}/\phi_{sa}\right)^{1/3} - 1} \tag{2.15}$$

λ increases for increasing concentration. The experiments proof that the total shear stress increases with increasing linear concentration.

A.D. Thomas did research to the increase of the viscosity and yield stress by the addition of sand in non-Newtonian fluids (A. D. Thomas, 1999). From experiments he derived that the increase in plastic viscosity μ is related to the sand volume concentration divided by the maximum volume concentration of sand to a certain power. The function is related to the Krieger-Doughetry approach. In contrast to eq. (2.14) the maximum concentration is bounded (Mueller et al., 2010).

$$\frac{\mu_{mixture}}{\mu_{carrier-fluid}} = \left(1 - \frac{\phi_{sa}}{k\phi_{sa,max}} \right)^{-2.5} \tag{2.16}$$

k is a constant to be determined empirically. Measurements show that the value of $k\,\phi_{sa,max}$ deviates between 0.6 and 0.9. For the concerned data in (A. D. Thomas, 1999) he used a value of 0.75. Likewise A.D. Thomas found that the formulation is applicable for the effect of sand on the yield strength as well.

In the work of (Jacobs et al., 2011, 2007) an investigation was done to the effect of sand (and silt) on the undrained shear strength and viscosity of sand-mud mixtures. Their conclusions are that the undrained shear strength and viscosity decrease for decreasing W_{rel} if the mixtures are in the cohesive regime. If the sand-silt structure dominates, the two rheological parameters increase with decreasing clay content. Due to the presence of clay particles it is more difficult for the granular material to build a skeleton. The rate of increase of the undrained shear strength for sand-mud mixtures is an exponential function based on the linear concentration theory of Bagnold. Factor α is constant to be determined empirically.

$$\frac{c_u}{c_{u,clay}} = \exp(\alpha\lambda) \tag{2.17}$$

Figure 2-6 presents on the horizontal axis the linear concentration and on the vertical axis the ratio between the viscosity of the mixture and the carrier fluid. A good correspondence is found between eq. (2.17) and the presented data for $\alpha = 0.2752$.
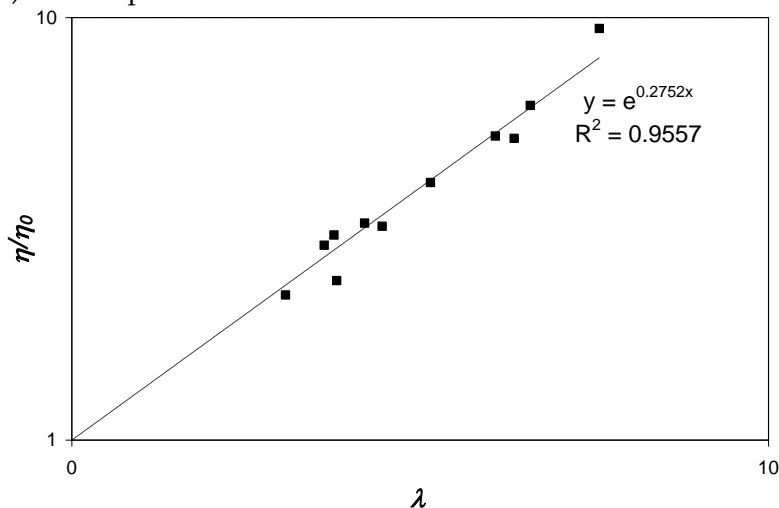

Figure 2-6 Relation between the increase in viscosity and the linear concentration compared with data. Figure by W. v. Kesteren, personal communication.

Figure 2-7 the approaches of A.D. Thomas and Jacobs et al. to quantify the effect of an increase in viscosity by sand are compared. The equation of Thomas is plotted three times with different values for $k\varphi_{sa,max}$ (0.6; 0.75; 0.9). The equation of Jacobs et al. is plotted using $\alpha = 0.2752$ and $\varphi_{sa,max} = 0.6$. For low volumetric sand concentrations (smaller than 30%) both models have a fair agreement.
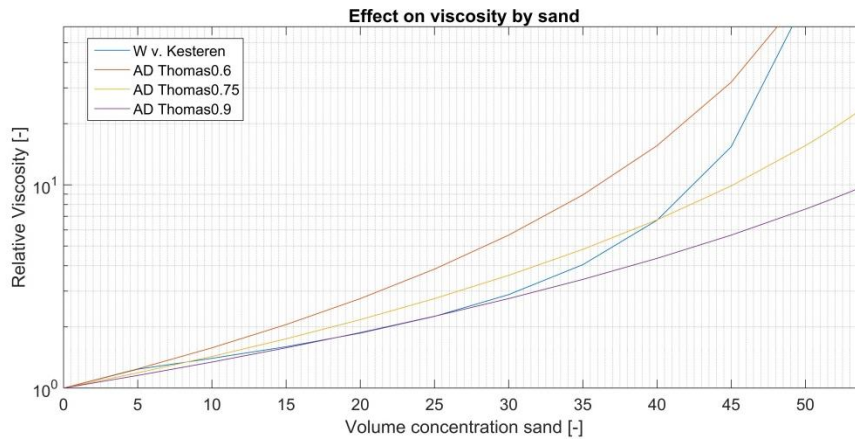
Figure 2-7 Comparison of formulas A.D. Thomas and W. v. Kesteren to describe the increase in plastic viscosity related to the sand concentration.

2.1.3. Hydrodynamics

The mud-sand flows under considerations are limited to (cohesive) non-Newtonian and laminar in an open channel. As discussed earlier in this chapter they have a yield stress and may have a dynamic viscosity which changes if the fluid is sheared. Depending on the hydrodynamic and rheological properties the flow is laminar or turbulent. A flow is called laminar if the flow lines of the fluid remain straight and parallel. The viscosity of the fluid dominates. Turbulence occurs due to variation in the flow velocity from the mean velocity. The Reynolds number Re is a function of the flow properties and the rheology. U, L, ν are the difference in velocity, length scale of velocity difference and kinematic viscosity respectively of the fluid.

$$Re = \frac{UL}{\nu} \tag{2.18}$$

For each fluid the Re of the transition between laminar to turbulent flow differs and can also be a range. This is especially true for non-Newtonian fluids. In open channels water alters to the laminar regime if $Re < 1000$ (Uijttewaal, n.d.). The flow adjusts from one state to the other until the Re is small enough and the flow is fully laminar. The Re for laminar and turbulent flow depends on the geometry and type of fluid. The concentration of solids influences the viscosity of the fluid and is able to reduce the amount of turbulence. If the viscosity dominates the advection a flow can shift into the laminar regime. Investigation towards the transition from laminar to turbulent flow for non-Newtonian flows is done by (T. G. Fitton & Slatter, 2013; Rainer Haldenwang & Slatter, 2006).

(T. G. Fitton & Slatter, 2013; Rainer Haldenwang & Slatter, 2006) found remarkable results. For non-Newtonian open channel flow an adapted Re was introduced (in analogy to pipe flow conditions), including the rheological properties and the flow properties. R_h is the hydraulic radius and n is the flow rate.

$$Re_2 = \frac{8\rho U^2}{\tau_y + \mu(2U / R_h)^n} \tag{2.19}$$

For low concentrated flows the transition from laminar to turbulent was at Re like in water. More viscous fluids had a transition region for lower Re (e.g. 700).

Figure 2-8 is a sketched situation of a non-Newtonian mixture flowing down a slope. The shear stress increases linearly with the water depth. The fluid can only flow if the wall shear stress exceeds the yield stress. The depth where stresses both are equal, h_{cr}, is an important transition

point for the velocity profile. Below h_{cr} the profile is parabolic in case of a Bingham model and a power function for a power law fluid. Above h_{cr} the profile is a straight line. The upper part is the ''Plug'' of the flow. In here the shear rate is zero. The lower part is the sheared region. This has consequences for the settling of particles as will be explained in Subsection 2.1.4.
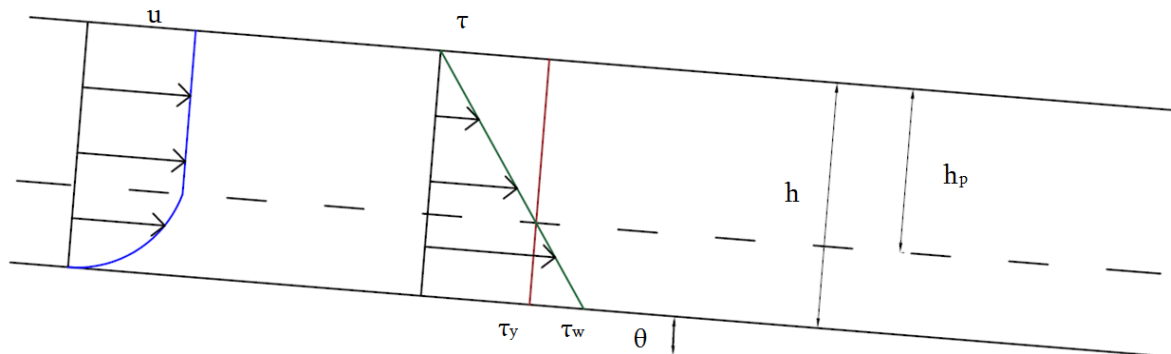

Figure 2-8 Non-Newtonian flow along a slope; velocity and shear stress profile

Eq. (2.20) presents the relation between the hydrodynamic properties and the rheological properties. For a homogeneous flow on a slope (P. T. Slatter & Williams, 2013) provided a new Re_4 and an analytical relation between the bulk shear rate and the rheological properties. The equation holds for Herschel Bulkley and Bingham ($n = 1$) fluids. They proved that it corresponds with data up to bulk shear rates of 200 1/s using the criterion the $Re_4 = 700$.

$$\frac{3\bar{u}}{h} = \frac{3n\mu}{\tau_w(2n+1)}\left(\frac{\tau_w}{\mu}\right)^{\frac{n+1}{n}}\left(1-\frac{\tau_y}{\tau_w}\right)^{\frac{n+1}{n}}\left(1+\frac{n}{n+1}\frac{\tau_y}{\tau_w}\right) \tag{2.20}$$

$\bar{u}$, h, τ_w, τ_y, μ, n are the average flow velocity, water depth, wall (or bed) shear stress, yield stress, dynamic viscosity and flow index respectively. By re-writing the equation it is possible to derive the mean flow velocity given the rheological properties and flow depth.

2.1.4. Segregation

The flow is homogeneous if the entire fluid has the same physical properties throughout the considered domain. Segregation is the settling of coarser particles. It results in differences in particle concentration and density over the vertical, leading to a separation of the flow into multiple layers; i.e. stratification.

In this study it is assumed that the clay particles will not settle in the considered time scale. The silt particles may settle depending on their diameter, the salinity of the fluid and viscosity of the fluid. A division can be made between the carrier fluid (defined here as the water-clay(-silt) portion of the slurry) and the whole mixture (i.e. water and all present inorganic fractions). The rheology for the flow calculations is governed by the whole sand-mud mixture as explained in Section 2.1.2. The segregation is determined by the rheology (inherent viscosity) of the carrier fluid (Thomas, 2010) and the flow behaviour, i.e. the shear rate.

Numerous studies are done to describe the (hindered) settling of sand in in Newtonian flows. Research towards the (hindered) settling of sand in non-Newtonian fluids utilizes this knowledge (Talmon et al., 2014; Talmon & Mastbergen, 2004). First the settling behaviour and related

17

equations of sand in a Newtonian fluid is explained. Thereafter the segregation of sand in a non-Newtonian fluid is considered.

Segregation in Newtonian fluids

The settling of a single Euclidean particle in a Newtonian fluid (e.g. sand particle in water) is commonly described by the well-known Stokes formula. The formula is derived from a force balance of the immersed weight of the particle (downward directed force) and the ability of the fluid viscosity to carry the particle (upward directed force). $w_{s,0}$ is the settling of a single particle, ρ_s, ρ_w is the density of the settling material and water respectively. g is the gravitational acceleration and d the nominal diameter of the settling particles. μ_w is the dynamic viscosity of water.

$$w_{s,0} = \frac{(\rho_s - \rho_w)gd^2}{18\mu_w} \tag{2.21}$$

Surrounding particles influence the settling of the single particle by the following physical aspects.

- Return flow and wake formation; if a particle settles, the flow around this particle in upward direction affects the settling velocity of surrounding particles. It reduces the settling velocity of the overall suspension. A particle caught in the wake of the settling particle, will settle faster.
- Dynamic effects; surrounding particles affect the shear rate of one particle (expressed in the viscosity of the fluid as well).
- Collisions; particles may hinder and collide while settling in the suspension, decreasing the overall settling velocity.
- Interactions; because of the movement of particles the attractive and repulsive forces of clay particles may change, affecting the viscosity of the fluid.
- Viscosity; Many studies proved that the increase of the viscosity of a fluid is related to an increase of material in the mixture.
- Buoyancy; the bulk density of the fluid will increase in the lower parts, reducing the settling velocity of remaining particles.
- Cloud formation; in the wake of a particle, other particles can be caught, enlarging the wake. A positive feedback mechanism resulting in higher velocities.

The concentration and its properties determine which process(es) dominate. The presiding physical aspects for a Newtonian fluid are viscosity enhancement, buoyancy reduction, return flow and wake formation.

Varies equations describe the hindered settling of sand. An overview can be found in (Scott, 1984). Commonly the formula of Richardson and Zaki (Richardson & Zaki, 1954) is used to characterize the hindered settling of sand in water and water-mud fluids (J C Winterwerp & van Kesteren, 2004). The formula is empirical derived from fluidization tests.

$$w_{s,eff} = w_{s,0}(1 - k\phi_{sol})^n \tag{2.22}$$

$w_{s,eff}$ is the hindered settling of particles. The parameters k and n are determined empirically and differ for each sample. φ_{sol} is the total volume fraction of solids. Herein it is assumed that these effects are all related to the same solids fraction to a certain power.

(J C Winterwerp & van Kesteren, 2004) found that eq.(2.22) is less suitable because the viscosity enhancement depends on the carrier fluid fractions whereas changes in buoyancy and return flow are due to the settling fraction as well. They presented a different segregation model; the reference velocity of sand is multiplied by a function accounting for these three physical phenomena.

- The return flow v_f reduces the settling velocity. It is found by continuity; the product of the particle concentration and the settling velocity is equal to the concentration of water times the return flow.

$$w_{s,0}^{sa}\phi_p^{sa} + w_{s,0}^{m}\phi^{m} - (1 - \phi^{m} - \phi_p^{sa})v_f = 0 \quad (2.23)$$

The superscript sa and m are for sand and mud respectively. φ is the volumetric concentration determined by c/c_{gel} and φ_p is the volumetric particle concentration. The return flow reduces for an increase of particles. It approaches zero if the maximum concentration is reached. This is the limit of the function. The function expressing the reduction of the settling velocity reads:

$$\frac{(1 - \phi^{m} - \phi_p^{sa})^n}{1 - \phi^{m}}(w_{s,0}^{sa} - w_{s,0}^{m}\phi^{m}) \quad (2.24)$$

n is an empirical parameter. Experiments done by (Dankers & Winterwerp, 2007; Dankers, Sills, & Winterwerp, 2008) verify eq. (2.24) for the hindered settling of sand in a (relatively) high concentrated mud mixture. They found that $n = 2$.

- The hindered settling formula uses the classical expression of Einstein for the modified viscosity of the mud fraction only. The method agrees with data of experiments. The superscript cl is clay. The reduction due to viscosity enhancement reads:

$$\frac{1}{1 + 2.5\phi^{cl}}(w_{s,0}^{sa}) \quad (2.25)$$

- The buoyancy reduction or enhancement is determined by the total mixture.

$$(1 - \phi_p^{m} - \phi_p^{sa})w_{s,0}^{sa} \quad (2.26)$$

The equation for the hindered settling of sand particles including these three effects reads:

$$w_s^{sa} = \frac{(1 - \phi^{m} - \phi_p^{sa})^n}{1 - \phi^{m}} \frac{(1 - \phi_p^{m} - \phi_p^{sa})}{1 + 2.5\phi^{cl}}(w_{s,0}^{sa} - w_{s,0}^{m}\phi^{m}) \quad (2.27)$$

Segregation in non-Newtonian fluids

In contrast to Newtonian fluids, non-Newtonian fluids comprise a yield stress. The yield stress influences the ability to carry the sand particles, i.e. the particle has to overcome the yield stress (Horsley, et al., 2004; Talmon & Mastbergen, 2004). This can be expressed by the following relation.

$$\tau_y \leq \alpha_{cr}(\rho_s - \rho_{cf})gd \quad (2.28)$$

τ_y is the yield stress and the coefficient α_{cr} has to be determined empirically. ρ_s, ρ_{cf}, g and d are the density of the settling solids, density of the carrier fluid, gravitational acceleration and nominal diameter respectively. Eq. (2.28) accounts for a single settling particle in a static non-Newtonian fluid.

The shear stress, or strength, of the carrier fluid depends on the shear rate. (Talmon & Huisman, 2005) derived a mathematical expression for the settling of a single particle in a non-Newtonian

sheared fluid. In a sheared fluid the shear stresses on a particle are assumed to be equal to the shear of the fluid at that location. The largest shear stresses are parallel or perpendicular to the flow. The particle co-rotates with the flow. This, together with the settling velocity of the particle, influences the direction of the shear stresses acting on a solid (compared to the situation without shear) as visualized in Figure 2-9.
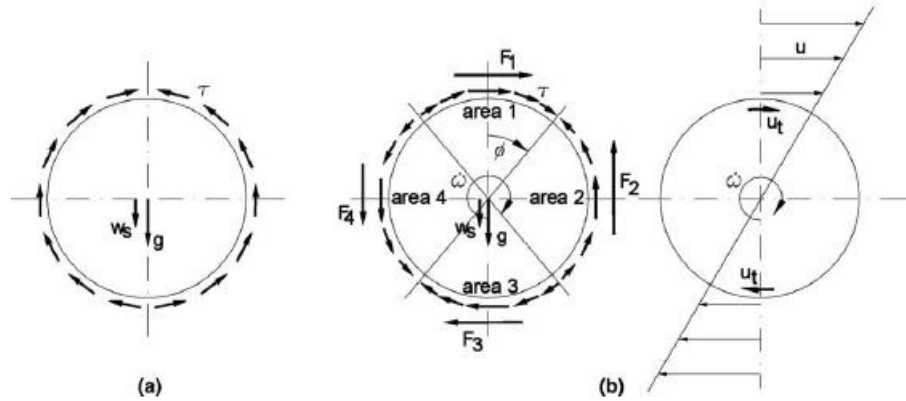

Figure 2-9 Schematization of forces on a particle in sheared flow (Talmon & Huisman, 2005)

The resulting forces *F4* and *F2* are in imbalance and the difference is equal to the immersed weight of the particle *G*.

$$G = \frac{1}{6}\pi(\rho_s - \rho_{cf})gd^3 \qquad (2.29)$$

The settling velocity is solved from the force balance and reads:

$$w_{s,0} = \alpha\frac{(\rho_s - \rho_{cf})gd^2}{18\mu_{apparent-cf}} \qquad (2.30)$$

$w_{s,0}$ is the settling of a single particle. Parameter α is an empirical factor found by experiments ($1/2 < \alpha < 2$) and $\mu_{apparent-cf}$ is the apparent viscosity of the carrier fluid.

Analogous to Newtonian fluids, the settling velocity of a single particle in a non-Newtonian fluid is influenced by surrounding particles. For non-Newtonian fluids the dynamic effects and the increased viscosity appear to be the leading processes. It is not certain if buoyancy effects and return flow effects in flowing non-Newtonian fluids are precisely equal to a Newtonian situation. Although, in stationary fluids, it has been proven that particles can settle faster if they are cached in the wake of another particle (Horsley et al., 2004). To account for the hindrance, a formula derived from eq. (2.22) is commonly used. The resulting formula for shear induced hindered settling of a sand particle in a non-Newtonian flow reads:

$$w_{s,eff} = w_{s,0}(1-k\phi_{sol})^n = \alpha\frac{(\rho_s - \rho_{cf})gd^2}{18\mu_{apparent-cf}}(1-k\phi_{sol})^n \qquad (2.31)$$

The parameters k and n are determined empirically (Pennekamp, Talmon, & van Kesteren, 2010; Sisson et al., 2012a; Spelay, 2007). The formula is verified with shear cell data in the work of (Pennekamp et al., 2010). Confirmation is also found in shear cell tests by (Sisson et al., 2012a; Talmon et al., 2014). For these experiments higher solid concentrations were used and a broader data set was obtained.

2.1.5. The coupled process

The processes explained in the previous sections are all coupled, producing a positive feedback mechanism. The process is visualized in Figure 2-10.

In a given volume of water, clay and sand, set into motion, the high clay fractions induces a non-Newtonian flow and the presence of sand particles influence the rheology. The rheological properties influence the flow velocity profile. The flow field generates a shear stress which affects the segregation of the sand particles. The particles in the plug portion of the flow hardly settle whereas the particles in the sheared region have a higher settling velocity.

In summary, the sand concentration changes have two effects:
1. Variation in the viscosity of the whole mixture, results in a different velocity profile and shear rate. The mutated shear rates affect the viscosity of the carrier fluid and therefore the settling velocity.
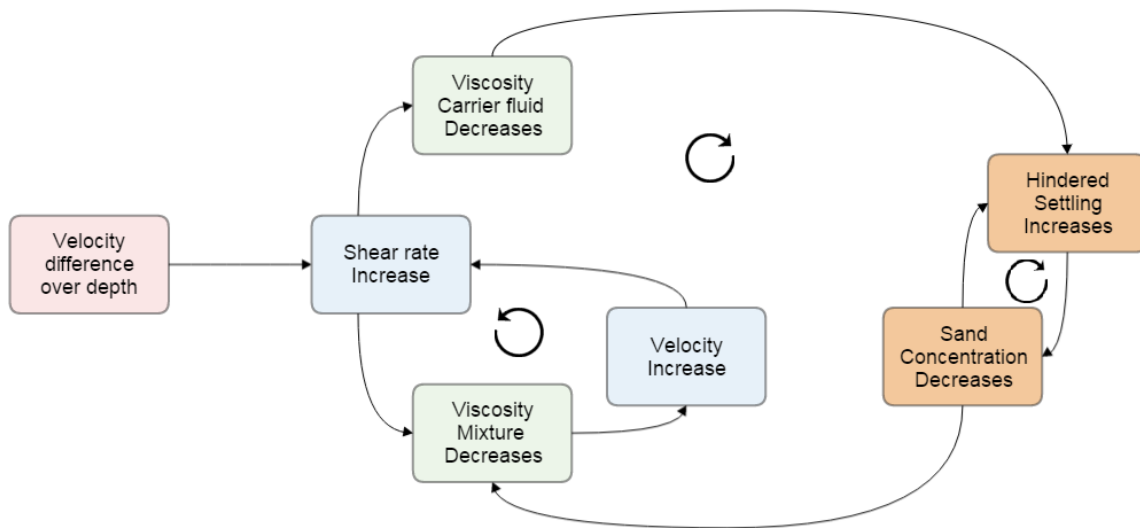2. Variation in the concentration influences the hindered settling.

Figure 2-10 The coupled process of hydrodynamics, rheology and segregation including feedback loops.

The settled material forms a gelled bed and if time allows the settled particles and mud dominated bed are able to consolidate. Mud is trapped in the bed forming a beach deposit with a composition depending on the flow and segregation process described in this thesis. Above the bed an inhomogeneous concentration profile over depth develops with an increase of particles towards the bottom.

2.2. State of the art

Over the last two decades progress is made in the research towards mud-sand flows, especially regarding the rheological properties. More recent is the work on the coupling between rheology, segregation and hydrodynamics and the numerical modelling of these flows.

2.2.1. Physical experiments

In experimental work of S. Sanders, R. Spelay and B. Pirouz research is done towards the development of the velocity profile and concentration profiles of the sand-mud flows. In the experiments of Sanders and Spelay the flow is through a half open pipe. Pirouz used a half open pipe and a rectangular channel. The discharge, the slope of the channel and the mixture properties were varied during the performance of the experiments.

Sanders - 2002

The study done by (Sanders et al., 2002) includes tests with a Bingham fluid in a flume. The used half open pipe had a diameter of 150 mm and a length of 15.7 m. The mixture contained fine particles (15 % by volume) and coarse sand having different nominal diameters and volume concentrations. The slope of the flume is varied during the tests. An overview of the experiment characteristics is presented in Table 2-3.

Table 2-3 Range of properties in experiment of (Sanders et al., 2002).

Q	θ	φ_{cl}	φ_{sa}	d_{50}
2.5 l/s	1.5 – 3.6˚	0.15	0.04 – 0.08	90 – 170 µm

The velocity profiles and concentration profiles were measured with a pitot-tube at 11.7 m from the inlet and traversing gamma ray densitometer near the discharge point respectively.

Flume test - Large sand diameter

Figure 2-11 presents the velocity (left) and concentration profile (right) of a slurry containing 8 % sand by volume and a nominal diameter of 170 µm. Initially the slope is 3.6˚ and gradually decreased to 1.5˚. The measured height y is presented as a function of the pipe diameter D. At an angle of 3.6˚ no deposition was observed. The velocity tends to zero near the bottom and has a curved shape in the sheared region. It is not perfect parabolic due to errors in the measuring procedure.
For slopes smaller or equal to 3.1˚ deposition was noticed. This can also be concluded from the velocity profile; the profile tends to zero at a higher level due to the increase in concentration near the bed.
For a decreasing slope, the driving force by gravity is reduced and the average velocity decreases. The discharge is kept constant. As the (average) velocity decreases, the water level increases. The water level increases due to both; the equilibrium flow and the deposition of sand near the bed.
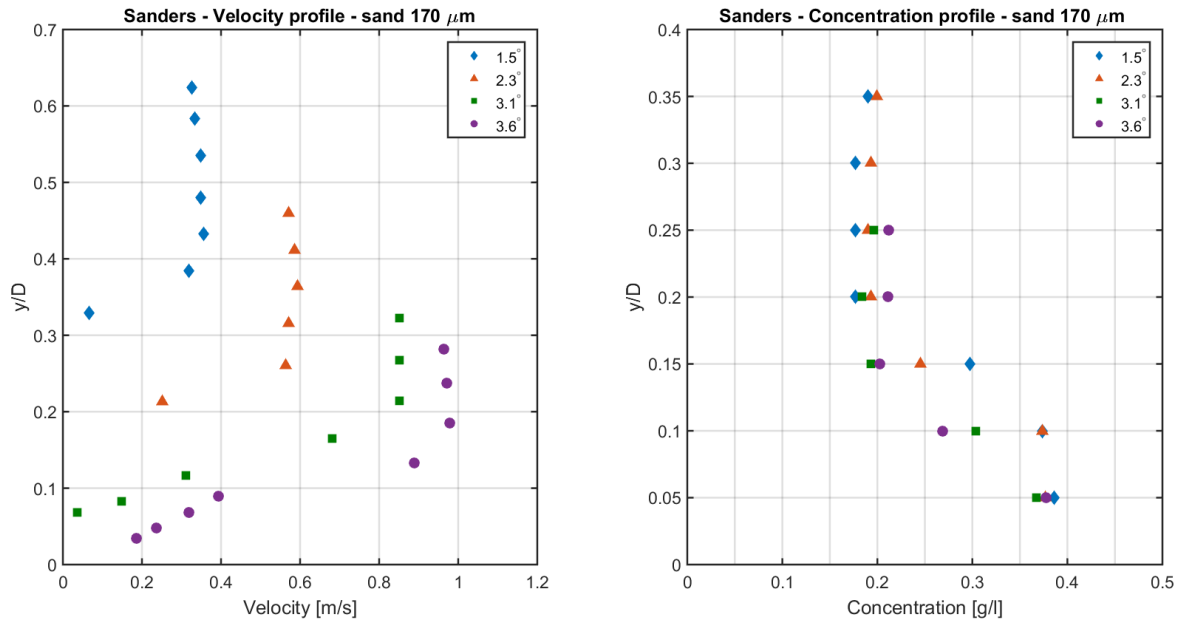
Figure 2-11 Measurement results of experiment with sand diameter 170 μm for different slopes. Left: velocity. Right: concentration.

The concentration profile displays the volume concentration of clay (15 %) and the measured total concentration for the indicated slope.

In every test the concentration increases towards the bottom, indicating that sand segregates for every angle.

In the plug of the flow the measured concentration profile is an (almost) straight line. From the presented theory it is known that the segregation rates should be zero. It is not likely that differences in the concentration occur over depth in the plug zone. These might be introduced by inaccuracies in the measurement procedure. At a smaller angle the concentration in the plug of the flow decreases slightly. It is not likely that smaller angles and lower velocities the settling velocity in the plug increases. The measured points are all still beyond the clay concentration line, which is a sign that over the full depth of the flow sand is present.

In the top of the sheared region the shear rate increases rapidly and at angles of 3.1 and 3.6 degrees a small set back is visible in the concentration profile. Likewise for the velocity profile, the top height of the concentration profile is higher in the flume for a decreasing angle. Near the bed the concentration increases for a smaller slope. This is an unexpected finding because for a larger slope the velocity is higher resulting in larger shear rates and a higher settling velocity. The increased bed level at smaller angles has probably two different causes. Firstly during the tests with larger slopes sediment already segregated which is not brought back into suspension when the slope was decreased. Secondly at larger angles the settling velocity is higher but the velocity near the bed is larger. It has a larger capacity to transport more sediment down the slope in comparison to a test with a smaller slope.

The maximum concentration of solids is 40 % by volume in the bed which is lower than the (average) maximum concentration of 60 %. This is in correspondence with the observation that during the test no stationary bed was formed.

A point of attention regards the measured heights. These differ for the pitot-tube measurements and gamma ray densitometer measurements. The water level height and increased bed height in the concentration profile are lower compared to the velocity profile. After (Sanders et al., 2002)

23

the measurements are likely influenced by the boundary conditions because the gamma ray densitometer is located near the discharge point (at the end of the flume).

Flume test - Small sand diameter

Figure 2-12 presents the measured data for of a slurry containing 8 % sand by volume and a nominal diameter of 90 µm. Initially the slope is 3.9° and gradually decreased to 1.5°.

The velocity profile (left) and concentration profile (right) present a similar behaviour as seen in Figure 2-11. A large difference between the two tests can be found in the flow speed, this is 0.2-0.5 times higher in Figure 2-12. The flow resistance might be reduced by the smaller sand diameter so that the fluid flows faster between the particles.

At a slope of 3.1° the velocity profile becomes zero close to the bottom. This indicates that deposition occurred at a smaller angle. This would be inconsistent with the fact that segregation increases for larger shear rates. It is possible that the deposited material is transported down the slope at a larger angle. The transport rates increase for a smaller particle diameter. This is in agreement with the less thick layer of deposits.

The total flow depth is smaller compared to the experiments with the coarser sand. This is initiated by two processes. First due to the higher flow speed and equal discharge the water level is lower. Secondly due to the smaller deposited layer the fluid is less propelled.
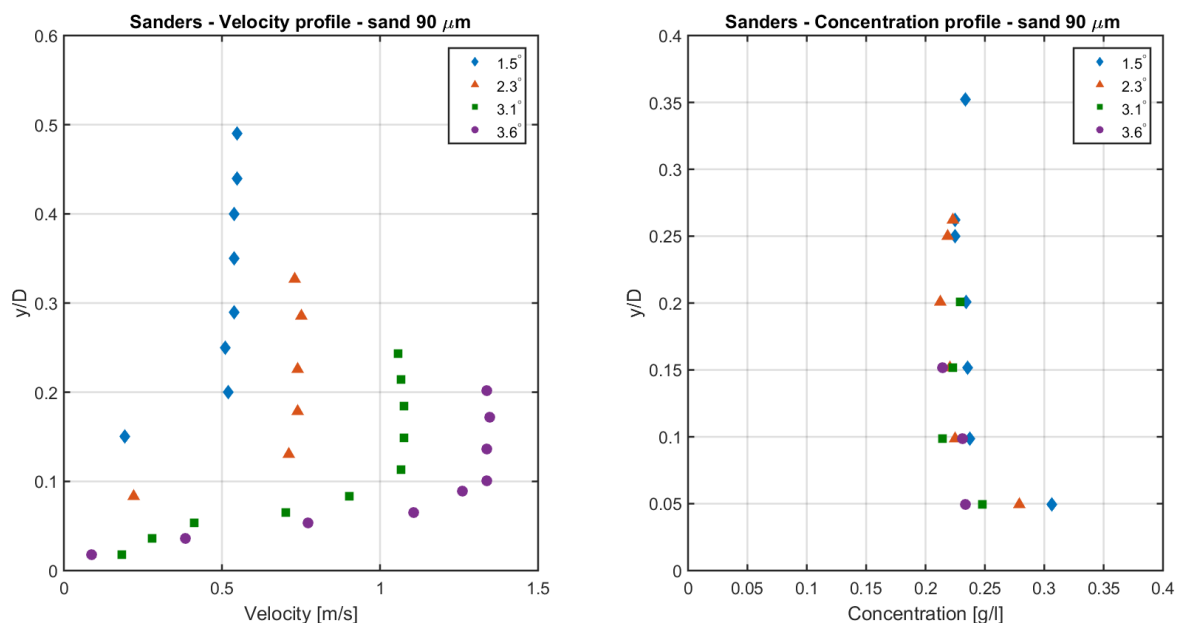

Figure 2-12 Measurement results of experiment with sand diameter 90 µm for different slopes. Left: velocity. Right: concentration.

There are also differences found in the concentration profile. At a slope angle of 3.9° the concentration profile is almost a straight line. Probably the angle and flow velocity were large enough that the flow was not fully laminar. Turbulent forces kept the particles suspended. Deposition was observed Sin the slope angles were smaller than 3.1°. Although the velocity is higher in this experiment- and therefore higher shear rates – it does not result in a wider distribution of the concentration profile. The deposition rates (near the bed) decrease with 40 %. The reduction of the nominal diameter of sand reduces the settling velocity. This is dominant in comparison to the changes in shear rates.

Again the gamma ray densitometer is located near the discharge point, the measurements are likely influenced by the boundary conditions.

Spelay - 2006

(Spelay, 2006) used the same flume as (Sanders et al., 2002) and extended it to a length of 18.5m. Four different Bingham fluids, as found in the oil sands industry, were used. Especially the sand concentration is larger compared to the experiments of (Shook et al., 2002). During the tests the slope of the flume and volumetric flow rates varied. An overview is presented in Table 2-4.

Table 2-4 Range of properties in experiment of (Spelay, 2006).

Q	θ	φ_{cl}	φ_{sa}	d_{50}
2.5 – 5.0 l/s	1.5 – 3.6˚	0.09 – 0.23	0.00 – 0.28	186 μm

The concentration profiles were measured a traversing gamma ray densitometer 14.8m from the inlet. The paper presents two concentration profiles of two different types of slurry. For both the plastic viscosity and yield stress were measured.

Flume test – low clay concentration

Figure 2-13 presents the results of a mixture containing 8.7 % clay and 28 % sand. The tests are conducted for different discharges (2.5 & 5 l/s) and at different slope angles (2.5˚ & 3˚). After (Spelay, 2007) the flow was not fully laminar. First the mixture was discharged at a flow rate of 5 l/s at an angle of 3˚. Secondly the slope was decreased to 2.5˚. In the third phase the slope was increased again and the discharge was decreased.

The plot presents the measured height y is presented as a function of the pipe diameter D. In the first phase the measured concentration profile is a straight line and no segregation occurred. In the second phase sediment settles. At a smaller angle and flow velocity, the turbulence is dampened after (Spelay, 2007). When the discharge is decreased and slope increased even more sediment settles. Probably the reduction of the discharge leads to a reduction of the flow velocity which is larger than the increase in velocity due to the larger slope. Therefore the turbulence dampened even more, enhancing sedimentation. The water level increased significantly in the third phase due to the lower flow velocity and sedimentation.
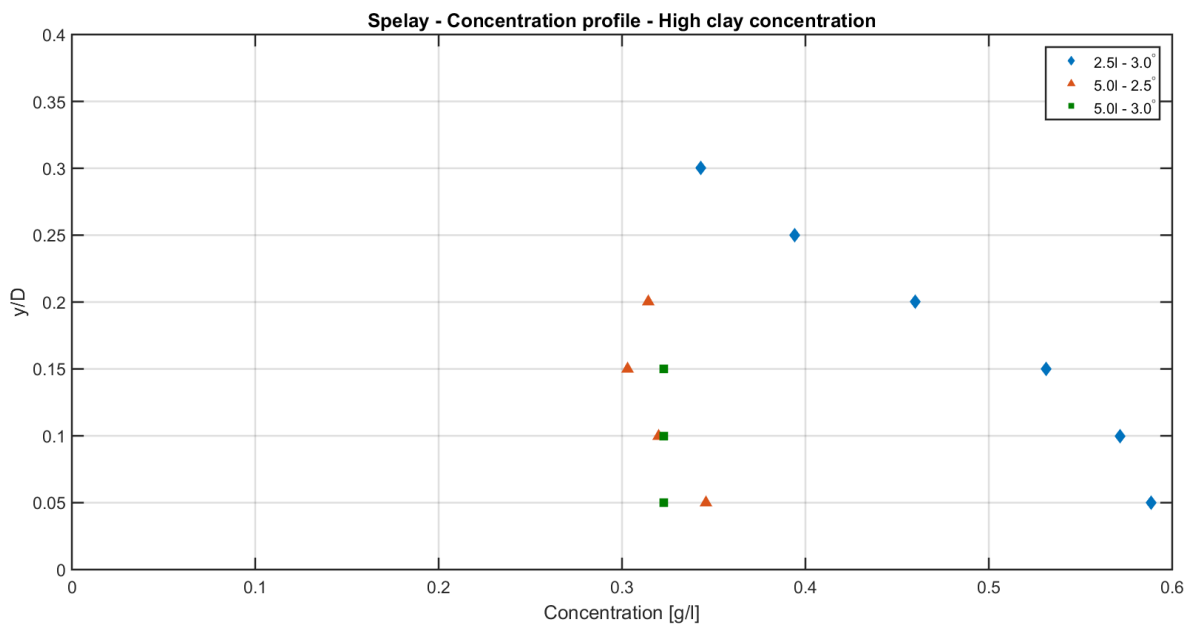

Figure 2-13 Concentration measurement of experiment with low clay concentration

Flume test – high clay concentration

The second mixture contained 15 % clay and 15 % sand. The increase of clay enhances the strength and the reduction of the sand decreases the strength of the mixture. Although the sand reduction was larger, the total strength increased. The hydraulic resistance increases due to the larger viscosity and yield stress. This corresponds with a high measured flow depth for the second mixture. The results are presented in Figure 2-14.

The tests are conducted for different discharges (2.5 & 5 l/s) and a slope angle of 4.5˚. The flow occurred in the laminar regime. First the mixture was discharged at a flow rate of 5 l/s. The concentration profile is an almost straight line between 0.25 and 0.57 y/D. The measured concentration is close to the average concentration of the mixture. Probably this part is the plug of the flow. Below 0.25 y/D the total concentration decreases. It is plausible that this is the sheared region and sand segregates. The sand deposits near the bottom and the total concentration is enhanced.

A second measurement was done for the same mixture and slope angle with a smaller discharge. The measured flow depth increases. Therefore the measured mean velocity must be lower compared to the high discharge test.

Comparable to the first test, in the top part of the flow (until 0.15 y/D) the concentration is almost constant. A decrease of concentration is not visible in the concentration profile. Near the bottom the concentration increases. The increase of concentration is smaller compared to the first test. This would be in agreement with the theory that the shear rates are smaller for smaller flow velocities and that the shear induced settling is smaller for smaller shear rates.
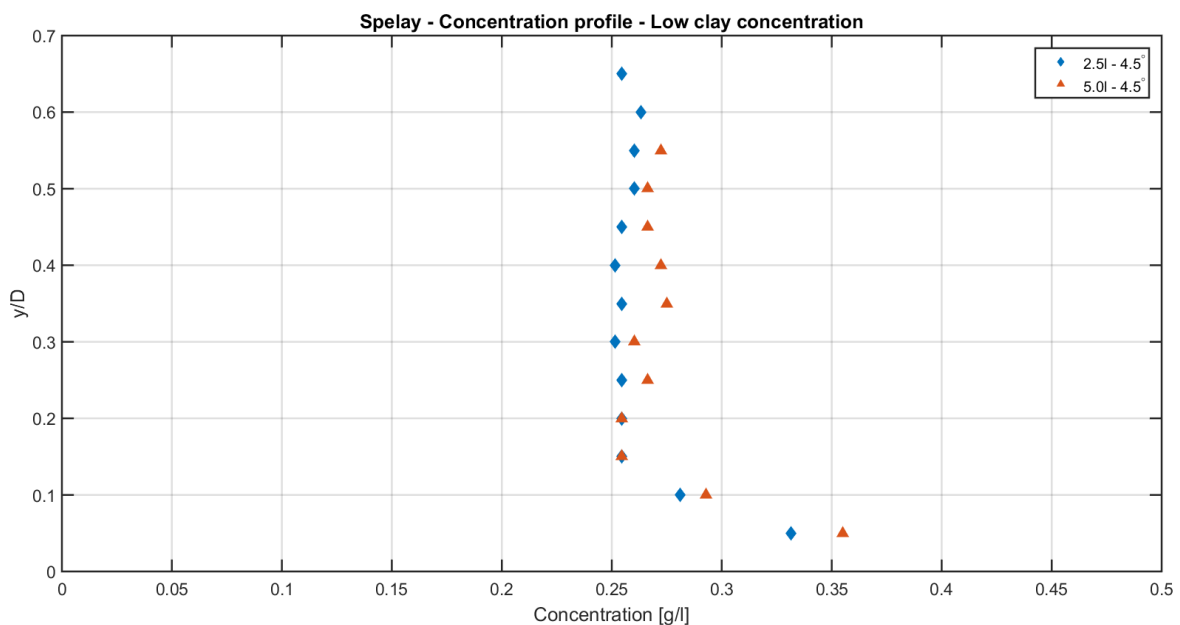

Figure 2-14 Concentration measurement of experiment with low clay concentration

Pirouz - 2013

Pirouz performed tests for different existing tailings, slopes and flow rates (Pirouz et al., 2013). The objective was to study the achievable tailings beach slope. In the flume half open pipes as well as rectangular channels were used. The rheology of the mixtures could be approximated with a Herschel-Bulkley model. Different tests were done on varies fluid compositions and different flume geometries. An overview is presented in Table 2-5.

Q	θ	φ_{cl}	φ_{sa}	d_{50}
5.5 – 18.0 l/s	2.5 – 5.5°	0.12-0.20	0.30 – 0.50	250 μm

In the paper a velocity profile and relative concentration profile are presented for a flow through a half open pipe (D = 326 mm, L = 10 m). The discharge was 13 l/s and the total concentration by weight was 64 %. A velocity profile is measured at 8m from the inlet. The concentration was measured with a rod shaped concentration probe. The dimensions of the tip were 2 x 10 x 10 mm. The flume is circulated through the test facility for a certain amount of time. Every new circulation the fluid passes a mixer and optionally material is added to obtain a constant homogenous solids distribution over depth. During this period a bed of deposited material can form.

Figure 2-15 presents the velocity and relative concentration profile. The velocity profile is an almost straight line from the waterline until 30 mm. It seems to be an unsheared region were no segregation occurs.
Below 30 mm the profile bends. The decrease of velocity over depth introduces shear stresses within the fluid. It would be expected that solids will segregate due to the shear. However the concentration profile does not depict a reduction of the concentration.
The last 5 mm towards the bottom the measured velocity is nearly zero. This coincides with the increase of the concentration near the bottom. Due to the higher concentration, the flow encounters more resistance and the velocity reduces.

The used method to measure the concentration of solids might be doubted. The measured points are obtained by different measurements in sequence. Every measurement requires a certain amount of time.
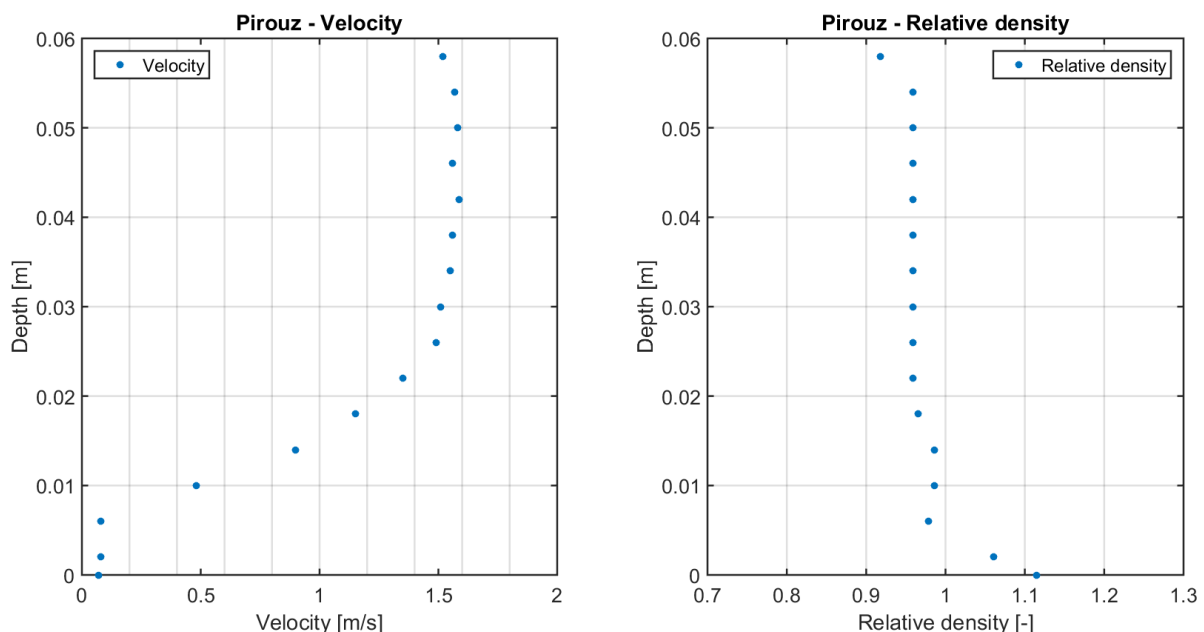

Figure 2-15 Measured velocity and concentration profile.

(Pirouz et al., 2013) and (Sisson et al., 2012b) discovered in their flume experiments the formation of stationary channels and meandering channels respectively. The experimental set-ups differ in length and slope conditions. (T. Fitton et al., 2007; Thomas A, 2011) investigated the width to depth ratio related to the flow rate. (T. G. Fitton & Slatter, 2013; T. Fitton et al., 2007) derived empirically a critical flow velocity criterion.

Currently three different methods exist to predict the beach slope (Talmon, 2015; Treinen, 2014). These are:
- Energy dissipation: based on stream power and entropy resulting in a concave shape.
- Channel formation theory: the channel slope determines the slope of the beach.
- Lubrication sheet flow: a flow prefers the shortest route down the valley. The formed beach has a convex shape.

(Treinen et al., 2014) studied the existing beach flow models and proposed a research trajectory to develop a new or improve a beach slope model. He proposes an integrated model of fluid motion (plug flow), rheology (separation between carrier fluid and mixture) and segregation (hindered settling). Thereafter he suggests a parametric study of various beach flows and path scenarios.

The formation of a beach by deposition is an essential process which determines the management of tailings and slurries. (Kesteren et al., 2015) performed a large scale flume experiment (length of 52 m) with a mud-sand mixture discharged along a beach. The deposited material and flow behaviour was studied. Initially the fluid was able to transport sediments. In the proceeding of the experiment the flow behaviour changed from sheet flow to a more dynamic flow and channel formation. Simultaniously the surface velocity profile transformed and enhancement of the segregation rate occurred. The decrease in strength of the mixture caused the slope of the mud line to decrease. Their conclusion is that the strength of the material dictates the flow behaviour.

Performing large scale experiments on sand-mud channel flows and beaching includes several challenges. The experimental set-up on actual scales (larger than 50m) has often space restriction (Spelay, 2007) and becomes costly. Scaling the experiments brings in artefacts. Outlet conditions may influence the upstream conditions and measurements (Sanders et al., 2002).
Performing the measurements is not effortless. Due to the high particle concentrations laser devices cannot be used to measure the velocities. Instead intrusive probes are used that can easily influence the flow channel (Pirouz et al., 2013).

2.2.2. Modelling

Analytical and numerical models can contribute to the conceptual understanding of the mud-sand flows. If a model is well calibrated and validated, time and length scales can easily be adjusted to study the development of the flow to study different scenarios. Research towards numerical modelling is relatively new in this field of work. To date most of the numerical models focus on the rheological properties and in some cases on segregation.

Research towards the equilibrium slope formation of non-segregating tailings led to a 3D model to predict a tailings stack in the work of (Fitton et al., 2007). The model is based on an empirical model to predict the minimum transport velocity and a methodology to predict the equilibrium slope. The stacks have a cone shape and the tailings are discharged from the top of the cone. The mixture flows downslope, forming a channel. This behaviour is modelled with the assumption

that the tailings spread radially from the top of the stack and flow down the slope. With this model concave shape beach slopes were obtained.

(Spelay, 2007) developed a one dimensional model to predict the behaviour of laminar non-Newtonian flows including coarse sediment in an open channel. The model was compared to experiments performed in the same study and others found in literature. His model is able to predict the segregation of the sand fraction in the non-Newtonian fluid. If the particles segregate, three regions form; the unsheared region with scarcely any difference in concentration, the sheared region where particles deplete and a particle rich region near the bed. For laminar flow the segregation is the governing process compared to re-suspension in vertical direction. The model cannot predict the sliding of the bed material en-bloc.

(Sisson et al., 2012a) presents an analytical model for the segregation of sand in different types of tailings and with different disposal settings of the tailings. Also for this model experiments were done to compare the results. The model is able to predict the behaviour of the mud-line elevation in time and changes in the sand to fines ratio. The concentration profile displays a decrease of the concentration in the sheared zone. The model cannot simulate the bed formation because of the set-up of the model.

In the work of (Sittoni et al., 2015) the first attempts are made to introduce coupling between non-Newtonian flow and sand settling in Delft3D. Different types of tailings where modelled in a 2DV version of Delft3D. The intention was to model these tailings qualitatively. It appeared possible to present slurry flow along a 400 m beach including segregation. Also differences in segregation depending on the slurry properties are clearly visible. The rheological function was not validated at that time and is still in development, which partly motivated this thesis.

2.2.3. Research gaps

The mining industry has a significant demand for understanding the development of tailings and slurry flows and especially to the critical flow velocities to prevent segregation. The accomplished studies increased the perception of the laminar non-Newtonian flows. Despite there is a large undiscovered area. Some examples of knowledge gaps and/ or topics that require additional research are: the interaction between hydrology, rheology and segregation (Haldenwang & Slatter, 2006; Haldenwang et al., 2010; Slatter & Williams, 2013; Spelay, 2007), thixotropy, time dependent viscosity changes, consolidation and stability of stratified flow are not well studied phenomena in flows. Concerning the channelization the evolution of the geometrical properties (width-depth ratios, channel slope) and hydraulics is not well understood.

Regarding the modelling, the formation of a gelled bed layer and transport properties (sliding) has not been modelled to date (Sisson et al., 2012a; Spelay, 2007). In addition, all these approaches are 1DV with attempt to 2DV as best. The translation to 3D, including processes like channel width, avulsion etc. is still virgin ground.

This thesis focusses on definition of the rheology of laminar non-Newtonian flows, segregation of granular material and the coupled process with the flume hydrology in an existing 1DV model directed towards the evolvement of the special 3D module for slurries: Delft3D-Slurry.

2.3. Conclusions

- Tailings and debris flows are mixtures consisting of sand, silt and clay. The clay content introduces a yield strength and is the cause of the non-Newtonian behaviour. Sand and silt influences the rheological properties. The fluid consist of a carrier fluid, water-clay(-silt), and the settling of the granular material.
- The viscosity of the mixture and the viscosity of the carrier fluid determine the hydrodynamics and segregation respectively. The rheology, hydrodynamics and segregation are coupled processes introducing positive feedback mechanisms.
- To date different types of research are conducted towards laminar, non-Newtonian open channel flow including segregation. Nonetheless there are still numerous challenges concerning the behaviour of the channel flow, segregation, and beaching. The use of analytical and numerical models enhances the understanding.

3. Rheology and Segregation

In literature different formulas exist to describe the rheological properties and segregation of solids in a sand-mud flow. This thesis presents three different rheological models and a segregation model for the settling of coarse grains (sand a/o silt).

The three rheological models originate from different fields of expertise, i.e. fluid mud and soft sediment dynamics in natural environments, oil-sand tailings and industrial concentrates. These are the models of Winterwerp&Kranenburg, Jacobs&v.Kesteren and Thomas respectively. Other models exist as well. The choice is made to study these three models for the following reasons. The Winterwerp&Kranenburg model is based on the fractal dimension theory. In Delft3D this theory is implemented to model the properties of clay in a Newtonian flow for numerous projects. The Jacobs&v.Kesteren model is often used in the oil-sand tailings and is used previous in an analytical model (Sisson et al., 2012b). The Thomas model is described in the work of (A. D. Thomas, 1999). It appears that the model is able to present the rheological properties for different solids concentrations and sand to solid ratios. The data in this paper are used to compare the three different analytical models.

The theory behind the three analytical models is simultaneously presented in the paper ''Implementation of Tailings Rheology in a Predictive Open-Channel Beaching Model'' which is submitted to the Paste 2016 conference.

The introduced segregation model is based on experimentally proven theory of Newtonian flow and non-Newtonian flow as presented in Chapter 2. The intention is to develop a physically based model which is in harmony with previous programmed (settling) formulations in Delft3D.

Section 3.1 presents the three rheological formulas. These are compared to data and a calibration example is given in Sections 3.2 and 3.3 respectively. The new segregation model is presented in Section 3.4. In Section 3.5 a brief summary is provided about measurement techniques for the various material and settling parameters. The conclusions are summed in Section 3.6.

3.1. Rheological formulas

The presented rheological formulas who describe non-Newtonian fluids include a yield stress and a shear rate dependent viscosity (Model 1) or constant plastic viscosity (Model 2 and 3). The first model is a power law model whereas the last two models are Bingham models.

For the shear stress τ determination the equation of the three models reads:

$$\tau = \tau_y + \mu\dot{\gamma}^n \quad \text{with} \quad 0 < n \leq 1$$

(3.1)

The three models differ in the formulation of the yield stress τ_y, (plastic) viscosity μ and flow index n of this equation.

3.1.1. Winterwerp and Kranenburg (Model 1)

Self-similarity and the related fractal dimension theory, presented in Chapter 2, often yield a power law behaviour and reads:

$$\tau = \tau_y + \mu \dot{\gamma}^n \quad \text{with} \quad 0 < n \leq 1 \tag{3.2}$$

Important to note is that μ consists of the dynamic viscosity of water and the viscosity of the material. For the first one the $n = 1$, for the latter $n < 1$ due to the shear rate dependency of eq. (3.4).

$$\tau_y = A_y \left(\frac{\phi_{cl}}{1 - \phi_{sasi}} \right)^{2/(3-n_f)} \exp\{\beta\lambda\} \tag{3.3}$$

$$\mu = \exp(\beta\lambda)\left[\mu_w + A_\mu \left(\frac{\phi_{cl}}{1 - \phi_{sasi}} \right)^{\frac{2(a+1)}{3}} \left[\frac{1}{\dot{\gamma}} \right]^{\frac{(a+1)(3-n_f)}{3}} \right] \tag{3.4}$$

The determination of the yield strength and viscosity are based on different physical properties of the sand-mud mixture. These are the solid fractions φ (subscripts *cl* and *sasi* are clay and sand-silt respectively). Their summed value will always be smaller than one, otherwise there is no water present. The fractal dimension n_f varies between 2.6-3 for high concentrated mud suspensions. A value of 2.64 is obtained from the data of A.D. Thomas. The value of the linear concentration λ depends on the present amount of sand a/o silt and their maximum concentration. *a* is a parameter accounting for the (non-symmetric) shape of the particle. μ_w is the viscosity of water typically it has a value of 1E-3 Pa s.

A_y and A_μ are empirical parameters depending on the clay type. In the data of A.D. Thomas they have a value of 7.3E5 and 9.3 respectively. The measured yield stress in the experiment of A.D. Thomas was relatively high (order 100 Pa). Therefore A_y might attain a value in the order of 1E4 as well. The measured viscosity was relatively small (order 0.01 Pa s). A_μ could be an order of magnitude larger. At least its value most be above the value of the dynamic viscosity of water. The reduction of the mud matrix due to the granular material is expressed in the denominator of eqns. (3.3) and (3.4). The clay fraction and n_f determine the yield strength and viscosity. The theory of Jacobs and van Kesteren (presented in Chapter 2) is used to determine the internal friction by the granular material. β accounts for the internal friction to be determined empirical as well.

In eqns. (3.3) and (3.4) the fraction of silt is included to the granular fraction which is settles. For mixtures where the silt fraction is part of the carrier fluid is also possible to rewrite these equations. The silt fraction will then be added to the clay fraction.

3.1.2. Jacobs and van Kesteren (Model 2)

The theory from the second model follows from the ratio of the water content W and plasticity index PI (which is a function of the clay content) as presented in Chapter 2. It is previously described in the work of Jacobs and v.Kesteren (Jacobs et al., 2011) and has been implemented in thick and non-segregating tailings (e.g. in the oil sands industry). This reads:

$$\tau = \tau_y + \mu\dot{\gamma} \tag{3.5}$$

$$\tau_y = K_y \left(\frac{W}{PI} \right)^{B_y} \times \exp(\beta\lambda) \tag{3.6}$$

$$\mu = \mu_w \exp(\beta\lambda)\left[1 + K_\mu\left(\frac{W}{PI}\right)^{B_\mu}\right] \tag{3.7}$$

In contrast to Model 1, the viscosity is constant for all shear rates as seen from eq. (3.5). This model is a Bingham model.

The strength of the clay decreases for increasing W or decreasing clay content (Chapter 2). Factors B_μ and B_y is there for smaller than one. The W and PI can be rewritten in terms of sand, silt and clay concentration, and clay activity (A_{clay}).

$$\frac{W}{PI} \approx \frac{\rho_w}{\rho_{solids}}\frac{1-\phi_{solids}}{\phi_{solids}}\frac{1}{A\xi_{cl}} = \frac{\rho_w}{\rho_{solids}}\frac{1-\phi_{solids}}{\phi_{solids}}\frac{\phi_{solids}}{A\phi_{cl}} = \frac{\rho_w}{A_{clay}\rho_{solids}}\left(\frac{\phi_{cl}}{1-\phi_{solids}}\right)^{-1} \tag{3.8}$$

Model 2 includes the following physical properties of the sand-mud mixture. The solid fractions φ_{cl} and φ_{sol} are always smaller than one. A_{clay} the clay activity and depends on the Atterberg Limits and present clay fraction. ρ_{solids} and ρ_w the mixture density and the density of water respectively. Depending on the solids type the value ranges between 1900 – 2860 kg/m³. Fresh water has a density of 1000 kg/m³, the value of salt water is about 1025 kg/m³. The linear concentration is λ. The effect of the granular material is once more represented by an exponential function and the linear sand concentration (eqns. (3.6), (3.7)).

K_y, B_y, K_μ and B_μ are empirical parameters depending on the clay type. The data of A.D. Thomas let to a value of 6.7E4 and 2.5 for K_y and K_μ respectively. K_y might be an order of magnitude smaller and K_μ an order of magnitude larger for other mixtures equivalently to A_y and A_μ of Model 1. β accounts for the internal friction to be determined empirical as well.

If the solids content in eq. (3.8) is increased the by the addition of sand, the clay matrix is reduced. Model 1 and 2 obtain a similar behaviour (eqns. (3.3), (3.4) and eq. (3.8)).

Likewise Model 1 the silt fraction is part of the settling material (eq. (3.8)). It is possible to incorporate the silt fraction in the carrier fluid by summing the clay fraction and silt fraction in eq. (3.8).

3.1.3. Thomas (Model 3)

A.D. Thomas (A. D. Thomas, 1999) developed a model for sand-mud mine tailings mixtures. For transparency the equation is rewritten. The rheological model is a Bingham model; the effect of shear thinning in viscosity is not accounted for eq. (3.9).

$$\tau = \tau_y + \mu\dot{\gamma} \tag{3.9}$$

$$\tau_y = C_y\left(\frac{\phi_{fines}}{\phi_{water} + \phi_{fines}}\right)^p\left[1 - \frac{\phi_{sa}}{k_{yield}\phi_{sa\,max}}\right]^{-2.5} \tag{3.10}$$

$$\mu = \exp\left(D\frac{\phi_{fines}}{\phi_{water}}\right)\left[1 - \frac{\phi_{sa}}{k_{visc}\phi_{sa\,max}}\right]^{-2.5} \tag{3.11}$$

The different solid fractions (φ_{fines} and φ_{sa}) water fraction φ_{wa} are the physical parameters within this model. C_y, P, D, $k_{visc}\varphi_{sandmax}$ and $k_{yield}\varphi_{sandmax}$ are empirical parameters depending on the clay and sand type. C_y = 4.75E5 for the mixture used in the experiment of (A. D. Thomas, 1999). A

relatively high yield stress was obtained. C_y might be 1 order of magnitude smaller for other clay types. (A. D. Thomas, 1999) found that $k_{visc}\varphi_{sandmax}$ and $k_{yield}\varphi_{sandmax}$ range between 0.6-0.9.

The yield strength of only the carrier fluid eq. (3.10) is described by a power function. The contribution of the granular material is expressed by the term containing $k_{yield}\varphi_{sandmax}$. This part of the equation is based on eq. (2.16) which A.D. Thomas derived from the experiment (Chapter 2). The viscosity of the carrier fluid eq. (3.11) is a, exponential function. The part between the second set of brackets containing $k_{visc}\varphi_{sandmax}$ expresses the contribution of the granular material likewise done for the yield strength.

The yield stress and viscosity of only the carrier fluid are determined by the fines and water content. For an increasing amount of fines or decreasing water content the yield stress and viscosity increase. The effect of the sand content is accounted for separately.

From the paper it is not directly evident if a silt fraction was present in the experiment and if it is added to the fines or sand.

3.1.4. Modification of the yield stress

The three analytical models do not account for a shear stress if it is smaller than the yield stress. It would not be possible to calculate the apparent viscosity in the plug zone. Therefore the constitutive shear stress eq. (3.12) as modified by (Papanastasiou, 1987) is used. The parameter m is an input parameter and defines the slope of the flow curve at low shear rates. In the sheared and unsheared region the equation is valid (Mitsoulis & Zisis, 2001). It allows computation of the shear stress and apparent viscosity in the plug of the flow.

$$\tau = (1 - \exp(-m\dot{\gamma}))\tau_y + \mu\dot{\gamma} \tag{3.12}$$

3.2. Comparison of the models

The three rheological models are compared to the experimental data of Thomas (1999) and research data of Deltares. The latter only gave the possibility to compare the results on the yield stress. The following describes the procedure to make the comparison with Thomas' experiment and drawn conclusions. For the data of Deltares the procedure was similar and only the conclusions are included.

3.2.1. Experimental set-up

The experiment of Thomas started with the carrier fluid containing fines and water, i.e. no sand. It is assumed that the fines consist of clay.

The yield strength and viscosity related to different total volume fractions of the carrier fluid were measured. Subsequently sand was added to the system obtaining a mixture with a certain sand to solids ratio (STS). For each STS the total concentration of solids (clay and sand) was increased and new measurements were done. Progressively the sand to solids ratio (STS) was increased and as a consequence the total volume concentration of solids of the sample.

The measured data points are presented by filled symbols in Figure 3-1 and Figure 3-2 for yield strength and (plastic) viscosity respectively. In both graphs the blue dots points depict the measurements of only the carrier fluid for different volume concentrations. Every subsequent set of data points (having the same colour and symbol) is a mixture with a certain STS. The STS increases towards the right.

The measured data prove that for a specific total solids concentration the yield strength and the viscosity of a mixture with a low STS (or even no sand) is higher than for a mixture with a higher STS. It is concluded that for a given specific solids concentration and density, the effect of the internal friction caused by the sand particles within the carrier fluid is smaller than the reduction in cohesiveness produced by inert sand particles substituting an equal amount of cohesive clay.

3.2.2. Determination of parameters

For Model 1 and 2 there was not enough information available to value all physical parameters. The models were fit using the data points of only the carrier fluid to obtain the (empirical) constants. The parameters who account for the influence of the internal friction are based on values found in previous work. They were used for a first estimate. The writer was aware that these values might differ. For Model 3 the parameters were already fit to the data as described in (A. D. Thomas, 1999). An overview of the parameters is presented in Appendix A.

3.2.3. Comparison

The predicted values of the three rheological models are compared to the measured data by the Root Mean Square Error (RMSE) method. At lower STS the range of the measured yield stress and viscosity is an order 10-1000 lower than for the high STS. Consequently the absolute value errors of the high STS have an exceptional large impact on the overall RMSE, governing the comparison. Therefore the Normalized Root Mean Square Error (NRMSE) is calculated and utilized to compare the predicted yield strength and viscosity.

Yield stress

In Figure 3-1 the predicted yield stress of the models is plotted against the measured data of (Thomas 1999). For each model a different line type is used. The different colours belong to the different STS. At low total volume concentrations the accuracy of the predicted yield stress of all three models is higher. As the STS increases, the error in the prediction increases as well. In general the performances of the models are comparable. Model 3 has the best fitting overall (note that this model was calibrated based on this data set). For low to medium volume concentrations and STS Model 1 and 2 perform also very well. At the large STS of 78.9% Model 1 and 2 over predict the measured yield stress by a factor 4.
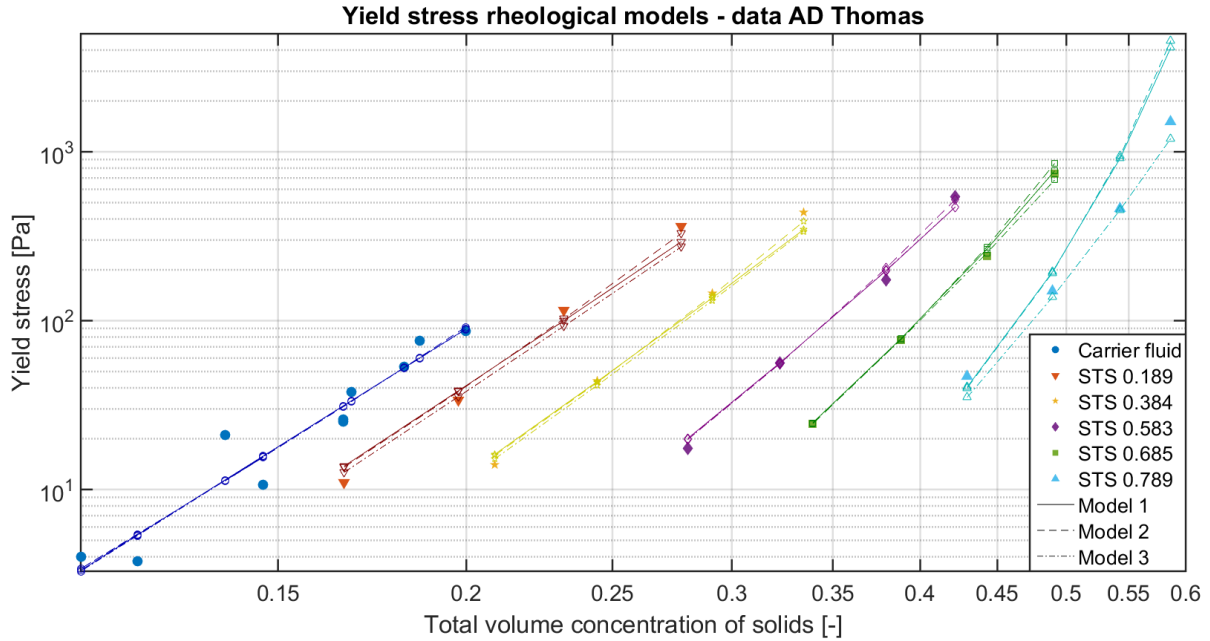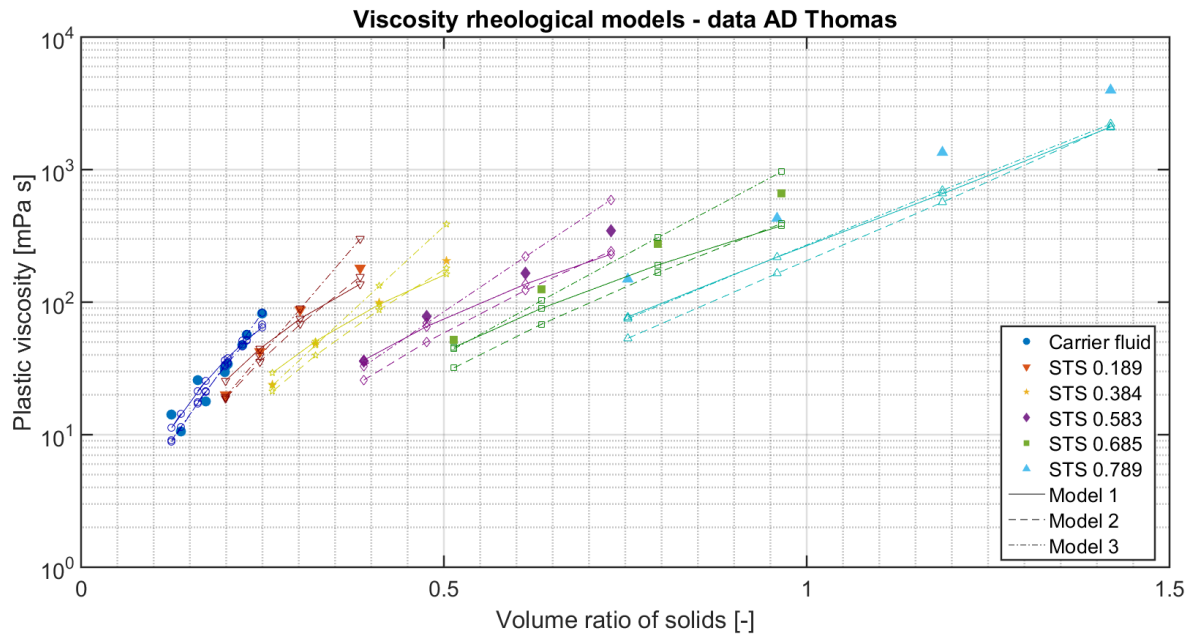
Figure 3-1 Yield stress: Data A.D. Thomas (filled symbols) and rheological model predictions. Model 1 continuous line. Model 2 dashed line. Model 3 dash-dot line.

Viscosity

Similarly as for the yield strength, the error in the prediction of the three models increases for increasing STS. The errors in the viscosity (especially for high STS) are much larger than for the yield strength for all three models. The errors increase with the order of the measured viscosity. Models 1 and 2 perform at times better than Model 3. The results are presented in Figure 3-2.

Figure 3-2 Viscosity: Data A.D. Thomas (filled symbols) and rheological model predictions. Model 1 continuous line. Model 2 dashed line. Model 3 dash-dot line

Concluding remarks

The high STS ratios contain 80 % sand and 20 % clay of the total solids concentration. Experiments done by (Jacobs et al., 2011) prove that mixtures move into the granular regime for high sand concentration. In their research a sand-silt skeleton formed if the STS is 50 % (by weight) depending on the clay type. For these situations the mud matrix is disturbed and the applicability of the three models is exceeded. The parameters concerning the internal friction in Model 1 and 2 might therefore be reconsidered for higher STS ranges.

The distribution and behaviour of the silt particles influence the mixture behaviour as well. If the particles are captured by the clay they will not contribute to the granular skeleton. Secondly if the fraction of silt contains mainly particles with a relatively large particle diameter it is more likely that they build up a granular skeleton.

Another reason for the large differences between the measured values and predicted values is attributed to the error that might occur during the experiment. At high concentrations – and especially high sand concentrations – it is more difficult to measure the yield strength and viscosity correctly.

3.2.4. Sensitivity analysis

A sensitivity analysis was done for the different parameters of the models. It turns out that especially the parameters that influence the internal friction (e.g. maximum sand concentration) and the exponents in the functions are most sensitive. The best fitting values of the parameters deviate for different STS and for different total volume concentrations as well.

- λ and $k_{yield}\varphi_{sandmax}$: Especially for the high STS an higher value of the maximum sand concentration would lead to a better fit. This does not influence lower STS ranges severely. In Figure 3-3 the maximum sand concentration for Model 1 and 2 is corrected to improve the yield strength prediction. The calculated yield strength for high STS was too high. The maximum sand concentration (0.6) is increased to a value of 0.65, resulting in lower values for the yield stress which is more in line with the measured data for high STS. Correction of $k_{yield}\varphi_{sandmax}$ does not lead to an improvement of the predicted yield stress of Model 3.

  Regarding the viscosity the improvement of the prediction is presented in Figure 3-4. All three models under predict the value of the viscosity. The maximum sand concentrations (0.6) of Model 1 and 2 are corrected to 0.55 and the parameter of Model 3 (0.75) is adapted to 0.7. The graph of the viscosity visualizes that it improves to fits to the measured data for the low and medium STS ranges. For high STS the error becomes larger.

- Exponents (n_f, a, B_y, B_μ, P) : The change in the exponent (parameters) has a large influences for all STS resulting in a larger error for smaller STS. This applies for the yield stress as well as for the viscosity

The resulting yield stress and viscosity are presented in Figure 3-3 and Figure 3-4 respectively.
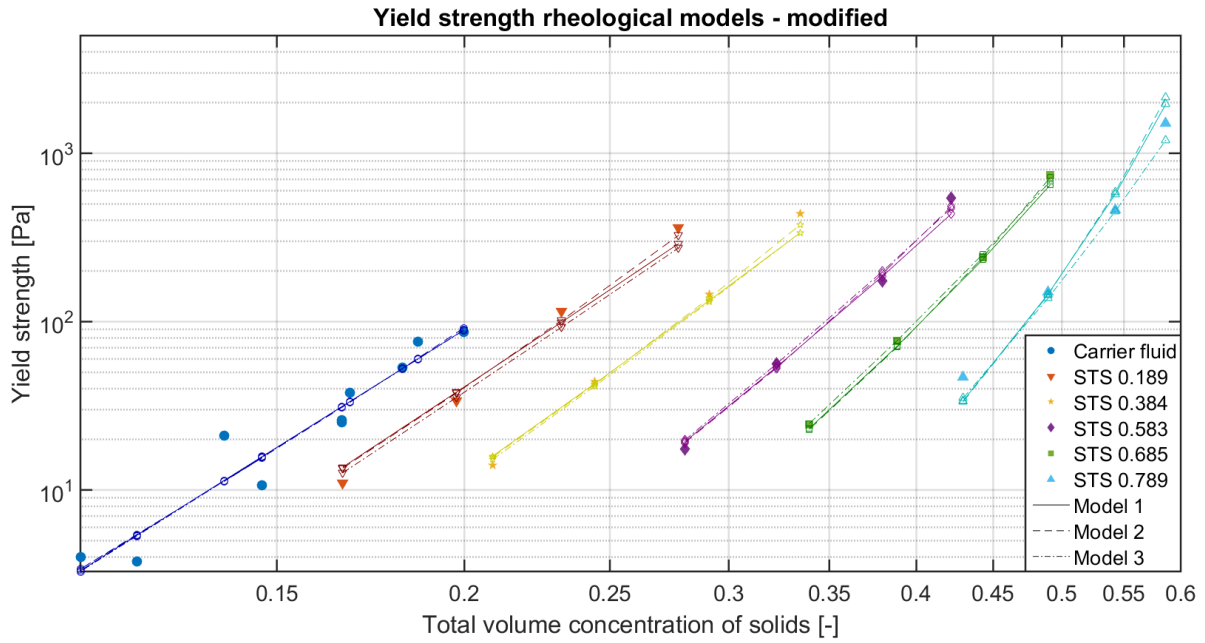
Figure 3-3 Calibrated yield stress: Data A.D. Thomas (filled symbols) and rheological model predictions. Model 1 continuous line. Model 2 dashed line. Model 3 dash-dot line
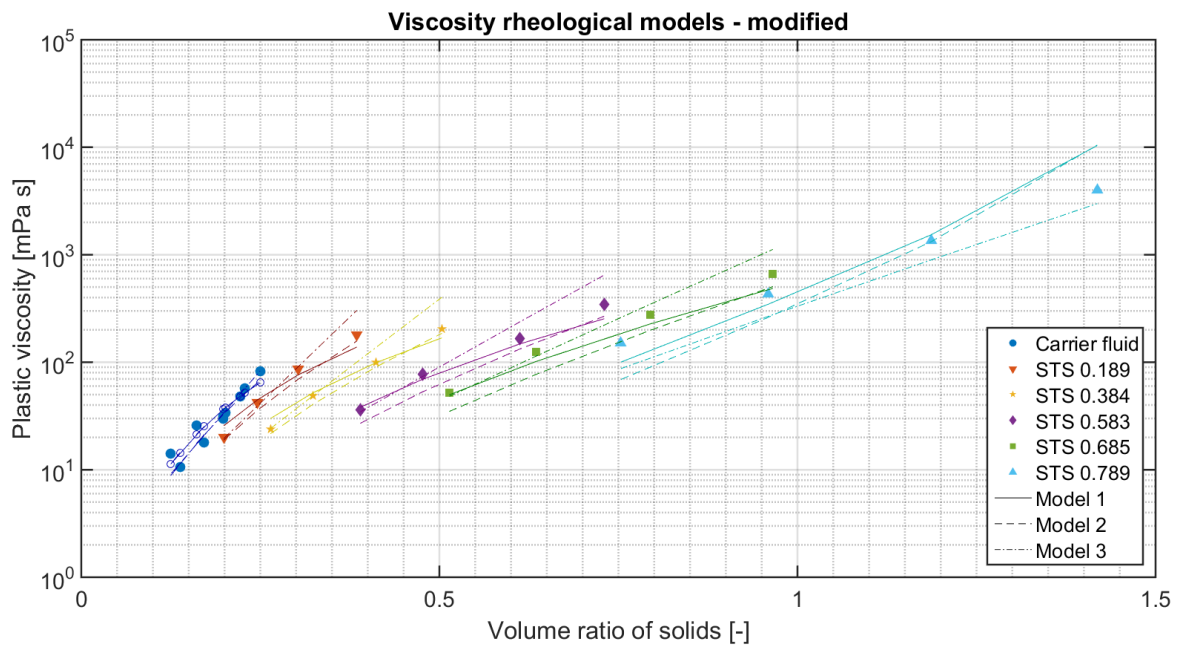

Figure 3-4 Calibrated viscosity: Data A.D. Thomas (filled symbols) and rheological model predictions. Model 1 continuous line. Model 2 dashed line. Model 3 dash-dot line.

3.3. Segregation

In this study a settling formula is presented by J.C. Winterwerp (personal communication) to determine the shear induced hindered settling of sand particles in a mud carrier fluid. First the initial concepts are explained followed by the final equation.

The model concerns the shear induced hindered settling of sand and silt in a non-Newtonian. Initially the total solids concentration is homogeneous distributed. In the initial situation the sand and silt fractions are below the granular regime, i.e. the particles are not able to form a granular skeleton. In the granular regime different processes contribute to the hindered settling which are not included into this model. In the work of (Jacobs et al., 2011) experiments prove that a mixture might shift into the granular regime if $\varphi_{sasi} \approx 0.25$. The exact value depends on the type of an-organic material. Therefore this settling model is limited to the mixtures where: $\varphi_{sasi} < 0.3\ \varphi_{sasi,max}$.

As explained in Chapter 2 the immersed mass of the settling particles has to overcome the yield stress of a non-Newtonian fluid. The settling of single sand particle is described by the formula of (Talmon & Huisman, 2005).

$$w_{s,0} = \alpha \frac{(\rho_s - \rho_{cf})gd^2}{18\mu_{apparent-cf}} \tag{3.13}$$

Parameter α accounts for the non-sphericity of the particle. ρ_s, ρ_{cf}, g and d are the density of the settling solids, density of the carrier fluid, gravitational acceleration and nominal diameter respectively. is the apparent viscosity. The formula is a function of the apparent viscosity of the carrier fluid $\mu_{apparent-cf}$ and therefore of the shear rate.

Below a certain critical shear stress, settling will not occur. The critical value is derived from the force balance between the reduced mass of a sand particle M_p in a mud matrix and the yield stress exhibiting an upward directed force on the particle, $F_{y,p}$ is reads:

$$M_p > F_{y,p} \tag{3.14}$$

$$M_p = \alpha \frac{1}{6}\pi(\rho_s - \rho_{cf})gd^3 \tag{3.15}$$

$$F_{y,p} = \tau_y \beta \pi d^2 \tag{3.16}$$

Parameter α and β account for the non-sphericity of the particle. τ_y is the yield stress. The criterion results in eq. (2.28).

Eq. (3.13) takes into account the (apparent) viscosity enhancement and dynamic effects of the carrier fluid. As seen in Chapter 2 (Sisson et al., 2012b; Talmon et al., 2014) accounted for the effects of buoyancy and return flow in one single addition to eq. (3.13). The obtained equation is valid for non-Newtonian fluids. Herein empirical parameters are imbedded.
To refine this equation the buoyance and return flow are considered analogous to the work of (Dankers & Winterwerp, 2007; Dankers, Sills, & Winterwerp, 2008; Winterwerp & van Kesteren, 2004). The physical processes are defined separately without the use of empirical parameters. To date this approach is validated for high concentrated Newtonian fluids solely.
- Buoyancy: reduction of the settling velocity due to all present particles.

$$(1 - \phi_s) \tag{3.17}$$

- Return flow: reduction due to the settling fraction limited by the minimum porosity.

$$\left(1 - \frac{\phi_{sa}}{\phi_{sa,\max}}\right)^2 \tag{3.18}$$

The final equation determining the shear induced hindered settling of sand is described by eq.(3.19) and (3.20).

$$\tau_y > \alpha_{cr}(\rho_s - \rho_{cf})gd: \quad w_{s,eff} = 0 \tag{3.19}$$

$$w_{s,eff} = (1 - \phi_s)\left(1 - \frac{\phi_{sa}}{\phi_{sa,\max}}\right)^2 w_{s,0s} = (1 - \phi_s)\left(1 - \frac{\phi_{sa}}{\phi_{sa,\max}}\right)^2 \frac{\alpha}{18} \frac{g(\rho_s - \rho_{cl})d^2}{\mu_{apparent-cf}} \tag{3.20}$$

3.4. Measurements

The rheological models and segregation model contain different (mixture) properties and parameters which can be measured or empirically determined. These measure techniques and/ or determinations are briefly discussed.

Rheometer test and Vane test
The yield stress, viscosity and flow index can be obtained by a rheometer test and/ or vane test. The rheometer test utilises a bob-cup method or plate-cone method. The soil sample is placed between the bob and cup (or plate and cone). The gab spacing between the bob and cup must be much larger than the maximum particle size. Then the sample is sheared by rotation of the bob. Either the stress is controlled and the strain is measured or vice versa. With the measured data the flow curve can be constructed. Typically the stress increases at low shear rates. It reaches the peak strength and decreases suddenly. The sediment structure is broken. Thereafter the shear stress increases for increasing shear rates.
The intersection with the y-axis is the yield stress. For a Bingham fluid the tangent of the curve is the actual Bingham function. The intersection with the y-axis is the yield stress measured for the smallest shear rate. It is difficult to measure this value and known that it may vary. The slope of the curve is the viscosity. If the slope is a function of the shear rate, the flow index can be determined as well. Figure 3-5presents the measured flow curve of a Bingham fluid. The measurements can be affected by the measurement procedure. For example particles may segregate while the sample is sheared. For high settling velocities it is impossible to measure the viscosity of the whole mixture.
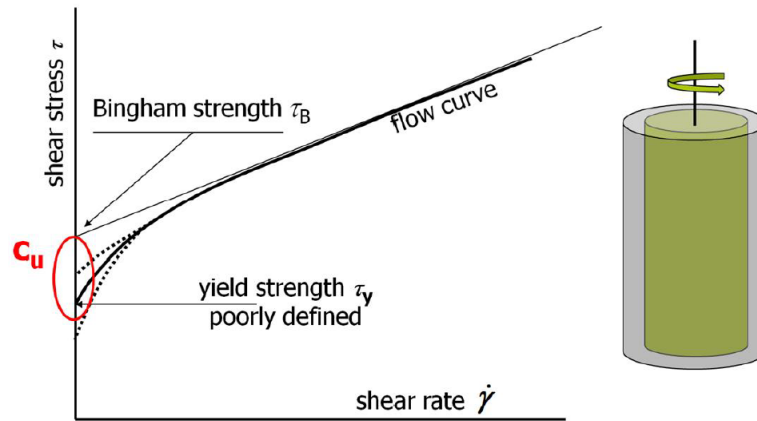
Figure 3-5 Schematization of rheometer and flow curve including approximation for Bingham model.

In a vane test the soil sample is placed in a bucket. A vane consists of four steel plates mounted in cross direction on a shaft. A system to measure the torque (when the vane is rotated) is connected to the top of the shaft. The tool is gently pushed into the sample, not disturbing the sample. By rotating the vane the sample is sheared. Again first a peak strength is measured where after the soil structure breaks down. Than the remoulded shear strength c_u can be measured. Peak strength is determined by the shear rate and there for not a clay property. The c_u is the yield stress of the clay.

It should be noted that for both tests the shear rates are low (<100 1/s) in order not to disrupt the clay properties.

The viscosity of the samples (and water) can also be obtained with a capillary viscometer. The mixture flows through a tube. The flow is forced by a prescribed pressure gradient. The resulting velocity profile provides information to determine the viscosity.

Concentration, particle size and density

The slurries are a mixture of water, clay and granular material.

In a settling column the granular material can deposit and separated from the mud fraction. The grain size distribution of the granular material can be obtained by a sieve curve analysis (after drying). The sample passes a number of sieves in a vertical row. The gap spacing reduces in downward direction. The mass weight of material on top of each sieve is measured and expressed as a percentage of the total weight. The particle seize distribution curve is often plotted on a log scale. The grains are categorized (sand, silt and clay) by size. The curve provides information on the grain size, nominal diameter and concentration by weight of the material.

It is also possible to measure the sediment concentration directly in the water column. Examples are the Optical Back Scatter sensors (OBS), Acoustic Doppler Current Profiler (ADCP) and Gamma densitometer. With the OBS method the backscatter of infra-red light is measured which is (amongst others) a function of the particle size distribution, shape and composition. The ADCP analyses the energy of the back scatter. Both methods request calibration and air bubbles might disturb the measurements. The OBS and ADCP are frequently used for (relative) dilute mixtures. The Gamma densitometer utilizes a radioactive source to measure the density. This apparatus is also used for thicker slurries, e.g. (Sanders, et al., 2002; Spelay, 2006). (Pirouz et al., 2013) uses an intrusive electrical conductivity probe to measure the density of the flowing mixture in his experiments with fairly dense mixtures. This instrument measures the conductivity of the solids

and water. In general the sediments are a poorer conductor than water. To perform these tests, the salinity of the pore water should be known and constant(Winterwerp & van Kesteren, 2004). Because the instrument is intrusive the mixture it disturbed which has a drawback. In a settling column a succeeding measurement of the same sample is aimless (L. M. Merckelbach & Kranenburg, 2004). In a flume the conductivity probe disturbs the morphology downstream of the probe (Pirouz et al., 2013).

For flocs the sieve procedure is not recommended to measure the floc seize. The floc structure will break-up due to the sieving. It is advisable to measure the floc size distribution in-situ to avoid any disturbance of the floc structure resulting in a measuring error. Commonly video techniques and laser beams are used to determine the floc size and particle distribution. In laboratories the (volume-based) floc size distribution can be measured with a laser diffraction technique. The sample is placed between a laser and a detector. The latter measures the intensity and angle of the light scattered by the particle. The light scatter is at a smaller angle and more intense for larger flocs (Zhenhua et al., 2000). In the work of (Zhenhua et al., 2000) the laser diffraction technique is used to determine the particle geometry as well. An example of a laser diffraction apparatus is the Malvern Mastersizer 2000 (Mietta et al., 2009).

The fractal dimension of a floc is a rather complex. (Winterwerp, 1998) found a relation between the settling velocity, particle diameter and fractal dimension. This theory is used by (Dyer & Manning, 1999) in combination with an INSSEV measuring system in coastal areas. The instrument is used in situ and measures optically the size, settling velocity and effective density. To determine the fractal dimension (L. M. Merckelbach & Kranenburg, 2004) made use of a consolidation experiment in settling columns. They derived a relation between the height of the interface between water and suspension, the settling time and the fractal dimension. (Alam et al., 2010) investigated the fractal dimension and floc size distribution of high concentrated coal plant tailings. Both properties where measured with a laser diffraction technique (Malvern Mastersizer 2000). An overview of the different measurement techniques – scattering, settling, image analysis – and a comparison is presented by (Bushell et al., 2002).

The density of water depends on the temperature and salinity of the water. A measure for the salinity is the conductivity. Temperature and conductivity can be measured with CTD-probes. The linear concentration is a function of the maximum sand and/ or silt concentration. This can be determined by the porosity. The porosity is a function of the present clay, silt and sand concentration.

Atterberg Limits and Water content

Two standard procedures are used to determine the Liquid Limit (LL) and Plasticity Limit (PL). Samples with different water content (W) are remoulded. To determine the LL a grove (having certain dimensions) is made in the sample. By blowing over the sample the groove can close if W is high enough i.e. at the LL. To determine the PL the sample is slightly rolled to a cylinder-shape. At PL the cylinder will fall apart. With the difference between the PL and LL and the clay fraction, the activity of the clay can be calculated (Winterwerp & van Kesteren, 2004).

Segregation

The settling velocity of particles in a flume must be measured to validate the segregation model. In situ this can be done with different techniques. An example is the settling tube. A sample is taken from the water column. Thereafter the gradients in sediment concentration or the particle size distribution can be used to determine the settling velocity. Another approach is to measure the settling velocity from succeeding optical images. The displacement of a particle within two subsequent images and the time-lapse between them determine the settling velocity. Both techniques cope with the occurrence of circulations diminishing the accuracy of the measurements (Winterwerp & van Kesteren, 2004).

In laboratory often settling columns are used to measure the settling velocity (Dankers et al., 2008; Merckelbach & Kranenburg, 2004). A prepared mixture is placed in a column with certain dimensions (e.g. height 1 m and diameter 150 mm). If the material settles, two interfaces occur. Up in the column the interface between water and the suspension. Down in the water column the interface between the suspension and the bed material. The two interfaces move towards each other. At certain time intervals both are measured. From which the settling velocity can be estimated.

To measure the settling velocity in a sheared flume (Talmon & Mastbergen, 2004; Talmon & Huisman, 2005) made use of a carrousel with on top a rotating rigid lid. The device is able to generate a Couette flow. The (glass) particle concentration was measured with an acoustic density meter. (Talmon et al., 2014) made use of shear cell tests to study the shear induced hindered settling velocity of mixtures. The mechanical operation of the shear cell is related to the bob-cup method, i.e. a static outer cylinder (diameter 100mm) and rotating inner cylinder. Conductivity sensors were mounted on the outer cylinder at different heights. The sensors measure the sand concentrations with certain time intervals. With the change in concentration over time and height the settling velocity can be quantified.

3.5. Conclusions

Three different rheological formulas and a segregation model are presented.

The rheological models originate from different fields of expertise. Model 1 is a power law model, Models 2 and 3 are Bingham models.
- All three models are a function of the concentration of the present solids. Additionally Model 1 and 2 include properties of the clay and the sand, e.g. fractal dimension, clay activity, material density and maximum solids concentration.
- The models describe the yield stress and viscosity of the carrier fluid. The effects of added granular material are expressed as an addition to the formulas of all three models. Thereafter for Model 1 and 2 the reduction of the mud matrix by the addition of sand is taken into account.
- The experimental data of (A. D. Thomas, 1999) are used to validate and calibrate the models. All three models are able to predict the behaviour of the yield stress and viscosity. Larger errors occur if the Sand To Solids and/ or volume concentrations are increased.

- From the sensitivity analysis we may concluded that in all cases, parameters have to be determined by experiments for yielding fair models results.
- The inclusion of physical properties has the advantage that an (initial) formula structure remains the same if it is used for a different mixture or if other physical processes are added (as seen in the shear induced hindered settling formula). An empirical formula depends on the experimental results and method to derive the parameters possibly leading to inaccurate results (Skvortsov & Sarychev, 2002). The formula structure might change if it is fit to results of a new experiment. Simultaneously an empirical formula gives less insight into the physical properties compared to an analytical formula (Lourenco & Pina-Henriques, 2006). There Model 1 and 2 account for a different fluid; the type of mixture determines which one of the two is preferred.

In the second part of this chapter a segregation model is presented. It takes into account the shear induced hindered settling of granular material.
- The shear induced settling of a single particle in a non-Newtonian fluid is defined by the equation of (A. Talmon & Mastbergen, 2004). The formula is proven by experiments.
- The hindrance due to the surrounding particles is commonly based on the empirical equation of (Richardson & Zaki, 1954). Within this thesis a physical based formula is presented. The theory is derived from Newtonian flows containing high mud concentrations and experimentally proven. Although for non-Newtonian fluids more research and data is required to validate this new shear induced hindered settling formula.

4. Numerical model

The second part of this thesis integrates the rheological properties and coarse particle segregation in a numerical model. In the work of (Sittoni et al., 2015) the first attempts are made to merge the rheological properties and coarse particle settling into Delft3D-Flow (Delft3D-Slib) towards the development of a Delft3D module specially designed to handle diluted and thick sand mud mixtures, or slurries and mine tailings. This work showed non-Newtonian behaviour (e.g. plug flow) of sand mud mixtures and sand settling in agreement with qualitative expectation. Yet thorough validation of the rheological model and sand settling models against theoretical and field measurements was necessary. This thesis begins with this objective in mind.

For controlled and thorough implementation and validation, the three rheological models and segregation model (discussed in Chapter 3) are implemented in a 1DV model, directed towards the evolvement of the special module for slurries: Delft3D-Slurry. The 1DV model is analogous to the processes in the vertical direction of Delft3D-flow. The objective to apply a 1DV model is to understand and test the numerical application of the formulas before they are implemented in (a more complicated) Delft3D. This is also the reason why Delft3D-Slurry is not directly exanimated in a 3D environment.

A summary of the characteristics of Delft3D and research objectives are presented in Section 4.1. The specifications of the 1DV application (equations and numerical scheme) are explained in Section 4.2. Section 4.3 presents the implementation of the theory developed in Chapter 3 in the 1DV model. This chapter ends with the conclusions in Section 4.4.

4.1. Delft3D-Slurry

Delft3D is an open source integrated modelling suite developed and maintained by Deltares. It has the capability to compute and visualize flow, sediment transport, morphological changes, water quality and ecology in two and three dimensions. Delft3D is open source software and used in numerous consultancy and research projects worldwide (https://www.deltares.nl/en/software/delft3d-4-suite/). Delft3D covers different sub suites or applications. Delft3D-Slurry is one of these. Figure 4-1 gives an overview of the structure of the development of Delft3D-Slurry.

DEVELOPMENT DELFT3D-SLURRY

Figure 4-1 Development of Delft3D-Slurry.

Clarification of Figure 4-1
- Delft3D-Flow: The open source main stream 'hydrodynamic engine' of Delft3D.
- Delft3D-Slib: New functionalities - described in (Winterwerp et al., 2007) - are incorporated in a special version of Delft3D-Flow to make it suitable for high concentrated (Newtonian) laminar and turbulent mudflows.
- Delft3D-Slurry: Rheology and shear induced hindered settling are integrated in Delft3D-Slurry.
- 1DV-Slib: The model includes the functionalities of Delft3D-Slib in 1DV.
- 1DV Slib to Slurry: This is the model used and improved in this thesis. The theory of three rheological models and segregation and the research questions of Delft3D-Slurry are included in 1DV-Slib.
- In time the tested rheology functions and segregation functions of the 1DV model will be incorporated in Delft3D-Slurry, thereafter in Delft3D-Flow with ''Slurry'' being a featured functionality.

The functionalities of these models are explained in the following.

Delft3D-Flow

Delft3D-Flow computes the hydrodynamics of shallow water flows, i.e. the horizontal scale is considerable larger than the vertical scale. Examples of these flows are: tidal flows, coastal flows, river flows, debris flows etc.
The fluid motion is described by the:
- Continuity equation
- Momentum equations (three dimensional)

The velocity components of the momentum equations consist of a mean velocity and a fluctuating part. The fluctuating part at the smallest scales of motion cannot be solved in a numerical model.

46

Therefore the velocity is decomposed by Reynolds decomposition and time averaged. The result is the 3D Reynolds Averaged Navier Stokes (RANS) equations.

The flows are considered as shallow water, the following assumptions are made for which the RANS equation are depth integrated (Deltares, 2014):

- Incompressibility; the particles are incompressible and the density does not depend on the pressure.
- Hydrostatic pressure assumption; the vertical velocity accelerations are insignificant compared to the horizontal variations and can be neglected. The vertical momentum balance reduces to a hydrostatic balance i.e. the pressure variation over depth is equal to the product of the gravity and the density. (This assumption only applies for the hydrostatic version of Delft3D).
- Velocity distribution: the horizontal velocity is uniformly distributed over depth.
- Boussinesq approximation; horizontal gradients in the density are negligible compared to the density and therefore neglected in the horizontal equations of motion. However the gradients are present in the Baroclinic pressure term.

The resulting 3D Shallow Water Equations (SWE) eqs. (4.1) - (4.6) are solved within each layer of the model.

- Momentum equations: u, v and w are the Reynolds averaged velocities in the x-, y-, and z- direction respectively. f is the Coriolis parameter. p, v_h, v_t are the pressure and horizontal and vertical eddy viscosity coefficients. g is the gravitational acceleration and ρ and ρ_0 are the density and average density of the fluid.

$$\frac{\partial u}{\partial t} + u\frac{\partial u}{\partial x} + v\frac{\partial u}{\partial y} + w\frac{\partial u}{\partial z} - fv + \frac{1}{\rho_0}\frac{\partial p}{\partial x} - 2v_H\frac{\partial^2 u}{\partial x^2} - \frac{\partial}{\partial z}\left(v_t\frac{\partial u}{\partial z}\right) = 0 \qquad (4.1)$$

$$\frac{\partial v}{\partial t} + u\frac{\partial v}{\partial x} + v\frac{\partial v}{\partial y} + w\frac{\partial v}{\partial z} + fu + \frac{1}{\rho_0}\frac{\partial p}{\partial y} - 2v_H\frac{\partial^2 v}{\partial y^2} - \frac{\partial}{\partial z}\left(v_t\frac{\partial v}{\partial z}\right) = 0 \qquad (4.2)$$

$$\frac{\partial p}{\partial z} = -\rho g \qquad (4.3)$$

- Depth-averaged continuity equation: H is the total water depth, d is the average depth and ζ is the fluctuation from the mean water level, $\bar{u}$ is the mean flow velocity determined by eq. (4.5) (an equal approach holds for $\bar{v}$).

$$H = d + \zeta \qquad (4.4)$$

$$\bar{u} = \frac{1}{H}\int_{-d}^{\zeta} u(z,t)dz \qquad (4.5)$$

$$\frac{\partial\zeta}{\partial t} + \frac{\partial\bar{u}H}{\partial x} + \frac{\partial\bar{v}H}{\partial y} = 0 \qquad (4.6)$$

The unknown velocity components, pressure and density can be solved with these equations. The water-mud-sand mixtures are modelled as a single phase fluid containing coarse material. The momentum and continuity equations are solved for the total mixture.

Besides the momentum and continuity equations, the model includes transport equations of dissolved matter (e.g. sand), salinity and temperature.

For the Reynolds stresses (a consequence of Reynolds averaging) the Boussinesq hypothesis is used. The stresses are expressed as a function of the viscosity and the velocity gradient. The

viscosity is determined by a turbulence closure model. In Delft3D the k-ε model is used to solve the Reynolds stresses. Therefore two additional transport equations for Turbulent Kinetic Energy k and Turbulent dissipation ε are defined.

Delft3D-Slib

Delft3D-Slib was developed to model high concentrated mud flows. It uses the model equations of Delft3D-Flow and is extended with new formulations described in (J. C. Winterwerp et al., 2007). The incorporated physical processes are:

- The effect of the suspended material on the turbulent motion.
- The inclusion of low-Re-damping function for turbulent fluids with a low Re permitting a smooth transition from turbulent to laminar flow.
- The bed roughness (hydraulic smooth beds, hydraulic rough beds or the transition between both) can be defined by the user.
- A flocculation model for the clay fraction and a hindered settling formula.
- Two formulations to account for the consolidation and erosion of the bed.

These processes occur at a small scale and/ or close to the bed and they request a very small grid spacing. Therefore a new grid feature is implemented, General σ-grid transformation. The grid spacing is a function of the concentration.

4.1.1. Delft3D-Slurry: Rheology and Sand Settling

Delft3D-Slib applies to high concentrated Newtonian flows. Delft3D-Slurry is developed to model high concentrated non-Newtonian flows. Delft3D-Slurry includes the physical processes of Delft3D-Slib and is extended with functions for rheology (as a function of sand and mud) and shear induced hindered settling.

Rheology

In Delft3D-Slurry a Bingham model is used to describe the rheological behaviour of the fluid. The viscosity of the mixture and the carrier fluid are calculated separately. The fractal dimension theory is used in Delft3D for the high concentrated (turbulent) mud flows. Therefore it was a first logical choice to use this formulation again for the rheological properties of a non-Newtonian flow (Sittoni et al., 2015). The model computes the rheology of the carrier fluid and the mixture separately. A detailed description can be found in (Sittoni et al., 2015) (R. Uittenbogaard internal communication.

Segregation

In Delft3D-Slurry it is assumed that exclusively sand particles settle according to the shear induced settling formula formulated by (Sisson et al., 2012a; Arno M. Talmon & Huisman, 2005). The apparent viscosity of the carrier fluid is substituted in the settling formula for a single grain.

4.1.2. Research objectives of Delft3D-Slurry

The work of (Sittoni et al., 2015) and an internal memo of R. Uittenboogaard is analysed. The following objectives require further research:

- To describe the rheology a Bingham model is used combined with the fractal dimension theory. As discussed in Chapter 2 the fractal dimension theory requires a power law model.
- The formulation incorporating the fractal dimension theory is not in line with the fractal dimension theory as presented in Chapter 2.
- An initial yield stress and plastic viscosity are input parameters. It is more beneficial if the model is capable to calculate both.
- The used equation to calculate the apparent viscosity results in a deviation of the actual apparent viscosity if the shear rate is sufficiently small.
- The applied shear induced hindered settling formula is analogous to the concept of Richardson&Zaki. In this approach the viscosity is accounted for implicit. The segregation model deviates from the segregation model as presented in Chapter 3.

The model requests customizations to agree with the theory presented in Chapter 2 and 3. These 'Lessons Learned' of the Delft3D-Slurry are used for the extensions of the 1DV model. The extensions concern: implementation of rheological formulas, inclusion of the shear induced hindered settling formula and general adaptions. This more indepth discussed in Section 4.3. First the model specifications of the 1DV model are described in Section 4.2.

4.2. 1DV Model specifications

Before implementing and adjusting the rheology and segregation in Delft3D-Slurry, adjustments to formulations and testing were done in a 1DV model. The 1DV model is similar to a vertical implementation of the processes of Delft3D-Slib (Delft3D-Flow) written in the programming language FORTRAN.

The code is developed by Deltares by R. Uittenbogaard. The code included an equation to calculate the viscosity of a mud flow. This differed from the three rheological models (discussed in Chapter 3) and is adjusted. Segregation was already programmed in the 1DV model; it contained an equation for hindered settling of sand, silt and flocs in water. This part requires an extension for the non-Newtonian fluids.

4.2.1. Governing Equations

The set of 3D SWE is reduced for the 1DV model. Only the (changes in) processes in the vertical direction (*z-direction)* are considered. The horizontal direction (*x-* and *y-*direction) are neglected by the following three assumptions:

$$u(x, y, z, t) \rightarrow u(z, t)$$
$$v \equiv 0$$
$$\frac{\partial}{\partial x} \equiv 0; \frac{\partial}{\partial y} \equiv 0$$

The reduced set of equations is presented below eq. (4.7) -(4.12).
Equations of motion: v and v_t are the viscosity of the fluid and turbulent viscosity (which is zero) respectively.

$$\frac{\partial u}{\partial t} + \frac{1}{\rho_0}\frac{\partial p}{\partial x} - \frac{\partial}{\partial z}\left[(v+v_t)\frac{\partial u}{\partial z}\right] = 0 \tag{4.7}$$

$$\frac{\partial p}{dz} = \rho g \tag{4.8}$$

The hydrostatic term p is a function of the atmospheric pressure p_{atm} and the weight of the water column.

$$p(z) = p_{atm} + g\rho_0\int_z^\zeta \rho_0 dz \tag{4.9}$$

Differentiating eq. (4.9) with respect to x and substituting it in eq. (4.7) results in eq. (4.10) for which $\Delta\rho$ is the difference between the actual density and average density:

$$\frac{\partial u}{\partial t} = \frac{\partial}{\partial z}\left[(v+v_t)\frac{\partial u}{\partial z}\right] - \frac{\Delta\rho}{\rho_0}g\left(\frac{\partial\zeta}{\partial x}\right) \tag{4.10}$$

The depth averaged continuity equation reads:

$$\frac{\partial\zeta}{dt} + \frac{\partial\overline{u}H}{\partial x} = 0 \tag{4.11}$$

This study focuses on laminar flow. To ensure the model does not account for any diffusion (except from molecular diffusion) the $k-\varepsilon$ model is turned off.
In this project it is assumed that there is no variation in temperature or salinity.
The sediment transport equation includes the settling velocity w_s which is a function of the sediment concentration. Furthermore the concentration c - where the subscript l defines each solid fraction - the molecular diffusion of the sediment D_s, and turbulent diffusion Γ_t (which is zero) are included. The equation reads:

$$\frac{\partial c_l}{\partial t} + \frac{\partial}{\partial z}\left[w_s(c_l)c_l\right] - \frac{\partial}{\partial z}\left[(D_s + \Gamma_T)\frac{\partial c_l}{\partial z}\right] = 0 \tag{4.12}$$

Forcing of the flow

The 1DV model includes two different flow situations. One option is a flow on a horizontal bed with an imposed mean velocity and flow depth. Both are preserved and therefore the specific discharge, is prescribed. The driving force is the depth averaged pressure gradient, found by rewriting eq. (4.7).

$$\frac{\partial p}{\partial x} = \frac{1}{H}\int_z^\zeta\left\{\frac{\partial}{\partial z}\left[(v+v_t)\frac{\partial u}{\partial z}\right] - \rho_0\frac{\partial u}{\partial t}\right\}dz \tag{4.13}$$

The user defines a mean velocity u_0. Due to physical processes there are variations in the velocity profile. To obtain the prescribed mean velocity the pressure gradient is corrected by eq. (4.14). Therefore the velocity time derivative is used as a relaxation. $\tau_{surface}$ and τ_{wall} are the shear stress at the surface and bottom respectively. $\overline{u}$ and u_0 are the average velocity calculated by the model and user-defined average velocity respectively. T_{relax} is the relaxation time. Figure 4-2 (right) visualizes this configuration.

$$\frac{\partial p}{\partial x} = \frac{\tau_{surface} - \tau_{wall}}{H} + \rho_0\frac{\overline{u} - u_0}{T_{relax}} \tag{4.14}$$

The second case is a flow along a predefined slope with an imposed specific discharge, q_0. The flow depth and mean velocity depend on the specific discharge, slope and rheology of the fluid. For this situation the driving force is the gravitational acceleration g and the slope θ.

$$\frac{\partial p}{dx} = g \sin(\theta) \tag{4.15}$$

The user defines an initial flow depth, h_0. The average velocity is calculated with the specific discharge and initial depth:

$$\bar{u}_0 = \frac{q_0}{h_0} \tag{4.16}$$

Due to different processes the velocity profile changes. Therefore a variation in the average flow velocity leads to a variation in the specific discharge at $t=n$.

$$q^n = h^n \bar{u}^n \tag{4.17}$$

This variation is corrected by correcting the flow depth for the new time step $t=n+1$.

$$h^{n+1} = \frac{q_0}{q^n} h^n \tag{4.18}$$

Figure 4-2 (left) presents the slope configuration. In the Input file the user selects one of the two options.
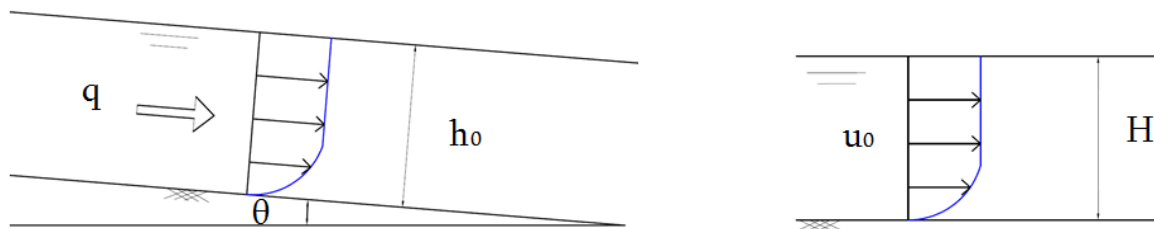
Figure 4-2 Schematization of slope configuration. Left: flow along a slope. Right: Flow above horizontal bed.

4.2.2. Grid

The computational domain of the model is divided in a number of layers in the vertical direction denoted by k. At each layer the unknown scalar quantities are defined. The 1DV model (as well as Delft3D) uses a staggered grid. The velocity and concentration are defined in the cell centre (position k) whereas the settling velocity, viscosity, turbulence and fluxes are defined at the cell interface (position k±1/2). Figure 4-3 visualizes the position of the variables on the vertical grid. The amount of layers and thickness of each layer is defined by the user at input.

The first layer beneath the surface is called k=1, the last layer above the bed is called k=kmax. The length of the computational loop of the centre values is k:1-kmax. The length of the computational loop of the interface values is k:0-kmax. To conserve continuity; the flux through the 'floor' of cell k-1 is equal to the transport through the 'roof' of k.
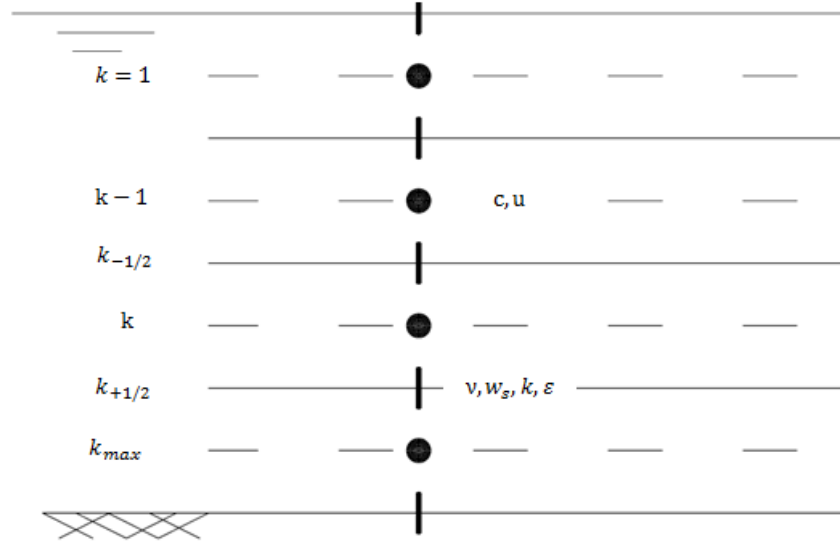
Figure 4-3 Staggered grid of the 1DV model

The grid spacing is a fraction of the total water depth. To convert the grid size of a z-layer distribution to a sigma layer distribution eq. (4.19) is used. The layers can be equidistant distributed over depth, i.e. the fractions of all grid cell are equal. Or an exponential function can be used. Than the fraction of the grid size increases exponentially towards the surface.

$$\frac{\partial}{\partial z} = \frac{1}{H}\frac{\partial}{\partial \sigma} \tag{4.19}$$

4.2.3. Numerical scheme

The equations (4.10) - (4.12) are discretized in time and space. The equations are integrated in time with an implicit numerical scheme, named Euler Backward. Eq. (4.20) is the general Euler Backward equation where y is the quantity to solve, t is the time, a is a constant, and superscripts n and $n+1$ are the old and new time step respectively.

$$\frac{\partial y}{\partial t} = f(t, y)$$
$$y^{n+1} - y^n = af(t^{n+1}, y^{n+1}) \tag{4.20}$$

The space discretisation is obtained with the central difference method eq. (4.21).

$$\frac{\partial T}{\partial z}(k\Delta z, t) \approx \frac{T_{k+1}(t) - T_k(t)}{\Delta z} \tag{4.21}$$

The set of equations of the model converges to the Steady-State solution, i.e. a time independent solution, which is non-trivial. For a certain cell k eq. (4.12) can be discretised into eq. (4.22).

$$\frac{\partial u_k}{\partial t} = \frac{1}{H^2}\frac{\partial}{\partial \sigma}\left(v\frac{\partial u_k}{\partial \sigma}\right) - \frac{\Delta \rho}{\rho_{slurry}}g\left(\frac{\partial \zeta}{\partial x}\right) \tag{4.22}$$

The discretization of the first term on the right hand side of eq. (4.22) on a staggered grid reads:

$$\frac{1}{H^2}\frac{\partial}{\partial\sigma}\left(\nu\frac{\partial u_k}{\partial\sigma}\right) = \frac{1}{\Delta\sigma_k H^2}\left[\left(\nu\frac{\partial u_k}{\partial\sigma}\right)_{k-\frac{1}{2}} - \left(\nu\frac{\partial u_k}{\partial\sigma}\right)_{k+\frac{1}{2}}\right]$$

$$\frac{2}{H^2\Delta\sigma_k}\left[\nu_{k-\frac{1}{2}}\frac{u_{k-1}-u_k}{\left[\Delta\sigma_k+\Delta\sigma_{k-1}\right]} - \nu_{k+\frac{1}{2}}\frac{u_k-u_{k+1}}{\left[\Delta\sigma_k+\Delta\sigma_{k+1}\right]}\right]$$

$$= \frac{2\nu_{k-\frac{1}{2}}}{H^2\Delta\sigma_k\left(\Delta\sigma_k+\Delta\sigma_{k-1_-}\right)}u_{k-1} \qquad (4.23)$$

$$- \left[\frac{2\nu_{k-\frac{1}{2}}}{H^2\Delta\sigma_k\left(\Delta\sigma_k+\Delta\sigma_{k-1}\right)} + \frac{2\nu_{k+\frac{1}{2}}}{H^2\Delta\sigma_k\left(\Delta\sigma_k+\Delta\sigma_{k+1}\right)}\right]u_k$$

$$+ \frac{2\nu_{k-\frac{1}{2}}}{H^2\Delta\sigma_k\left(\Delta\sigma_k+\Delta\sigma_{k+1}\right)}u_{k+1}$$

The discretization of the second and third term of eq. (4.12) read:

$$\frac{1}{H}\frac{\partial}{\partial\sigma}\left(w_sc\right) = \frac{1}{\Delta\sigma_k H}\left[\left(w_sc\right)_{k-\frac{1}{2}} - \left(w_sc\right)_{k+\frac{1}{2}}\right]$$

$$= \frac{1}{H\Delta\sigma_k}\left[w_{sk-\frac{1}{2}}\left(c_{k-1}-c_k\right) - w_{sk+\frac{1}{2}}\left(c_k-c_{k+1}\right)\right]$$

$$= \frac{w_{sk-\frac{1}{2}}}{H\Delta\sigma_k}c_{k-1} \qquad (4.24)$$

$$- \left[\frac{2w_{sk-\frac{1}{2}}}{H\Delta\sigma_k\left(\Delta\sigma_k+\Delta\sigma_{k-1}\right)}\right]c_k$$

$$+ \frac{w_{sk-\frac{1}{2}}}{H\Delta\sigma_k}c_{k+1}$$

$$\frac{1}{H^2}\frac{\partial}{\partial\sigma}\left((D_s+\Gamma_T)\frac{\partial c_k}{\partial\sigma}\right) = \frac{1}{\Delta\sigma_k H^2}\left[\left((D_s+\Gamma_T)\frac{\partial c_k}{\partial\sigma}\right)_{k-\frac{1}{2}} - \left((D_s+\Gamma_T)\frac{\partial c_k}{\partial\sigma}\right)_{k+\frac{1}{2}}\right]$$

$$\frac{2}{H^2\Delta\sigma_k}\left[(D_s+\Gamma_T)_{k-\frac{1}{2}}\frac{c_{k-1}-c_k}{\left[\Delta\sigma_k+\Delta\sigma_{k-1}\right]} - (D_s+\Gamma_T)_{k+\frac{1}{2}}\frac{c_k-c_{k+1}}{\left[\Delta\sigma_k+\Delta\sigma_{k+1}\right]}\right]$$

$$= \frac{2(D_s+\Gamma_T)_{k-\frac{1}{2}}}{H^2\Delta\sigma_k\left(\Delta\sigma_k+\Delta\sigma_{k-1_-}\right)}c_{k-1} \qquad (4.25)$$

$$- \left[\frac{2(D_s+\Gamma_T)_{k-\frac{1}{2}}}{H^2\Delta\sigma_k\left(\Delta\sigma_k+\Delta\sigma_{k-1}\right)} + \frac{2(D_s+\Gamma_T)_{k+\frac{1}{2}}}{H^2\Delta\sigma_k\left(\Delta\sigma_k+\Delta\sigma_{k+1}\right)}\right]c_k$$

$$+ \frac{2(D_s+\Gamma_T)_{k-\frac{1}{2}}}{H^2\Delta\sigma_k\left(\Delta\sigma_k+\Delta\sigma_{k+1}\right)}c_{k+1}$$

53

To be able to solve the equations, they can be rewritten in matrix-vector notation. The matrix is a Tridiagonal matrix; only the main diagonal and adjoining diagonals contain non-zero values. By using a double sweep method the matrix values on the diagonal are set to 1 and the system of linear equations can be solved. The solutions are the velocities, pressure, density, water level and concentrations at the new time step.

Numerical schemes (e.g. central differences) may produce spurious oscillations (wiggles). To dampen these wiggles a first order numerical Upwind scheme is used to calculate the new concentrations as a result of the settling of particles. The amount of sediment in the next grid cell determines the amount of settling sediment from the previous cell. In this manner the concentration cannot exceed the maximum concentration in a computational cell.

4.2.4. Calculation sequence

The code consists of several subroutines, i.e. a book with different chapters. Every subroutine contains relations for the computation of a certain physical process (e.g. velocity components, viscosity). One subroutine, the main file, prescribes the order of the calculation procedure. The sequence in which the variables are solved starts with an initialization of the parameters, hereafter a time loop computation pursues. The initialization is stored in an output file. The time loop computations are stored after a (user defined) time interval. The fainted processes are included in the model but not used in the 1DV computation. Explanation is given in Section 4.3.

1. Initialization of:
   - Input parameters are read from the input file
   - Water density depending on initial density, salinity and temperature distribution.
   - Stability parameters for the turbulence closure.
   - Bed roughness height.
   - Wind friction velocity components.
2. Time loop computations:
   - Mean water depth and mean flow velocity update
   - Bottom roughness height
   - Forcing by the tide, waves and wind
   - Friction component of the wind
   - Turbulence terms
   - Momentum equation in u direction
   - Water level update (if the flow is along a slope)
   - Bed friction
   - Transport equations for turbulent kinetic energy and turbulent dissipation
   - Role and surface waves
   - Apparent viscosity
   - Transport constituants: salt, diffusion and sediment concentration
   - Water density depending on salt, temperature and concentration

4.3. Model Extensions

To enable the model to compute the physical features of laminar non-Newtonian flow including segregation, extensions were made upon the general model settings, rheology and segregation.

4.3.1. General adaptions

No-slip condition and bed roughness

For laminar flow the velocity at the bed is zero. Secondly the bed is supposed to be hydraulic smooth. In the model a 'No-slip' condition is implemented, i.e. the boundary conditions at the bed are changed. The velocity is defined in the cell centre of the last grid cell. There it is not zero. Therefore a 'fictive' grid cell (*kmax+1*) is used with condition(4.26).

$$u_{k\max+1} = -u_{k\max} \tag{4.26}$$

With eq. (4.26) the interpolated value at the cell interface between *kmax* and *kmax+1* is zero.

The discretised viscosity term at the bottom reads now:

$$
\begin{aligned}
\frac{\partial}{\partial z}\left(\nu \frac{\partial u_k}{\partial z}\right)\Big|_{k\max} &= \frac{1}{\Delta \sigma_k H^2}\left[\left(\nu \frac{\partial u_k}{\partial \sigma}\right)_{k\max-\frac{1}{2}} - \left(\nu \frac{\partial u_k}{\partial \sigma}\right)_{k\max+\frac{1}{2}}\right] \\
&= \frac{2}{H^2 \Delta \sigma_{k\max}}\left[\nu_{k\max-\frac{1}{2}}\frac{u_{k\max-1}-u_{k\max}}{\left[\Delta\sigma_{k\max}+\Delta\sigma_{k\max-1}\right]} - \nu_{k+\frac{1}{2}}\frac{2u_{k\max}}{\left[\Delta\sigma_{k\max}\right]}\right] \\
&= \frac{2\nu_{k\max-\frac{1}{2}}}{H^2 \Delta\sigma_{k\max}\left(\Delta\sigma_{k\max}+\Delta\sigma_{k\max-1\_}\right)}u_{k\max-1} \\
&\quad -\left[\frac{2\nu_{k\max-\frac{1}{2}}}{H^2\Delta\sigma_{k\max}\left(\Delta\sigma_{k\max}+\Delta\sigma_{k\max-1}\right)} + \frac{2\nu_{k\max+\frac{1}{2}}}{H^2\Delta\sigma_{k\max}\left(\Delta\sigma_{k\max}\right)}\right]u_{k\max}
\end{aligned}
\tag{4.27}
$$

Separation of carrier fluid and mixture

The model was not able to distinguish between the mixture, carrier fluid and type of carrier fluid. In the Input file an option is introduced to define the fractions of the carrier fluid; i.e. water, water-clay or water-clay-silt.

The calculation of the average density of the mixture in a grid cell is reformulated. Adjacent to it the computation of the average density of the carrier fluid is added. The computation is performed in a loop, the densities are calculated in each grid cell.

Initially only the viscosity of the mixture was calculated in the 1DV model. A new subroutine is coded to compute the viscosity of the carrier fluid. The content is discussed in Subsection 4.3.2.

Computation sequence

Three mutations are made in the computation sequence.

- In the initialization phase the viscosity of the mixture is computed based on the initial concentration and shear rate.
- In the time loop the viscosity of the mixture was calculated before the segregation of the material. An incorrect assumption because this computed viscosity is substituted in the momentum equation of time step *t+1* without taken into account the new viscosity due to segregation in time step *t*.
  In the modified sequence the viscosity of the carrier fluid is calculated and hereafter used in the fall velocity calculation of the granular material. Then the concentration and density of this new state are computed. The new viscosity of the mixture is established on this value and used in the momentum equation of the next time step.

The sequence of the adjusted model is presented in Figure 4-4.
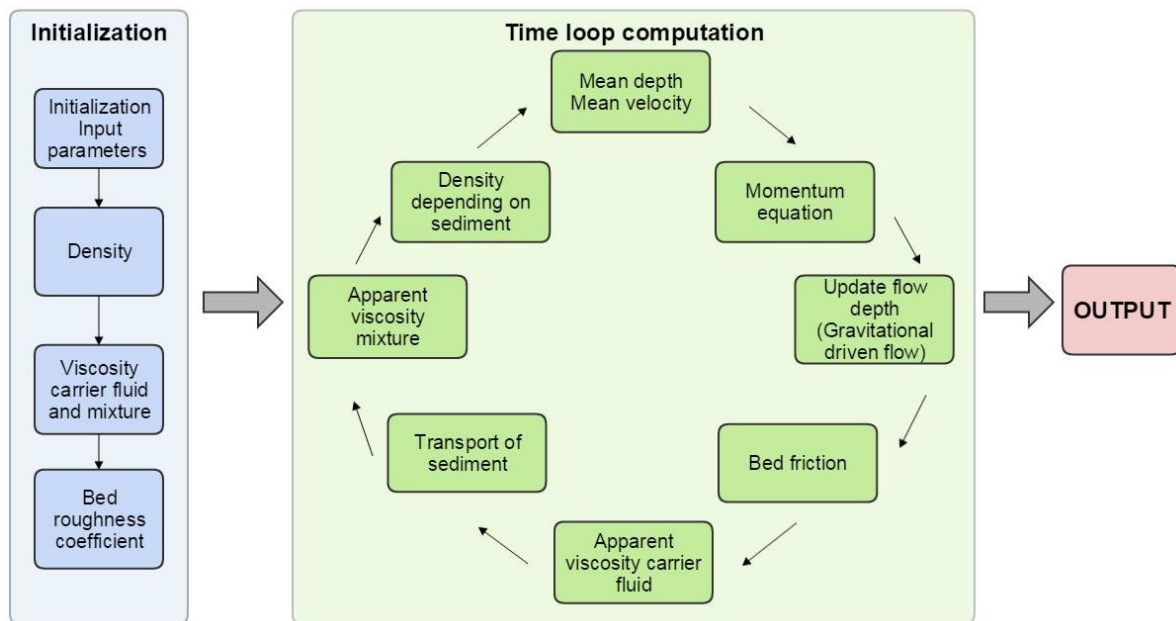
Figure 4-4 Computation sequence of 1DV Model

Storage and Output

Every subroutine contains two different types of parameters; parameters that are only used within the subroutine and parameters used as input in other subroutines or Output file. The latter must be initialized in the Initialization file. Furthermore the code requires the instruction where to store the data through an Inclusion file.

4.3.2. Rheology

Rheological models

The three rheological models, presented in the Literature survey, are programmed in the 1DV model. As mentioned in 4.3.1 the viscosity of the mixture and the carrier fluid is coded in two different subroutines. The coded equations for the carrier fluid and the mixture of all three models are presented in Appendix B. The code is included in Appendix C.

Both subroutines calculate the yield stress, dynamic viscosity, apparent viscosity and kinematic viscosity depending on the input parameters and (input) concentrations. The yield stress is defined at every interface in a loop-calculation. Both viscosities are computed in one loop at the cell interface. Every sediment type (clay, silt or sand) is separately defined. It is optional to define different fractions for a certain sediment fraction.

The rheology of the carrier fluid depends on the fractions within the carrier fluid. The subroutine derives this information from the Input file. It includes two different calculations for the choices water-clay and water-clay-silt.

The concentrations and densities are defined in the cell centre, whereas the viscosity is defined on the cell interface. The concentrations and densities are interpolated to the cell interface to calculate the yield stress and viscosity on the interface.

Modification of the yield stress

The formula of the yield stress is adapted to enable the model to calculate a shear stress (and related apparent viscosity) in the plug of the flow (presented in Chapter 3).

Apparent viscosity

The apparent viscosity is the ratio between the shear stress and shear rate and varies over depth. The shear is the ratio of the velocity difference and distance between two cell centres. The absolute value is implemented to prevent negative viscosities. To prevent a division by zero shear rate an 'IF-statement' is introduced. If the shear rate equals zero, the apparent viscosity has a predefined value. The apparent viscosity increases for shear rates smaller than one. Therefore a high value (order of 10E4) is chosen for the apparent viscosity at zero shear rate. The apparent viscosity is divided by the density to obtain kinematic viscosity which is variable throughout the computational domain and it is used in the momentum equation.

Linear concentration

In Model 1 & 2 the internal friction of the granular material is described by the linear concentration theory. The linear concentration is a function of the present concentration and maximum concentration of granular material. In the model three adaptions are made compared to the theoretical formulas.

First the fractions governing the internal friction depend on the fractions belonging to the carrier fluid. Table 4-1 is an overview of the two possible carrier fluids and which fraction is part of the granular material.

Table 4-1 Division between carrier fluid and granular material.

Carrier fluid	Granular material or linear concentration
Water-clay	Silt and sand
Water-clay-silt	Sand

The second mutation concerns the maximum concentration itself. The maximum concentration is derived from the porosity of the material (sand or sand and silt) (J C Winterwerp & van Kesteren, 2004) as presented in Chapter 2. In the code the maximum sand (and silt) concentration is an input parameter independent on the present sand and silt concentrations. It is a simplification of the model.

Lastly an 'IF-statement' is included to prevent a division by zero due to the present sand and silt fraction. The linear concentration approaches zero for decreasing values of the total sand/ silt concentrations. If there is no granular material present the value is set to 10E-99.

4.3.3. Segregation

The model contains an equation for settling of sand, silt and flocs in water. The subroutine was extended with the formula for segregation presented in the literature study (Chapter 2).

The settling of the particles occurs within the carrier fluid, which has an imposed zero settling velocity. The settling of clay particles in insignificant compared to the settlement of the granular material in the considered time free. The selected type of carrier fluid determines the carrier fluid

properties to be taken into account in the equation and the settling fraction(s). Table 4-2 gives an overview.

Table 4-2 Division between carrier fluid and settling fraction.

Carrier fluid properties	Settling fraction
Water-clay	Silt and sand
Water-clay-silt	Sand

For the two different circumstances, different calculations are made. With an 'IF-statement' the code derives the state of the carrier fluid from the Input file.

First the subroutine calculates the settling of a single grain in the viscous fluid. The density and diameter of settling material is obtained from the Input file. The density of the carrier fluid is calculated in a separate subroutine. The fall velocity of particles is defined at the cell interface. Therefore the average densities of the carrier fluid are interpolated on the cell interface. The kinematic viscosity of the carrier fluid is computed in its subroutine. Therefore the parameter must be multiplied with the density to obtain the apparent viscosity.

Upwind scheme
The hindered settling formulas utilize an Upwind approach; i.e. the concentration of the succeeding grid cell dictates the amount of material that is able to segregate. In addition a limit is defined to prevent that material will 'fall upwards'. The amount of settling concentration is:

$$\max\left[0.0; \left(1 - \frac{\varphi_{sasi}}{\varphi_{sasi,\max}} \right) \right] \qquad (4.28)$$

As explained in Chapter 2 the maximum granular concentration depends on the porosity of the present fractions. In this model it is an user defined input parameter.

The coded equation for the three models is presented in Appendix D. The code is included in Appendix E.

4.4. Conclusions

The knowledge gaps on the numerical modelling of laminar non-Newtonian flows and the demand to advanced modelling from the industry formed the incentive to merge the rheological properties of the non-Newtonian flows and the hydrodynamics of Delft3D-flow in a new 2DV application called Delft3D-Slurry (Sittoni et al., 2015).

The incorporation of the rheology and segregation was limited to fluid mud applications already available in Delft3D, which deviate from the theory as presented in Chapter 2 and 3. Therefore the first attempts are made to extend Delft3D with typical formulations for thick mixtures.

The alterations are performed in a 1DV model analogous to Delft3D-flow. The objective is to understand the numerical application of the formulas in a 1DV model before they are implemented and used in a (more complicated) 2D and 3D environment.

The model utilizes the Euler Backward computation scheme and a double sweep method is used to solve the scheme. The calculation of the fall velocity is solved with an Upwind scheme.

The extensions concern:
- General adaptions: The initial conditions, boundary conditions and computation sequence are modified. Additionally the option is introduced to divide the different fractions into carrier fluid or mixture.
- Rheology: two new subroutines are established to calculate the viscosities of the carrier fluid and mixture separately. The three theoretical rheological models as presented Chapter 3 are coded.
- Segregation: Supplementary to segregation in water, the shear induced hindered settling formula (Chapter 3) for granular material in a non-Newtonian fluid is programmed.

The computation of the yield stress is numerically modified compared to the theoretical model to ensure a value for zero shear rate.

The maximum concentration of granular material is assumed to be a constant value.

5. Numerical simulations

This chapter presents the results of the performed numerical simulations. The projected end result is the modelling of a channel beach flow including segregation. To achieve this result, preparatory simulations were done. Section 5.1 presents the model geometry and boundary conditions. To test the rheological models separately from the segregation model a division is made between non-segregating flows and segregating flows. These are analysed in Paragraph 5.2 and 5.3 respectively. Model is verified with analytical results and validated with experimental results found in literature. Model validation is treated in Section 5.4. Section 5.5 concludes the numerical simulations.

5.1. Method and imposed conditions

The 1DV model includes two types of forcing of the flow (Chapter 4); the prescribed mean velocity and water depth on a horizontal bed or a prescribed discharge along a slope. The first named has a drawback. It forces the fluid to flow consistently (prescribed mean velocity), also if the yield stress surpasses the wall shear stress (prescribed mean water depth). Physically this is impossible. Simulations for which this condition occurred are excluded from the analysis.

First the models are tested excluding segregation in Simulations B1.1 – B1.4. Each of the rheological models is tested for multiple sand and clay concentrations and different hydraulic conditions. None of the simulations contains silt, but only sand and clay. As a starting point the concentrations and parameter settings are used who follow from the theoretical analysis in Chapter 3 in Simulation B1.1. The data of A.D. Thomas incorporate relatively high yield stresses and low plastic viscosities, resulting in an almost horizontal slope of the flow curve in the shear rate range of $0 < \dot{\gamma} < 50$ 1/s. In succeeding model runs the input parameters are altered to obtain a larger (plastic) viscosity.
As stated in Chapter 3 and 4 the yield stress is adapted in the numerical model. This new formulation influences the velocity and shear rate profile. In Simulation B1.3 the value of the parameter m is adjusted to minimize this influence.
A qualitative assessment of the coupled processes is done by comparing the model predictions with the observations found in literature. Therefore the concentrations of sand and clay are modified in Simulation B1.4. The models are verified with the analytical solution of (P. T. Slatter & Williams, 2013) presented in Chapter 2.
An overview of the adapted parameter per simulation is presented in Table 5-4.

Secondly simulations are done including segregation. Results of the flow on a horizontal bed (Simulations A2.1-A2.3) and on a slope (Simulations B2.1 – B2.5) are evaluated. The results of the horizontal bed configuration led to complications. These are explained in Section 5.3.1. The model is not further analysed with this configuration. The numerical robustness of the model

schematization is verified by changing the grid spacing (0.1mm – 150mm) and the time step (0.01s – 0.1s) in simulations B2.2 and B2.3 – B2.3.1 respectively.

Adjacent to the numerical modifications, variations in the physical properties are studied. As a starting point the concentrations and parameter settings are used who follow from the reference model of the non-segregating flow. In successive simulations the concentration (tailings property), discharge (operational parameter) and slope (geometry) are varied. None of the simulations contains silt. First the coupled process is verified with experiments found in literature. Then channel slope is decreased in Simulation B2.4 to 1/500 or 0.11˚. Generally flow depths and flow velocities range between 0.1-0.5 m and 0.1-0.6 m/s respectively but higher values occur as well. Initially a specific discharge of 0.1 m²/s is chosen. In Simulation B2.5 the discharge is increased to 0.5 m²/s.

An overview of the adapted parameter per simulation is presented in Table 5-10.

In literature different physical studies are found on (segregating) non-Newtonian flow (presented in Chapter 2). The model is validated with the experiment performed by B. Pirouz (Pirouz et al., 2013) considering no segregation and flow on a horizontal slope. Thereafter the experiment is simulated for segregating flow a slope. Only the velocity profile is validated.

A complete overview including the parameter settings is presented in Appendix F and G.

5.2. Non-segregating flow

The analysed non-segregating flow simulations concern the Simulations B1.1-1.4 (flow along a slope). To obtain a non-segregating flow the settling velocity of all particles is set to zero manually. The parameters in Table 5-1, Table 5-2 and Table 5-3 are used.

Table 5-1 Parameters Model 1 for non-segregating flow simulations.

Model 1	Sim B1.1	Sim B1.2	Sim B1.3	Sim B1.4
n_f	2.64	2.64	2.64	2.64
a	3.65	3.65	3.65	3.65
A_y	7.3E5	7.3E5	7.3E5	7.3E5
A_μ	9.3	930	930	930
β	0.27	0.27	0.27	0.27
$\varphi_{sasi,max}$	0.6	0.6	0.6	0.6
μ_w	0.001	0.001	0.001	0.001
φ_{clay}	0.16	0.16	0.16	0.12
φ_{sand}	0.04	0.04	0.04	0.16
φ_{sol}	0.20	0.20	0.20	0.28
SFR	1 : 4	1 : 4	1 : 4	4 : 3
ρ_{clay}	2670	2670	2670	2670
ρ_{sand}	2860	2860	2860	2860
$\rho_{mixture}$	1336	1336	1336	1348
m	5	5	5000	5000

Table 5-2 Parameters Model 2 for non-segregating flow simulations.

Model 2	Sim B1.1	Sim B1.2	Sim B1.3	Sim B1.4
B_μ	2.64	2.64	2.64	2.64
B_y	4.75	4.75	4.75	4.75
K_y	6.7E4	6.7E4	6.7E4	6.7E4
K_μ	2.5	250	250	250
α	0.27	0.27	0.27	0.27
$\phi_{sasi,max}$	0.6	0.6	0.6	0.6
μ_w	0.001	0.001	0.001	0.001
φ_{clay}	0.16	0.16	0.16	0.12
φ_{sand}	0.04	0.04	0.04	0.16
φ_{sol}	0.20	0.20	0.20	0.28
SFR	1 : 4	1 : 4	1 : 4	4 : 3
ρ_{clay}	2670	2670	2670	2670
ρ_{sand}	2860	2860	2860	2860
$\rho_{mixture}$	1336	1336	1336	1348
m	5	5	5000	5000

Table 5-3 Parameters Model 3 for non-segregating flow simulations.

Model 3	Sim B1.1	Sim B1.2	Sim B1.3	Sim B1.4
C_y	4.75E5	4.75E5	4.75E5	4.75E5
p	5.61	5.61	5.61	5.61
D	17.7	17.7	17.7	17.7
$k_{yield}\,\phi_{sasi,max}$	0.9	0.9	0.9	0.9
$k_{visc}\,\phi_{sasi,max}$	0.75	0.75	0.75	0.75
$\phi_{sasi,max}$	0.6	0.6	0.6	0.6
Multiplication μ	–	100	100	100
φ_{clay}	0.16	0.16	0.16	0.12
φ_{sand}	0.04	0.04	0.04	0.16
φ_{sol}	0.20	0.20	0.20	0.28
SFR	1 : 4	1 : 4	1 : 4	4 : 3
ρ_{clay}	2670	2670	2670	2670
ρ_{sand}	2860	2860	2860	2860
$\rho_{mixture}$	1336	1336	1336	1348
m	5	5	5000	5000

The sand and clay contents in gram per litre and mass fraction are included in Appendix F.

An overview of the altered model input (red parameter) per simulation is given in Table 5-4. The grid spacing, time step, slope angle and discharge are provided for completeness.

	φ_{sand} [-]	φ_{clay} [-]	τ_{yield} [Pa]	μ_{tot} [Pa s]	m [-]	Grid [#]	Time [s]	$Sin(\theta)$ [-]	q [m²/s]	W_s [m/s]
B1.1	0.04	0.16	38	0.04	5	200	0.1	0.01	0.1	0
B1.2	0.04	0.16	38	4.3	5	200	0.1	0.01	0.1	0
B1.3-REF	0.04	0.16	38	4.3	5000	200	0.1	0.01	0.1	0
B1.3.1*	0.04	0.16	38	4.3	5E6	200	0.1	0.01	0.1	0
B1.4	0.16	0.12	32.6	3.5	5000	200	0.1	0.01	0.1	0

5.2.1. Flow curve

Because the flow is non-segregating a Steady-State can be achieved. The model requires a spin-up time, 300-1000 time steps, to converge from the initial conditions to the Steady-State solution. The exact time needed depends on the difference between the chosen initial conditions and the Steady-State solution.

(Plastic) Viscosity

From the flow curve of the data of A.D. Thomas we can conclude that the viscosity is orders of magnitude smaller than the yield stress, i.e. the curve is almost horizontal. Therefore the viscosity is adapted with a factor 100. The original flow curve and the adapted flow curve of Model 1(power law) and Model 2 and 3 (Bingham) is visualized in Figure 5-1.
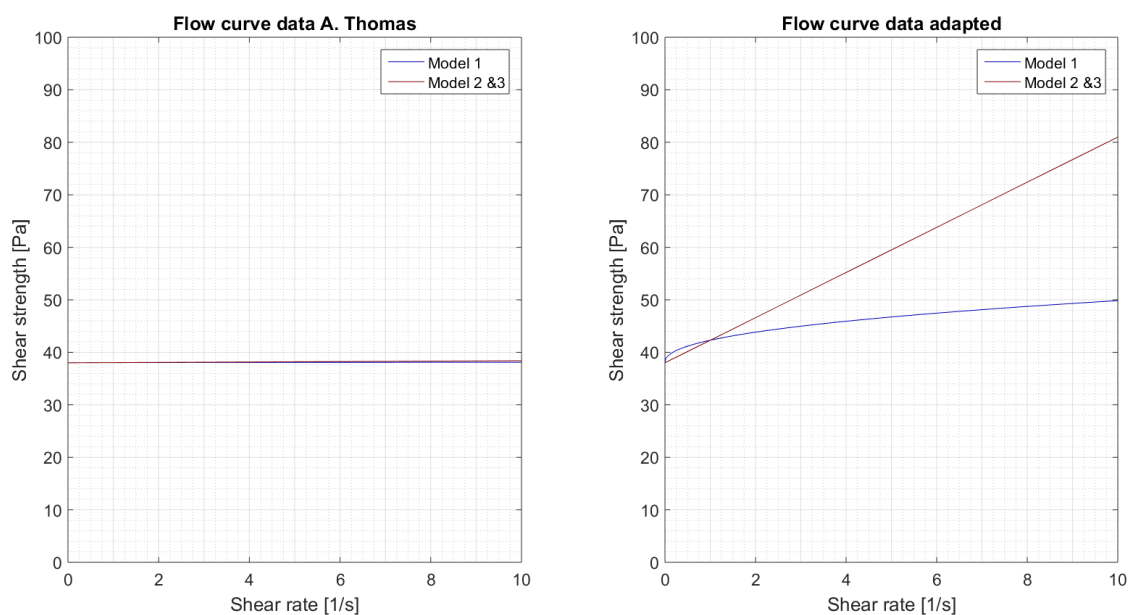
Figure 5-1 Flow curve of Model 1 (power law) and Model 2 (Bingham). Left: Based on data A.D. Thomas. Right: including modified (plastic) viscosity.

Simulation B1.1 includes the original parameters of the data A.D. Thomas obtained. Figure 5-2 presents this simulation for all three models the flow velocity, shear rate, yield stress and shear stress after 2000 s. The yield stress is close to the wall shear stress and the sheared zone covers only a few (4-10) grid cells in the models. Therefore this simulation will not suite as acceptable reference simulation.
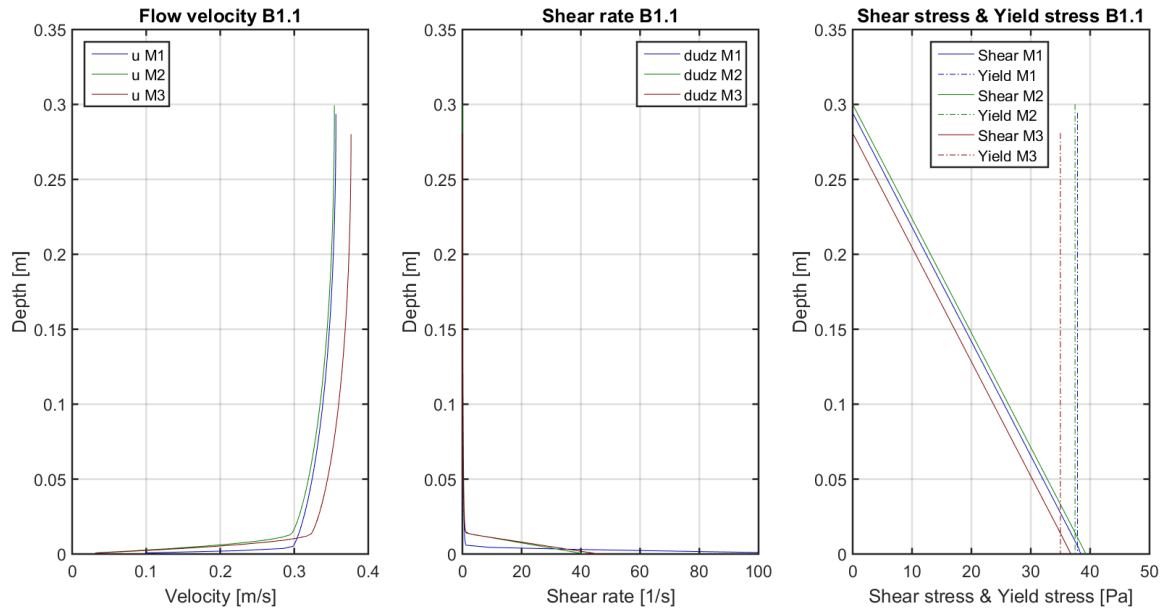
Figure 5-2 Sim. B1.1 original data A.D. Thomas. Results of all three models after 2000 s.

Figure 5-3 presents Simulation B1.2 (after 2000 s). The viscosity is 2 orders of magnitude larger compared to Simulation B1.1. Therefore the shear stress exceeds the yield stress at higher mud level. The intersection between the yield stress and wall shear stress is at 25-30% of the flow depth. As stated in Section 4.3 the yield stress is adapted in the numerical model to enable a flow calculation if $\dot{\gamma}$=0. As a result the value of the parameter m does not only influence the steepness of the flow curve, it influences the velocity profile as well.

If the shear stress exceeds the yield stress the velocity profile becomes more curved and the shear rate increases. Model 1 includes a power function and the shear stress does not linearly increase with the shear rate. Model 2 and 3 are Bingham models. Their shear stress increases linearly with shear rate. Therefore the behaviour of these two models is more similar. The calculated shear stress of Model 1 is lower compared to Model 2 and 3. Therefore the flow resistance is lower resulting in a lower flow depth. A more in-depth analysis follows in Subsection 5.2.3.
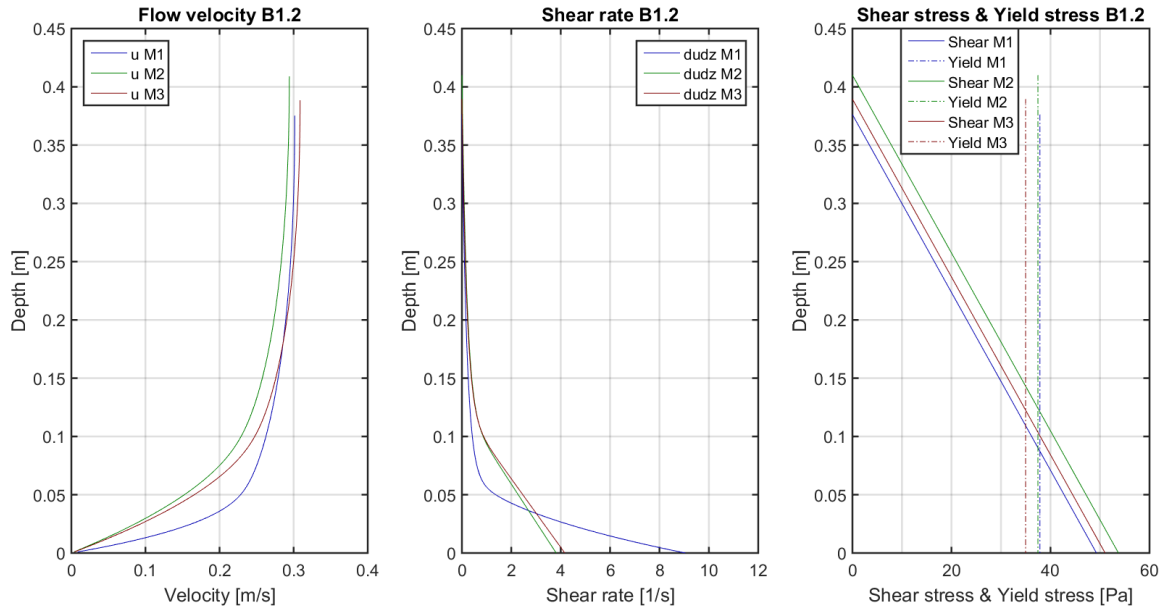
Figure 5-3 Sim. B1.2 adapted coefficient of the (plastic) viscosity. Results of all three models after 2000 s.

Modification of yield stress

A calculation is made including the modification of the yield stress for a Bingham and Herschel-Bulkley model. The resulting flow curves are displayed in Figure 5-4. From the shear rate profile of Simulation B1.2 it is evident that shear rates smaller than one occur. Figure 5-4 presents the flow curve for $m=5$. If $\dot{\gamma}=0.001$ the modified shear stress is two orders of magnitude smaller than the actual shear stress. The flow curve approaches the Bingham/ power law profile if a high value of m is chosen, resulting in a more accurate representation of the flow velocity and shear rate.
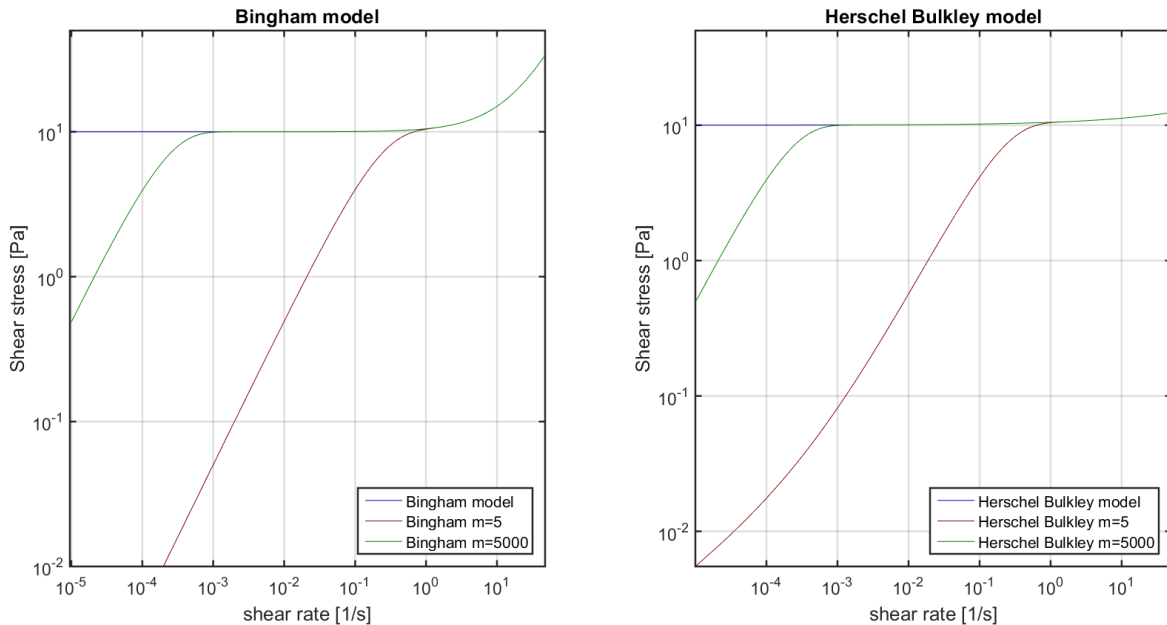
Figure 5-4 Influence of parameter m on flow curve. Left: Bingham model. Right: Herschel Bulkley model. $\tau_y = 10$; $\mu = 0.5$. Therefore at small shear rates the curve does not rise.

Figure 5-5 presents Simulation B1.3 (after 2000 s) with an adapted value of m. Figure 5-6 presents the velocity profile of Simulation B1.2 and B1.3.
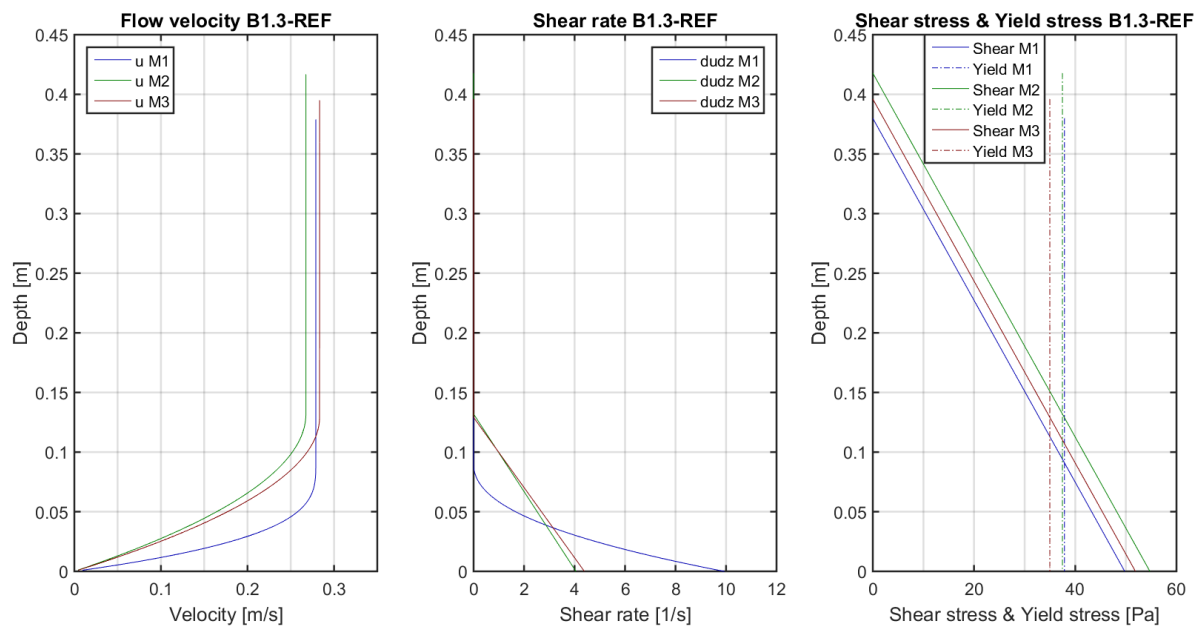
Figure 5-5 Sim. B1.3 Reference simulation. Result of all three models after 2000 s.
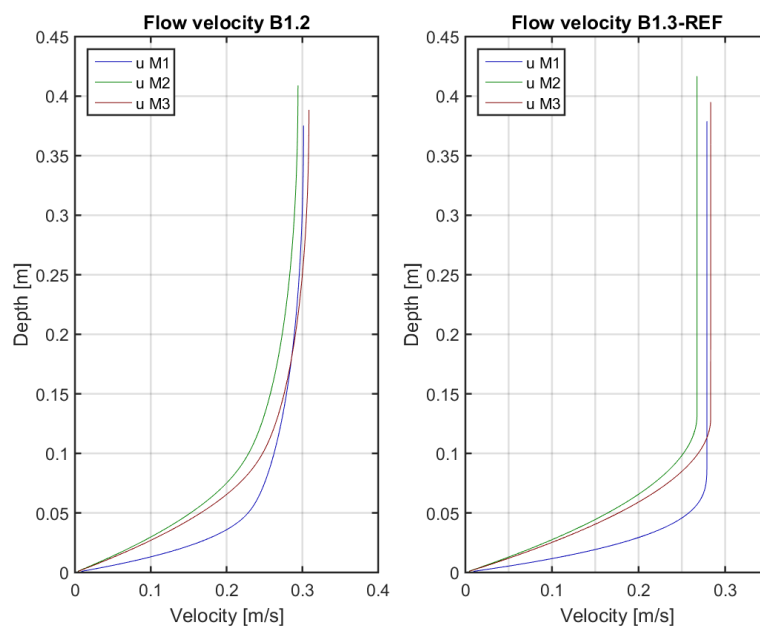
Figure 5-6 Velocity profile of B1.2 (left) & B1.3 (right) of all three models to visualize influence of parameter m after 2000 s.

The difference in shape of the velocity profile is clearly visible. Comparing Simulations B1.1, B1.2 and B1.3 results in the following conclusion. For low values of m the velocity profile attains a more parabolic shape in to the unsheared region. In this region - where the yield stress dominates the shear stress - non-zero shear rates occur, disturbing the plug-flow conditions. The shear stress profile is not affected by the value of m, it is determined by the slope and water depth. This consequence was observed in all simulations, i.e. for the horizontal bed model as well as for the slope model, in all three rheological models, for segregating and non-segregating flow.

If m has a value of 5E3, the shear rate values are in the order of 1E-6 in the plug of the flow. For Model 1 an additional simulation (B1.3.1) is done with m = 5E6. The results are compared to the reference simulation in Figure 5-7. There is no difference visible from the graphs. Figure 5-8 visualizes that m = 5E6 results in a decrease of the shear rates in the plug of the flow to an order of 1E-9 which increases the apparent viscosity in the plug of the flow as well. Because this difference does not influence the flow velocity profile, shear stress and yield stress notably, a value of m = 5E3 is chosen. In Section 5.3 the effects for segregating flow are analysed.
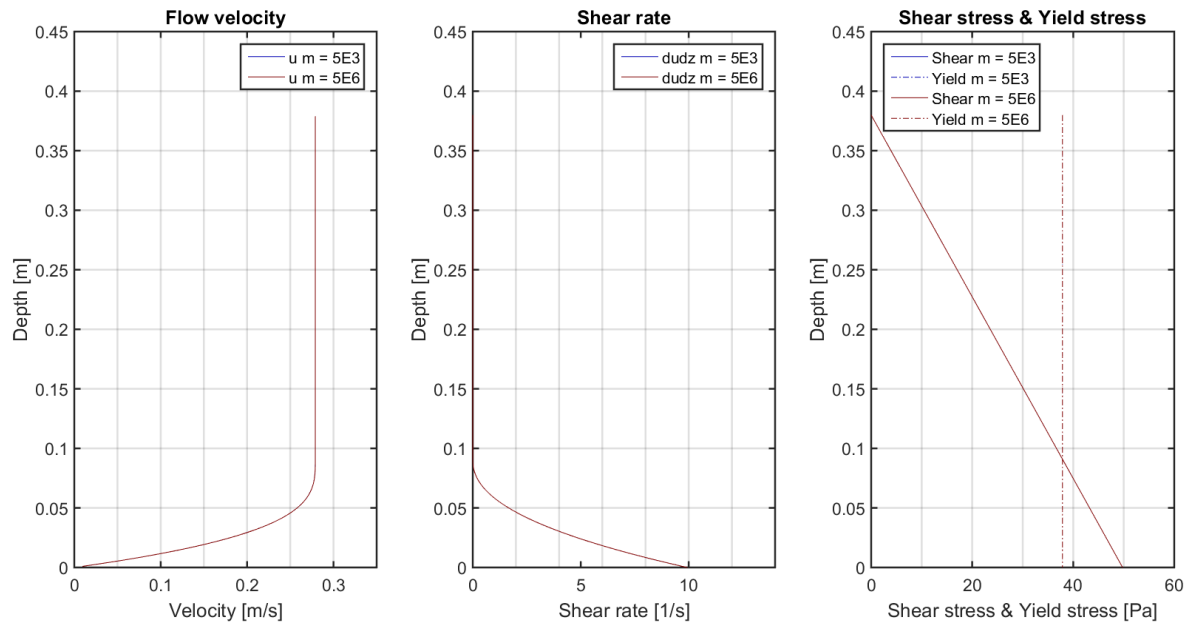
Figure 5-7 Sim. B1.3.1. m = 5E6. Results of Model 1.
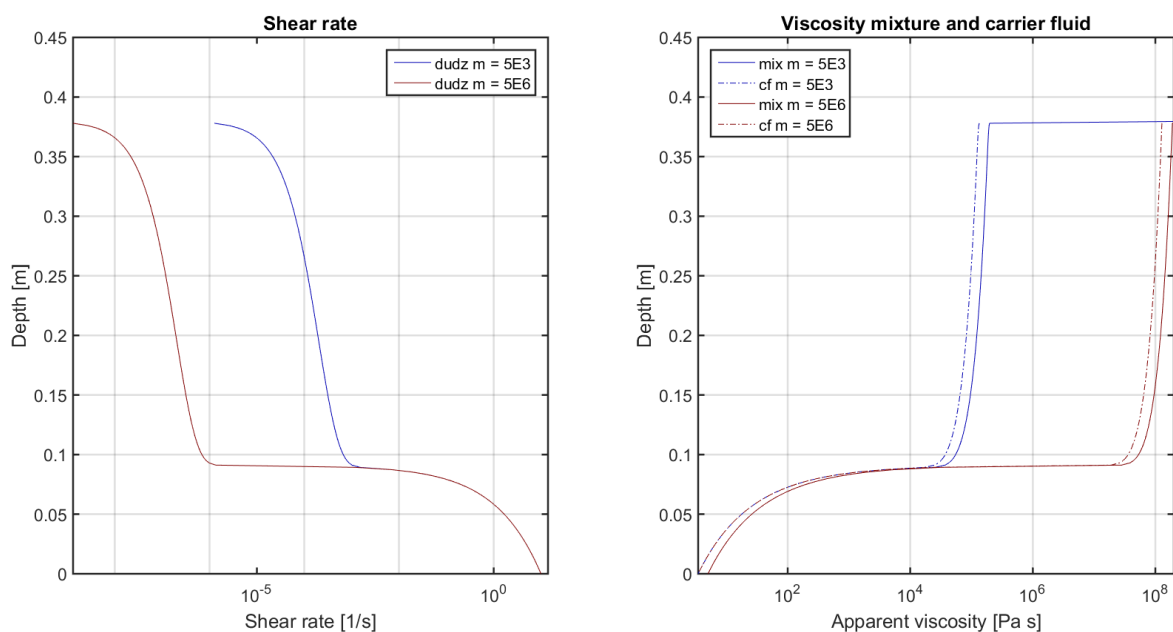
Figure 5-8 7 Sim. B1.3.1. m = 5E6. Shear rate and apparent viscosity of Model 1.

Simulation B1.3 is chosen as the reference simulation.

5.2.2. Qualitative assessment of physical properties

The rheology and velocity are coupled processes as discussed in Chapter 2. The results of the simulations present this coupling. In Simulations B1.3 and B1.4 the velocity profile is almost a straight line in the unsheared region. If the shear stress exceeds the yield stress the velocity profile becomes parabolic (Model 2 and 3) or a power law shape (Model 1) and approaches 0 m/s at the bottom (no-slip condition). The shear rate increases in the sheared region and decreases again if the velocity becomes zero. For Model 1 the shear rate is non-linear due to the power law shape of the velocity profile. The shear rate Model 2 and 3 increases linearly.

In the sheared region the apparent viscosity is (on average) three to seven orders of magnitude smaller compared to the apparent viscosity in the plug-zone. This depends on the parameter m and the resulting velocity profile and shear rate. In all model runs there is no segregation observed of any concentration, consistently with imposing non-segregating (settling velocity is zero) conditions.

Simulation B1.4 (after 2000 s) is presented in Figure 5-9. In Simulation B1.4 the sand and clay concentrations are increased and decreased respectively. The concentrations follow from the data of A.D. Thomas. Although the total concentration of solids increases it results in a decreased yield strength and viscosity compared to the reference simulation. Reduction of the strength of the clay is larger than the increase in strength by the sand. This is in accordance with the conclusion of Chapter 3. Due to the decreased yield strength and viscosity the (hydraulic) resistance of the mixture is reduced, resulting in an increased flow velocity, larger shear rates and lower flow depth.

These observations are in line with the conclusions on hydrology and rheology as seen in the physical experiments of (Pirouz et al., 2013; Sanders et al., 2002; Spelay, 2007) discussed in Chapter 2.
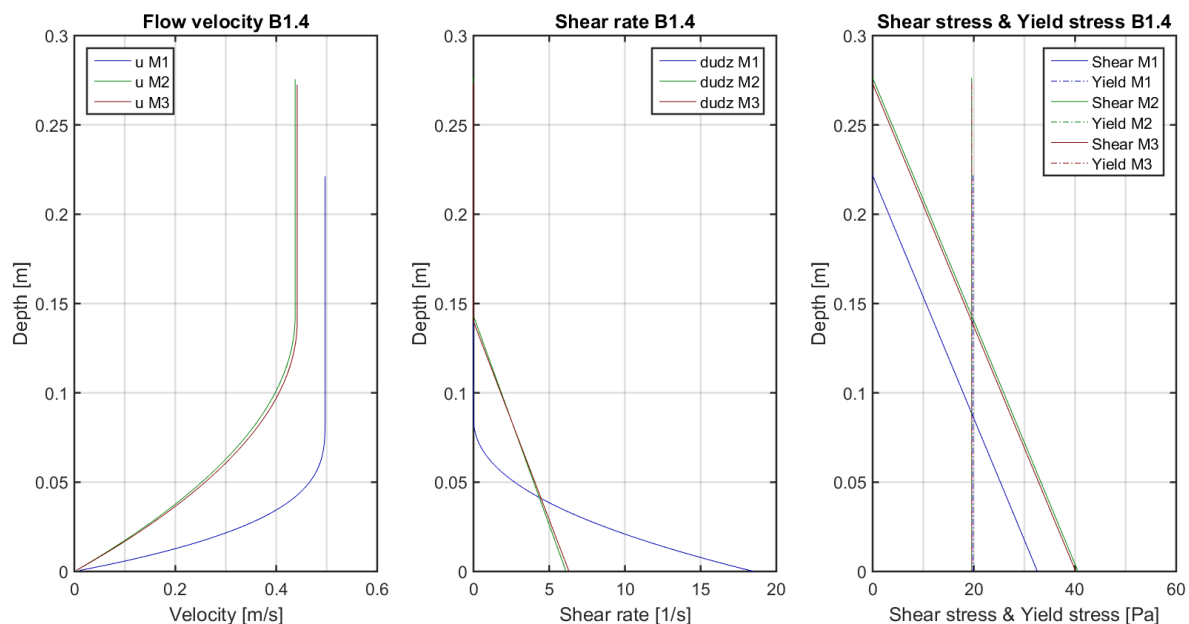
Figure 5-9 Sim. B1.4 adapted clay and sand concentrations. Result of all three models after 2000 s.

Simulations B1.1 and B1.2 prove that an increase in viscosity results in relatively larger differences between the three models. Simulations B1.3 and B1.4 prove that the same holds for an increase in solids concentration. From the data of (A. D. Thomas, 1999) it was also observed that the model predictions deviate more for higher concentrations. It is an expected result which originates from differences between the six different formulations (yield stress and viscosity of each rheological model). Model 1 utilizes the ratio of the clay fraction and sand fraction whereas Model 2 and 3 replace this sand fraction for the total solids fraction.

Secondly Model 1 is based on a power law behaviour for the material viscosity whereas Model 2 and Model 3 are Bingham models. Consequently Model 2 and 3 agree more. For the comparison to data in Chapter 3 the assumption is made that $\dot{\gamma}$ = 1 1/s. Hence the difference of the power (1 or 0.44) between the models does not influence the results. If the shear rate does not equal one the deviations of the predictions between Model 1 and Model 2 and 3 are more pronounced.

Lastly the approach to include the influence of the granular material diverges between the models. Model 1 and Model 2 use an identical equation (linear concentration theory) whereas Model 3 approximates this behaviour differently (power law equation).

In Simulation B1.4 the calculated viscosity, yield stress and shear stress of Model 1 are smaller compared to Model 2 and 3. As a result the velocity is higher (less hydraulic resistance) and the shear rate becomes larger.

5.2.3. Comparison to analytical results

For every simulation the solutions of the yield stress, viscosity and shear stress (given the shear rate) are analytically verified in Excel, i.e. verifying the code on physical reality grid cell to grid cell. No discrepancies were found.

Thereafter the coupling between the hydrodynamics and rheology is reviewed. The resulting wall shear stresses of the non-segregating flow simulations are compared to the analytical solution of P. Slatter.

$$\frac{3\bar{u}}{h_0} = \frac{3n\mu}{\tau_w(2n+1)}\left(\frac{\tau_w}{\mu}\right)^{\frac{n+1}{n}}\left(1-\frac{\tau_y}{\tau_w}\right)^{\frac{n+1}{n}}\left(1+\frac{n}{n+1}\frac{\tau_y}{\tau_w}\right) \tag{5.29}$$

An overview is given in Table 5-5,

Table 5-6 and Table 5-7. In the last column of each table the difference between the analytical solution and the simulation result is expressed as a percentage of the analytical solution.

Table 5-5 Calculated analytical solution and numerical solution of Model 1.

Sim	Model 1								
	h	u	τ_{yield}	τ_{wall}	μ_{tot}	n	3u/h	M1	Diff %
B1.1	0.294	0.340	37.871	38.410	0.044	0.446	3.460	3.580	3.448
B1.2	0.376	0.266	37.871	49.287	4.272	0.446	2.122	1.836	-13.486
B1.3 REF	0.380	0.263	37.871	49.773	4.272	0.446	2.078	2.077	-0.027
B1.4	0.222	0.451	19.846	32.566	3.454	0.446	6.100	6.102	0.028

Table 5-6 Calculated analytical solution and numerical solution of Model 2.

Sim	Model 2								
	h	u	τ_{yield}	τ_{wall}	μ_{tot}	n	3u/h	M2	Diff %
B1.1	0.300	0.333	37.457	39.275	0.044	1.000	3.333	2.837	-14.900
B1.2	0.301	0.332	37.457	53.729	4.263	1.000	3.311	1.559	-52.922
B1.3 REF	0.418	0.239	37.457	54.744	4.263	1.000	1.719	1.718	-0.062
B1.4	0.276	0.362	19.581	40.599	3.438	1.000	3.938	3.929	-0.247

Table 5-7 Calculated analytical solution and numerical solution of Model 3.

Sim	Model 3								
	h	u	τ_{yield}	τ_{wall}	μ_{tot}	n	3u/h	M3	Diff %
B1.1	0.280	0.357	34.979	36.753	0.039	1.000	3.827	3.282	-14.233
B1.2	0.282	0.355	34.979	51.036	3.854	1.000	3.780	1.760	-53.442
B1.3 REF	0.396	0.253	34.979	51.892	3.854	1.000	1.913	1.912	-0.036
B1.4	0.273	0.366	19.580	40.140	3.260	1.000	4.025	4.019	-0.160

In all simulations (small) deviations occur. B1.1 and B1.2 have the largest error for all three models. The reason is the adapted yield stress, resulting in a modified velocity and shear rate profile. The results of Simulations B1.3 and B1.4 correspond very well to the analytical solution; the error is less than 0.3%. The results of Model 2 and 3 are very close because they are both Bingham models whereas Model 1 attains a power law behaviour.

5.3. Segregating flow

In these simulations segregation of the granular material is permitted, the clay fraction may not settle. First the observations of the flow along a horizontal bed are discussed, followed by the results of the flow along a slope.

5.3.1. Horizontal bed

Three simulations different simulations are made with flow along a horizontal bed. The used rheological parameters follow from the data of A.D. Thomas and are presented in

Table 5-8. Table 5-9 presents the modified parameters.

Table 5-8 Parameters of Model 2 for segregating flow on a horizontal bed. Simulation A2.1 – A2.3

Model 2			A21 – A23			
B_μ	[-]	2.64	φ_{clay}	[-]	0.16
B_y	[-]	4.75	φ_{sand}	[-]	0.04
K_y	[-]	6.7E4	φ_{sol}	[-]	0.20
K_μ	[-]	2.5; 25; 250	ρ_{clay}	[kg/m³]	2670
α	[-]	0.27	ρ_{sand}	[kg/m³]	2860
$\phi_{sasi,max}$	[-]	0.6	$\rho_{mixture}$	[kg/m³]	1336
μ_w	[Pa s]	0.001	SFR	[m]	1 : 4
M	[-]	5000	u	[m/s]	0.4
			h	[m]	0.5

Table 5-9 Adapted parameters of Model 2 for segregating flow on a horizontal bed. Simulation A2.1 – A2.3.

	φ_{sand} [-]	φ_{clay} [-]	τ_{yield} [Pa]	μ_{tot} [Pa s]	m [-]	Grid [#]	Time [s]
A2.1	0.04	0.16	38	0.04	5000	200	0.1
A2.2	0.04	0.16	38	0.43	5000	200	0.1
A2.3	0.04	0.16	38	4.3	5000	200	0.1

The model requires a spin-up time. During these time steps sand segregates but the quantities are negligible. Figure 5-10 presents the results of Simulation A2.1 after 500, 1000 and 2000 s. As a remark, the downward settling velocity is negative defined in the chosen coordinate system. After the spin-up time the velocity profile is again a straight line in the unsheared region and attains a parabolic shape in the sheared region. In the sheared region the shear rate increases significantly. As a result the apparent viscosity decreases for an increasing shear rate. The settling velocity increases rapidly at the critical height where the yield stress is equal to the shear stress. At this point sand starts to segregate and the concentration decreases.

A decreasing concentration results in a decreasing viscosity and yield stress and hence an adapted shear stress. The shear stress and yield stress profile cross three times in the sheared region. The flow velocity does not decrease where the shear stress is smaller than the yield stress. A step in the velocity profile is visible and the shear rate is almost zero. In the sheared region an unsheared belt appears with an enhanced apparent viscosity and reduced settling velocity.
For longer computation times the yield stress and shear stress cross multiple times and several regions of segregation occur resulting in alternating layers of high and low concentrations.
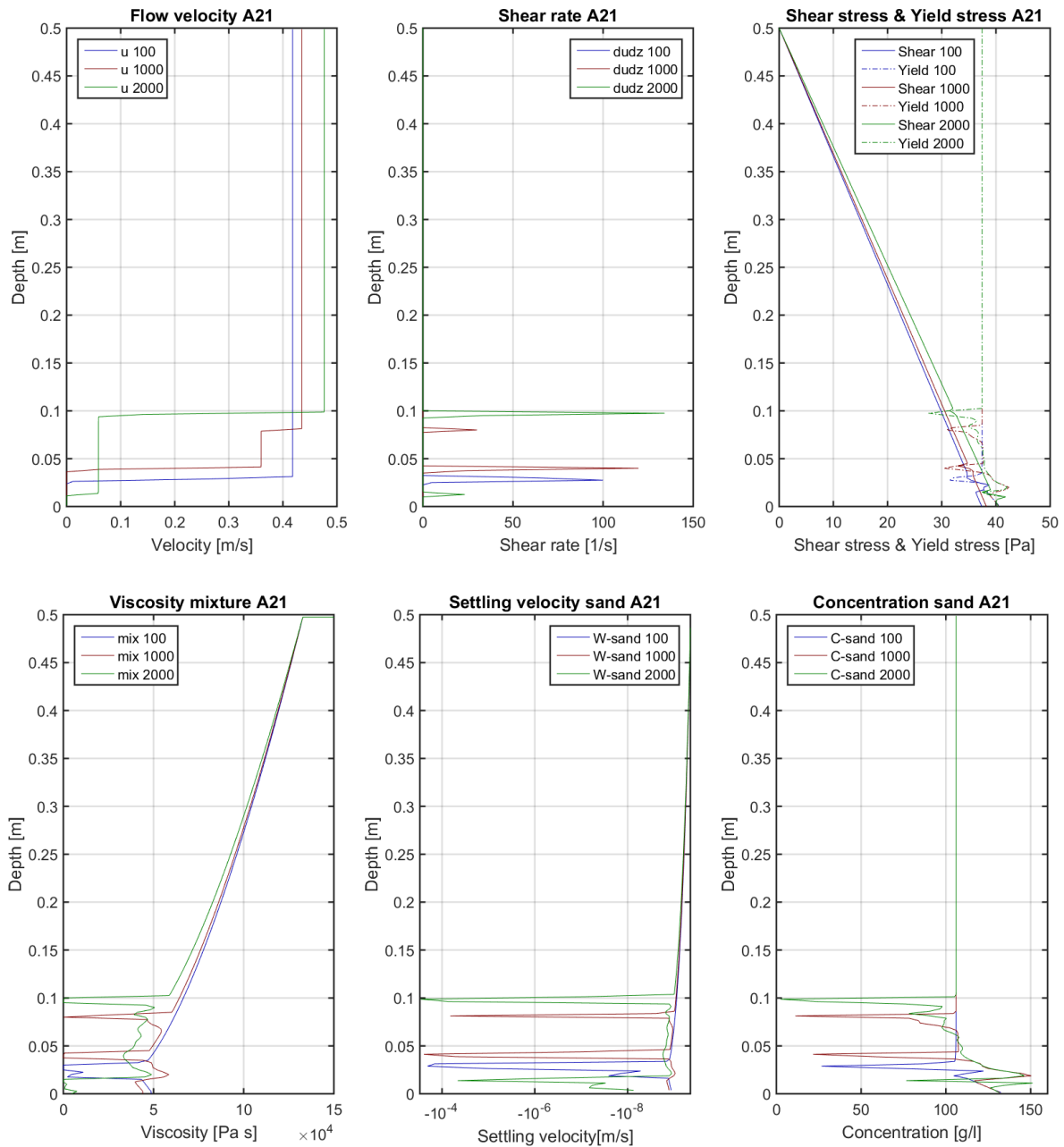
Figure 5-10 Sim. A2.1 Flow over a horizontal bed of Model 2 with original parameters A.D. Thomas after 100, 500, 1000 and 2000 s.

In Figure 5-11 the results of simulations A2.1-A2.3 are compared after 2000 s. Due to the higher viscosity in simulation A2.3, the difference between the yield stress and wall shear stress is larger. The instabilities do not occur of sand segregates. Segregation of material does not immediately lead to large changes in the apparent viscosity.
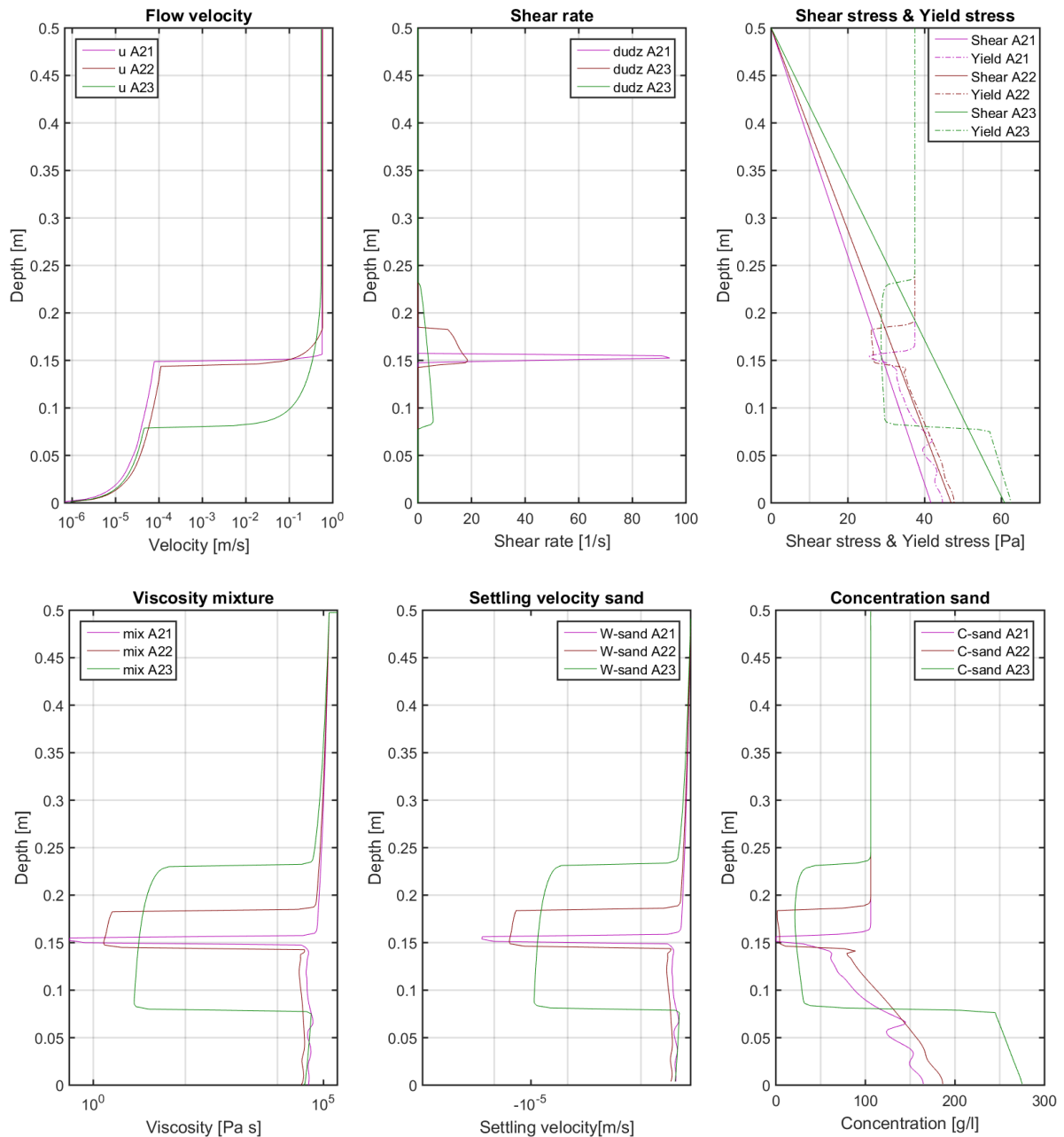
Figure 5-11 Sim. A2.1-2.3 adapted viscosities. Results of Model 2 after 2000 s.

All processes are very stiff coupled; i.e. a small change in the concentration has a substantial impact on the results. These strong changes, especially in apparent viscosity, are unexpected from nature. There is time needed for the flocs to break up and particles need time to accelerate in a viscous fluid.

In this configuration the flow depth and mean velocity are prescribed. The flow has not the ability to adapt the water level or mean velocity for the changes in concentration and deposition near the bottom.

The phenomenon was observed for different kinds of concentrations and parameter settings. Mutations of the following parameters affected the wiggling behaviour.

- Remarkably the alternating behaviour was less drastic for a low value of the parameter m. This results in one of the explanations. Due to the steep gradient of the flow curve the difference in apparent viscosity just below and above the yield stress is enormous. As a result the differences of the settling velocities are considerable. From a detailed view on the different grid cells it is clear that these coupled processes occur in the same grid cell.
- If the grid size is enlarged the amount of 'wiggles' decreases. The opposite occurs for smaller grid cells. The reason is that the concentrations are averaged over the de grid cells and interpolated on the interface. For larger grid cells the concentration decrease is more uniform distributed resulting in less strong transitions. In effect this is a manner of numerical diffusion.
- Smaller flow velocities result in smaller shear rates and especially smaller differences of the shear rate over depth. The alternation from high to low apparent viscosities becomes smaller. The wiggles appear to dampen but are not vanished.
- For longer simulations the amount of wiggles did not significantly decrease. The wiggles move upward in the system due to the increased concentration near the bottom.
- If the shear rate is decoupled from the settling formula, i.e. a constant viscosity in the settling formula, the wiggles do not appear.

Two alternatives may reduce the wiggling behaviour. First by programing a relaxation term in the settling velocity in the model. The segregation rates will be reduced, the changes in the viscosity will be less pronounced and the model behaves less stiff. Secondly the use of a flow along a slope can offer a solution. In the current model the fluid has to flow in any case due to the imposed mean flow velocity and water depth at the boundary. The first option is not studied. The latter follows hereafter.

5.3.2. Slope

Reference Simulation B1.3 is adjusted; by allowing settling of granular material. This new simulation is reference Simulation B2.1 and presented in Figure 5-19 top (velocity, shear rate, shear stress and yield stress) and bottom (apparent viscosity, settling velocity and sand concentration) after 2000 s.

The used model parameters are equal to simulation B1.3 (except from the segregation formula). These are presented in Appendix G together with the sand and clay contents in gram per litre and mass fraction. In Table 5-10 the adjustments to the reference run are presented.

Table 5-10 Input parameters of Sim. B2.1 - B2.5. Segregating flow along a slope. (*) this simulation is only done for Model 1.

	φ_{sand} [-]	φ_{clay} [-]	τ_{yield} [Pa]	μ_{tot} [Pa s]	m [-]	Grid [#]	Time [s]	$Sin(\theta)$ [-]	q [m²/s]	W_s [m/s]
B2.1 REF	0.04	0.16	38	4.3	5000	200	0.1	0.1	0.1	#
B2.1.1*	0.04	0.16	38	4.3	5E6	200	0.1	0.1	0.1	#
B2.2	0.04	0.16	38	4.3	5000	600	0.1	0.1	0.1	#
B2.3	0.04	0.16	38	4.3	5000	200	0.01	0.1	0.1	#
B2.31	0.04	0.16	38	4.3	5000	200	1	0.1	0.1	#
B2.4	0.04	0.16	38	4.3	5000	200	0.1	0.025	0.1	#

B2.5	0.04	0.16	38	4.3	5000	200	0.1	0.1	0.5	#

Once more the effect of factor m is studied. In Simulation B2.1.1 the value is increased to $m =$ 5E6. The test is done for Model 1 only. Compared to Simulation B2.1 the grid size (200 to 600 layers) is varied in Simulations B2.2 and the time step is decreased and increased in Simulations B2.3 and B2.31 respectively. In Simulations B2.4 and B2.5 the slope and discharge are adjusted, respectively.

The settlement of only sand results in changes in the flow curve of the mixture. The flow curve of the carrier fluid remains the same. Figure 5-12 presents the flow curve of the carrier fluid and mixture for a Bingham model and Herschel Bulkley model. The (rounded off) values are equal to the initial values of model simulations B2.1 – B2.5; $\tau_{y,mix} = 38$; $\mu_{mix} = 4.3$; $\tau_{y,cf} = 25$; $\mu_{cf} = 3.2$; $n = 1$ (Binham); $n = 0.45$ (Herschel Bulkley).
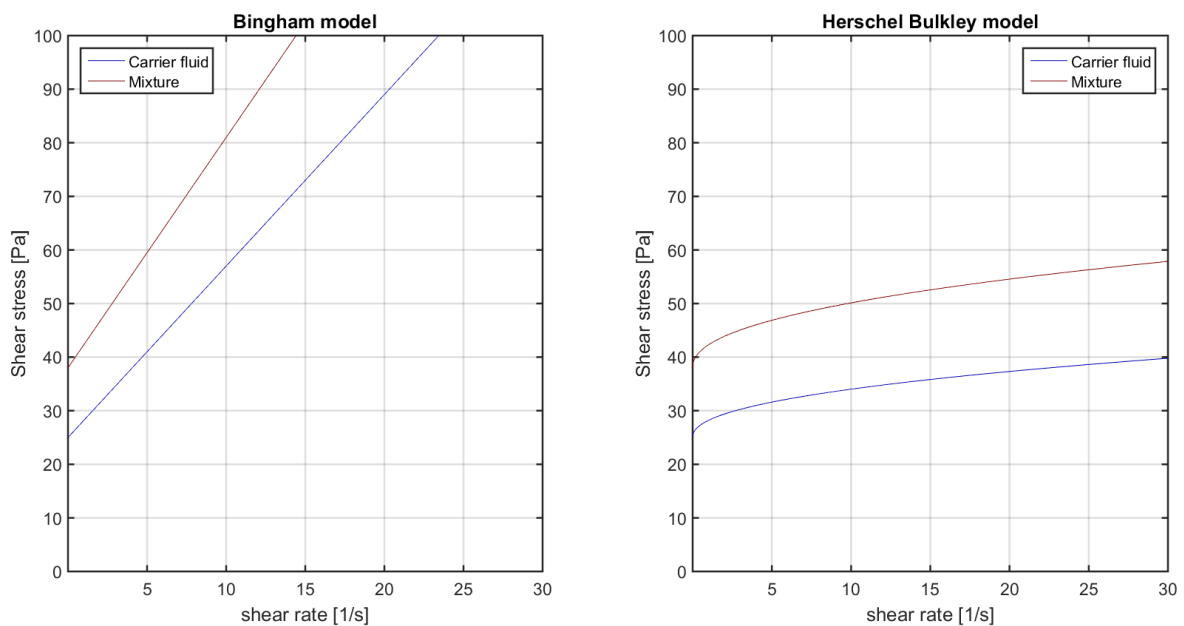
Figure 5-12 Flow curve Bingham model left ($n = 1$). Herschel Bulkley model right ($n = 0.45$). $\tau_{y,mix} = 38$; $\mu_{mix} = 4.3$; $\tau_{y,cf} = 25$; $\mu_{cf} = 3.2$.

In the plug of the flow the rheological properties of the mixture will approach the properties of the carrier fluid due to the segregation of sand. At the bed the material deposits and the concentration increases. In this area the flow curve of the mixture will deviate more from the carrier fluid flow curve. From this figure it is also evident that the calculated shear stress of a Bingham model and power law model deviate considerably for shear rates above 10 1/s. This is caused by the flow index n. Therefore the differences between Model 1 and Model 2 and 3 becomes larger for higher shear rates.

Numerical assessment

Similar to the non-segregating the simulations are analytically verified. It is not possible to use the analytical solution of P. Slatter. Due to the segregation the shear rate in the last grid cell, yield stress and wall shear stress vary. The results are compared to a calculation in Excel. Given a certain shear rate and the solids concentrations in a grid cell, the yield stress, viscosity, settling velocity and changes in concentration in time are verified. No discrepancies were found.

Modification of yield stress

Figure 5-13 presents the comparison of the results of Simulation B2.1 and B2.1.1 of Model 1. Likewise in Simulation B1.3.1 the differences in flow velocity, shear rate, yield stress and shear stress don not seem to differ. However in the plug of the flow the shear rates are in the order of 1E-6 and 1E-9 for simulation B2.1 and B2.1.1 respectively. The difference in the velocity and shear stress between the two simulations is in the order of 1E-3 or smaller.
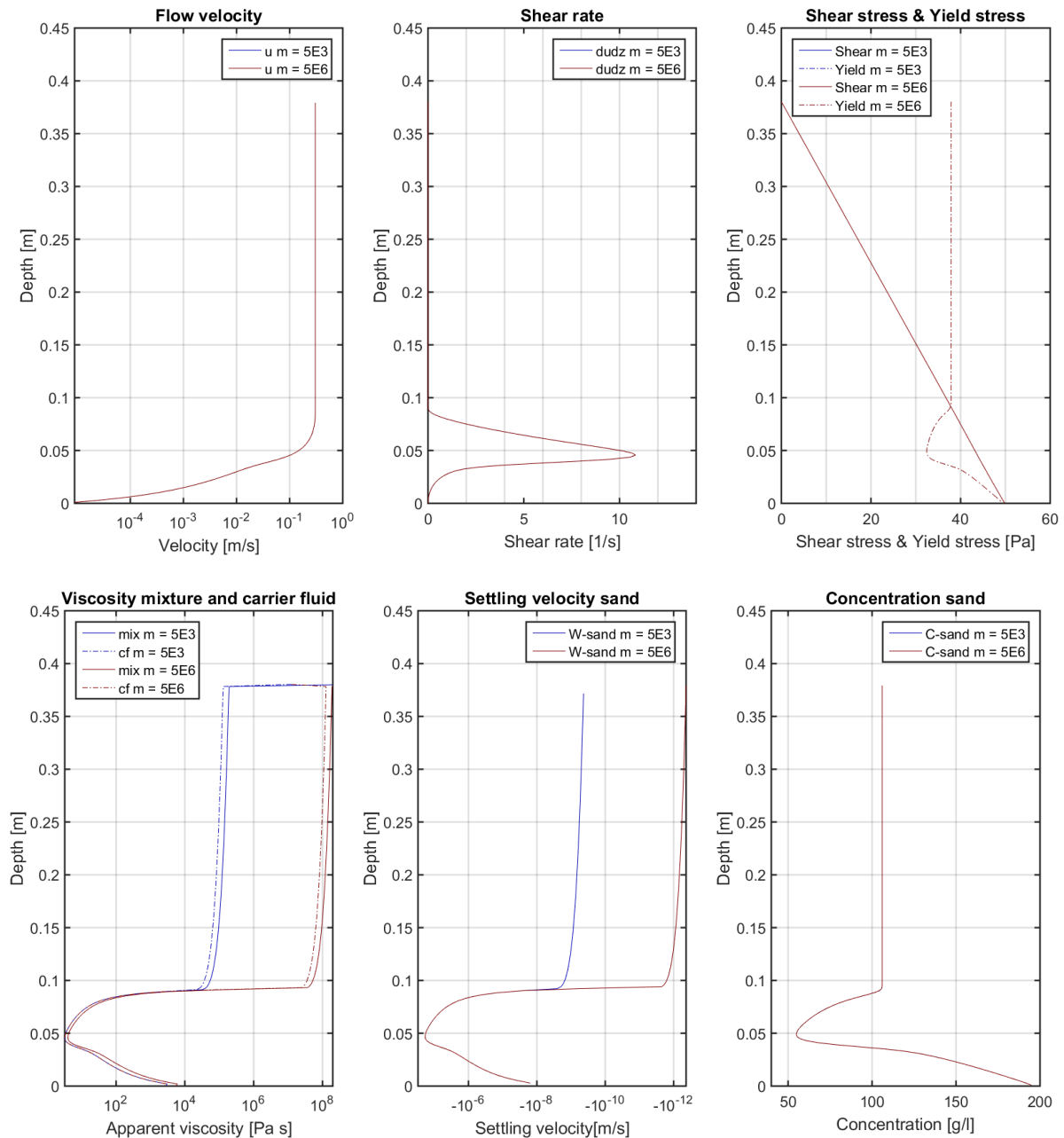
Figure 5-13 Sim. B2.1: m = 5E3 and B2.1.1: m = 5E6. Results Model 1 after 2000 s.

The apparent viscosity profile presents a large deviation between the two simulations in the plug of the flow. This is the result of the deviations present in the shear rate and diverge three orders of magnitude as well. Consequently the settling velocities in the plug of the flow differ three orders of magnitude. In the sheared zone the difference between the simulations is smaller than 1E-10. The resulting concentration profile does not seem to vary. From a detailed view it is observed that the concentration differences are in the order of 1E-3 in the plug, sheared zone and

near the bed. A value of m = 5E3 does not seem to result in large differences in segregation compared to higher values. However a thorough analysis of the upper bound of m is still required.

Grid size

The grid size is adapted for all three models Simulation B2.2. The results are compared with the reference Simulation B2.1 (after 2000 s). Figure 5-14 presents the results of Model 1. Figure 5-15 presents the results of Model 2. Model 2 and 3 comprise a similar behaviour. Therefor only the results of Model 2 are presented.
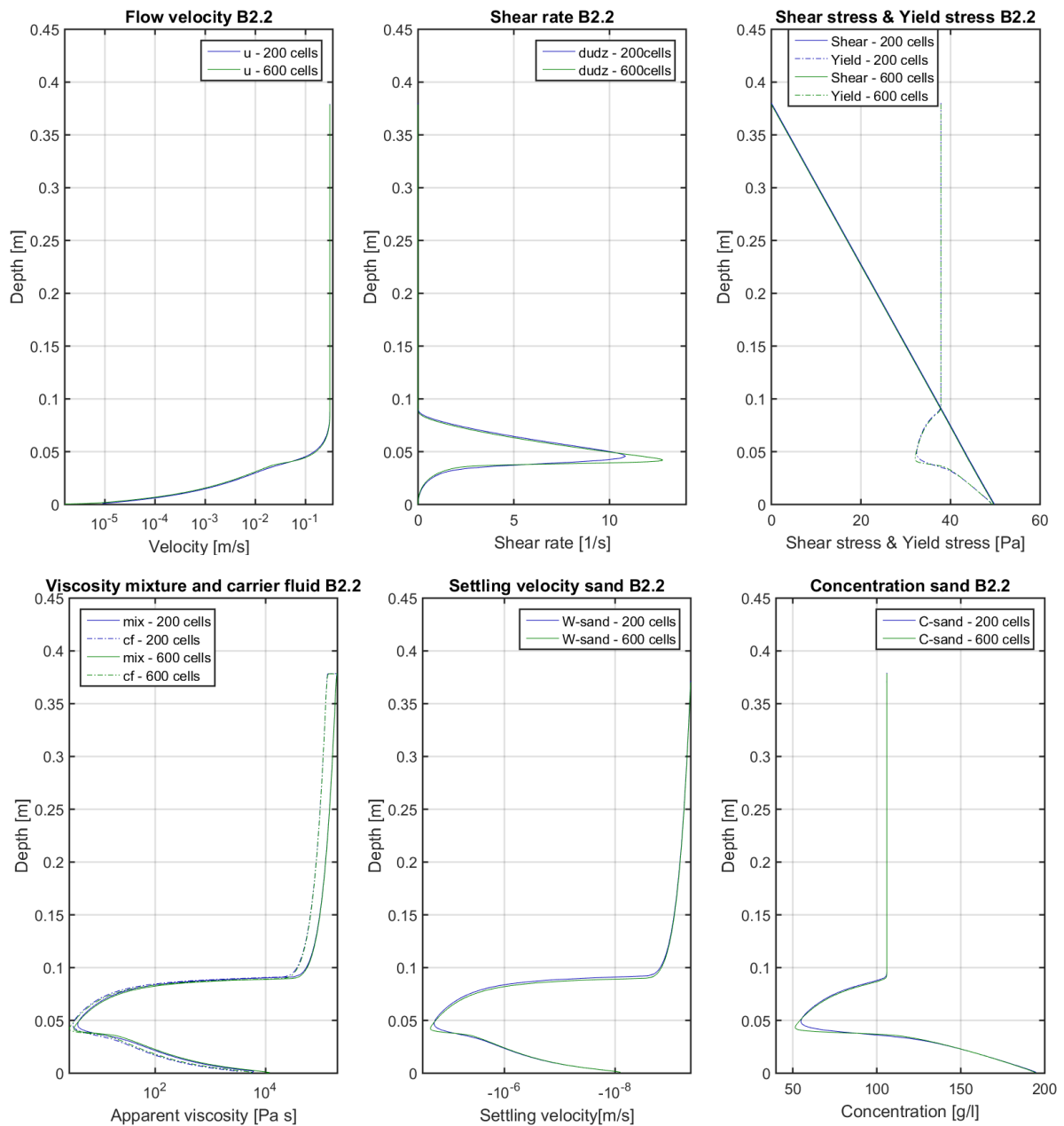
Figure 5-14 Sim. B2.1 – 200 grid cells and B2.2 – 600 grid cells. Results Model 1 after 2000 s.
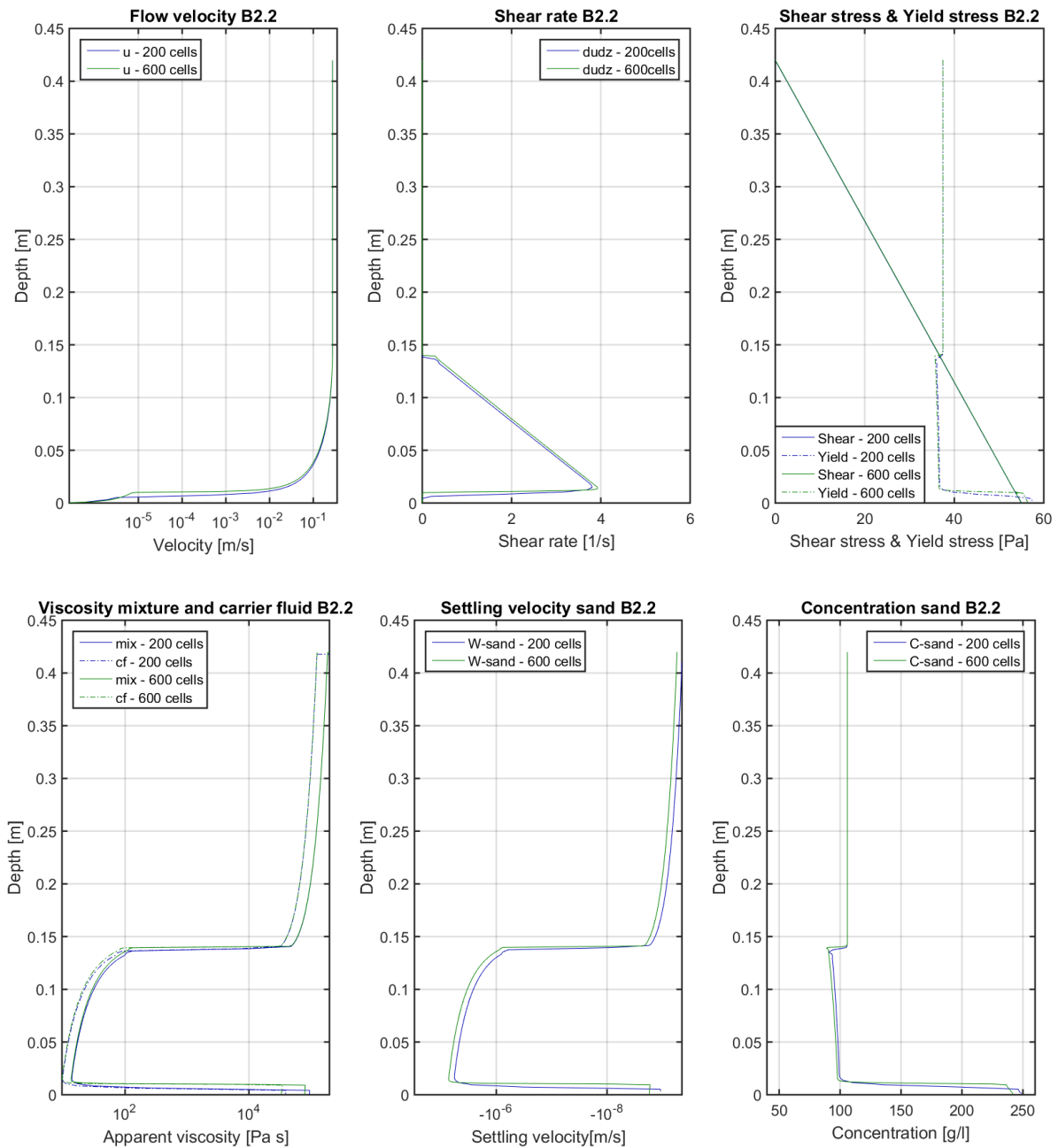
Figure 5-15 B2.1 – 200 grid cells and B2.2 – 600 grid cells. Results Model 2after 2000 s.

In this simulation the number of layers in the grid is increased from 200 to 600. The shape of the profiles remains the same if the grid size is decreased. The minimum and maximum values of the shear rate, viscosity, settling velocity and concentration of sand are smaller and larger respectively and the profile of Simulation B2.2 becomes more smooth. The values of the parameters are averaged over the grid cell. The accuracy of the computation increases if a finer grid size is used. The effect is more pronounced if the difference between yield stress and wall shear stress is very small.

The wiggle seen in Simulation B2.1 in Model 2 and 3 is smoothed. The smaller grid size results in a smaller concentration gradient. Again it affects the other parameters as well.

Time step

The numerical schemes are an approximation of the real differential equations. There exists a (small) numerical error between these two. The scheme is consistent if in the limit of Δt to zero the error becomes zero. For a certain Δt the error is small enough that a further decrease of the time step does not lead to a significant optimization of the calculation. The value of this time step depends on the type of numerical scheme that is used. The time step directly influences the duration of a simulation, therefor a as high as possible time step that does not compromise the quality of the results is always desired.

Figure 5-16 presents a comparison of Simulations B2.1, B2.3 and B2.3.1 of Model 1. Figure 5-17 the results of Model 2. Model 2 and 3 attain a comparable behaviour as seen in the previous simulations. It is assumed that the comparison of the time steps of Model 3 is similar to Model 2.
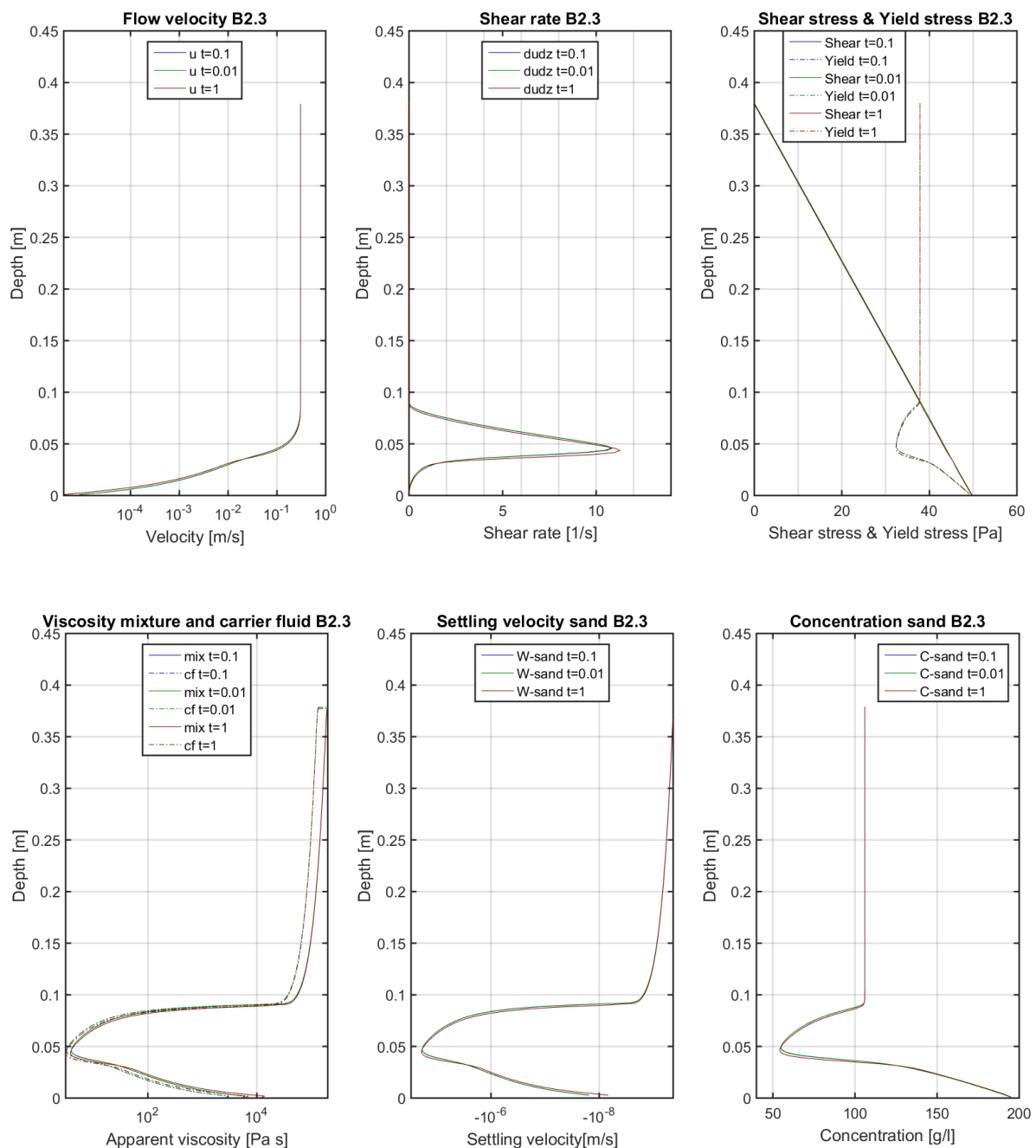
Figure 5-16 Sim. B2.1 – time step 0.1 s, B2.3 – time step 0.01 s, B2.3.1 – time step 1 s of Model 1 after 2000 s.

For all three models the time step was decreased in Simulation B2.3. It appeared that there is no significant difference visible if the time step is smaller than 0.1 s. Therefore the time step is also increased to 1 s in Simulation B2.31. For Model 1 and 2 the results of Simulation B2.1, B2.3 and B2.31 after 2000 s are compared. The increased time step for Model 1 leads to small differences mainly in the sheared zone. This is sound because in this region the properties of the fluid change significantly. For Model 2 the differences are even smaller.
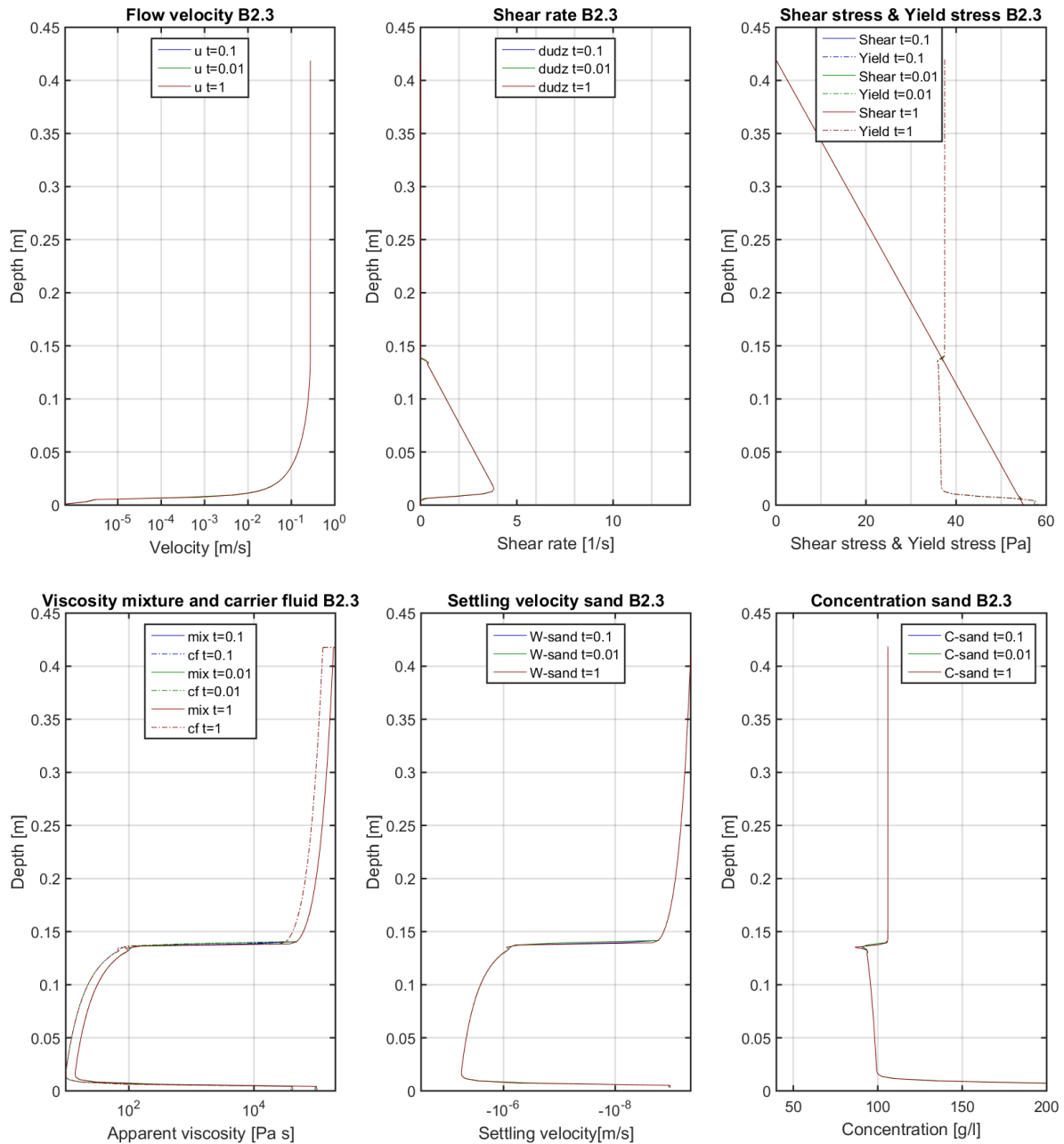
Figure 5-17 Sim. B2.1 – time step 0.1 s, B2.3 – time step 0.01 s, B2.3.1 – time step 1 s of Model 2 after 2000 s.

Qualitative assessment of physical properties

Evolution in time

Figure 5-18 presents the evolution of the flow in time for Simulation B2.1, Model 1. Each line in the graphs is a different moment in time (500, 1000, 2000 s). The profile (at t = 2000 s) differs from Simulation B1.3 due to the non-uniform concentration profile. The velocity profile is modified in the sheared region. In the plug the profile is still (almost) a straight line. This results in a shear rate which is almost zero in the plug-flow and increases in the sheared zone. The apparent viscosity of the carrier fluid and the mixture decrease due to the increasing shear rate. A reduced apparent viscosity of the carrier fluid increases the settling velocity of the sand, resulting in a decrease of the concentration of the sand.
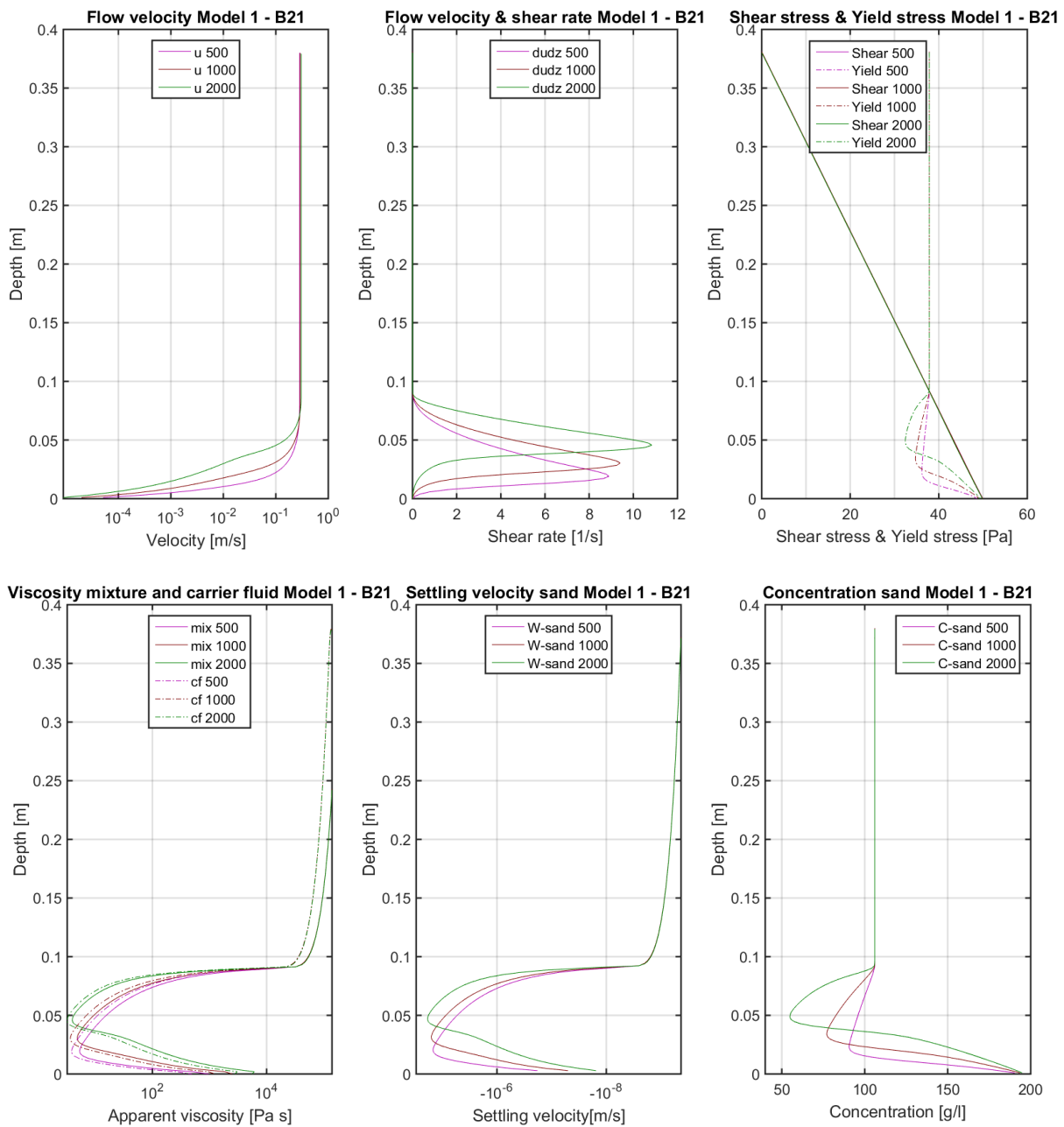
Figure 5-18 Sim. B2.1 of Model 1. Evaluation in time. t = 500 s, t = 1000s, t = 2000 s.

Due to the increased concentration of sand near the bed the yield strength and wall shear stress increase, reducing the velocity near the bed strongly, possibly approximating gel bed behaviour (Talmon et al., 2014; A. Talmon & Mastbergen, 2004).

As sand settles the profiles move upward in time. The height of the plug zone does not decrease significantly because the location of the intersection between the yield stress and shear stress depends on the concentration in the plug and no sediment settles from this region. Due to the settled material the velocity is very small near the bed but not zero. The viscosity, shear stress and yield stress increase and the settling velocity decreases. This region increases if more material settles. The discharge is predefined and the flow depth does not change significantly resulting in a larger mean flow velocity in time. At t=500 seconds the shear rate is largest 20 mm above the bed where most of the material segregates. The change in concentration changes the rheology and velocity profile. The maximum shear rate moves upward resulting in a higher segregation rate higher in the fluid column. This behaviour was visible in all computations of each model.

Comparison of the models

Simulation B2.1 of the three models is compared in Figure 5-19. Again there are clear differences between the three models. The differences are even more pronounced compared to the simulations without segregation. Due to the segregation the flume becomes in-homogeneous. The initial rheology differs per model. Hence the segregation rates differ per model resulting in different concentration profiles over depth. Consequently this enhances the difference in segregation rate.

Model 2 and 3 show the same behaviour. Model 1 predicts a smaller (wall shear) stress (as seen in the non-segregating simulation as well). As a result the sheared region becomes smaller and the hydraulic resistance is reduced. These two effects lead to a higher shear rate (over a smaller depth), diminish the apparent viscosity and increase the settling velocity. These processes enhance each other and the differences between Model 1 and Model 2 and 3 become larger over time. The concentration declines at a smaller depth but is more notable. Due to the power law behaviour of Model 1 the increase or decrease in concentration leads to more gradual changes in the yield stress, velocity, shear rate, apparent viscosity, settling velocity and concentration profile.

Model 2 and 3 have a wiggle in the upper part of the sheared zone. This is very clear in the concentration profile and if one zooms in in the profile of the shear rate, viscosity and settling velocity the wiggle is visible as well. The reason is a steep gradient in the concentration profile. There the system is stiffly coupled, the wiggle appears in the other profiles as well.
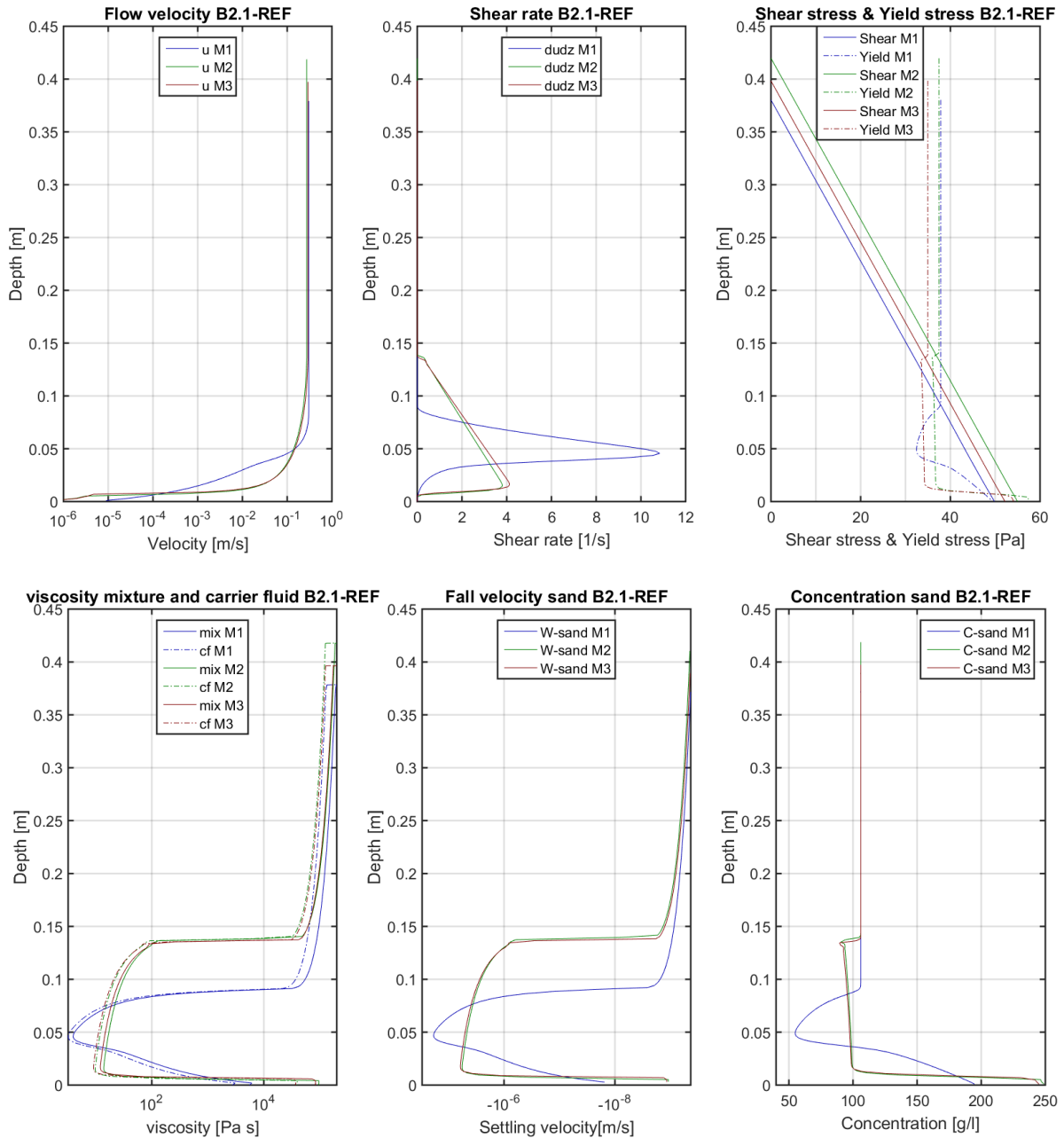
Figure 5-19 Sim. B2.1 Reference simulation. Results of all three models after 2000 s.

Geometry and discharge

In Simulations B2.4 and B2.5 the slope and discharge are adjusted respectively.

Simulation B2.4 (at t=2000) is presented in Figure 5-20. Due to a smaller slope angle, the velocity decreases resulting in smaller shear rates. The discharge is predefined and therefore the flow depth increases. The wall shear stress is closer to the yield stress, i.e. the sheared zone is smaller compared Simulation B2.1. The settling velocity is smaller due the smaller shear rates and increased apparent viscosity and less segregation. Because of the reduced velocity the results of the three models are closer to each other.
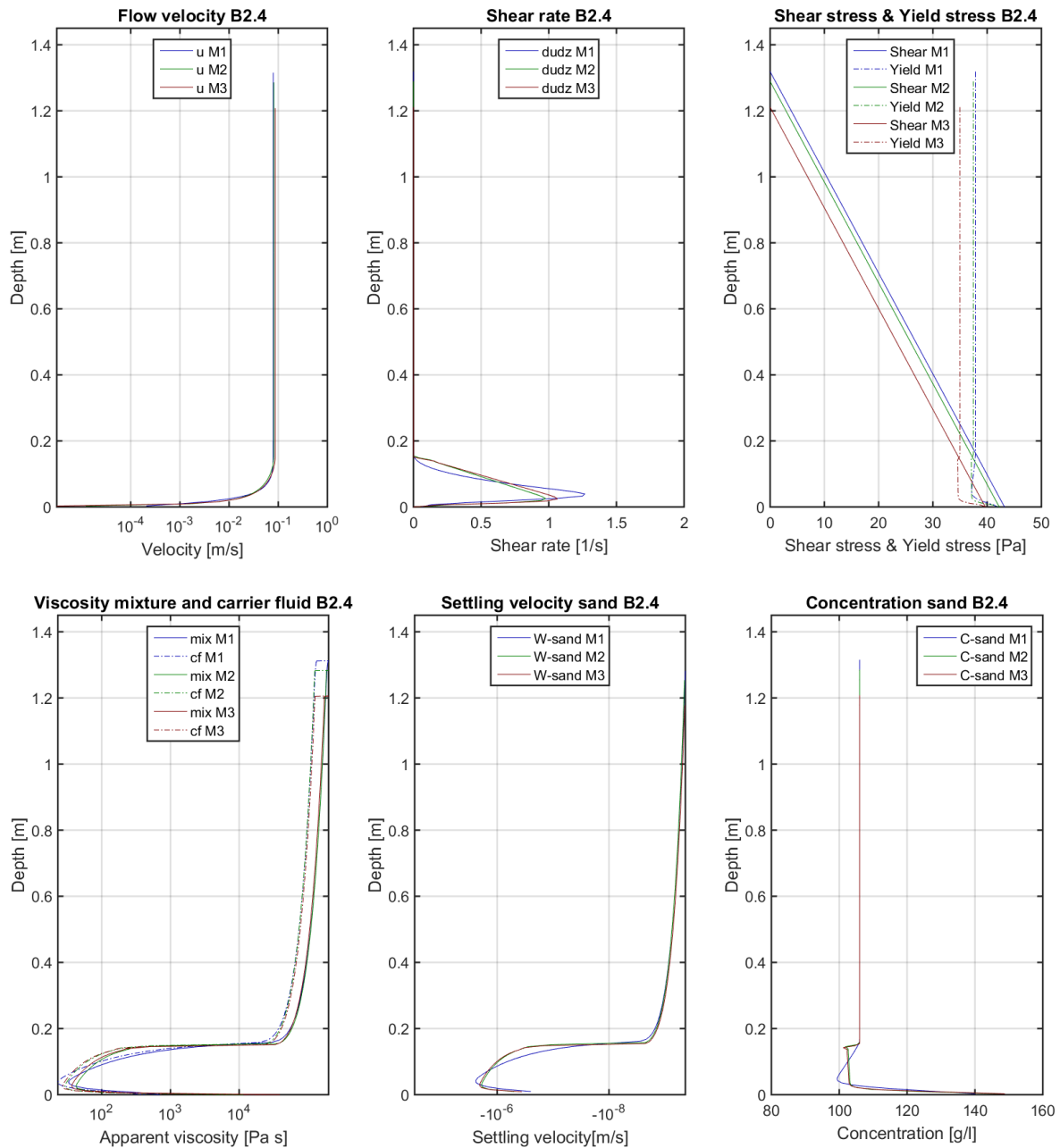
Figure 5-20 Sim. B2.4 – decreased slope angle. Result of all three models after 2000 s.

Simulation B2.5 (at t=2000 s) is presented in Figure 5-21. The increased discharge enhances the flow velocity, the shear rate and flow depth. Due to the larger flow depth the wall shear stress is larger compared to simulation B2.1 and the sheared zone is larger. The apparent viscosity is smaller in the sheared zone resulting in a higher deposition rate.

The wiggle of Model 2 and 3 is not enlarged due to the higher discharge. In Model 1 a new wiggle is present in the sheared region above the gelled bed formation. Also this disturbance has no physical background and is caused by a relatively large gradient in the concentration profile.
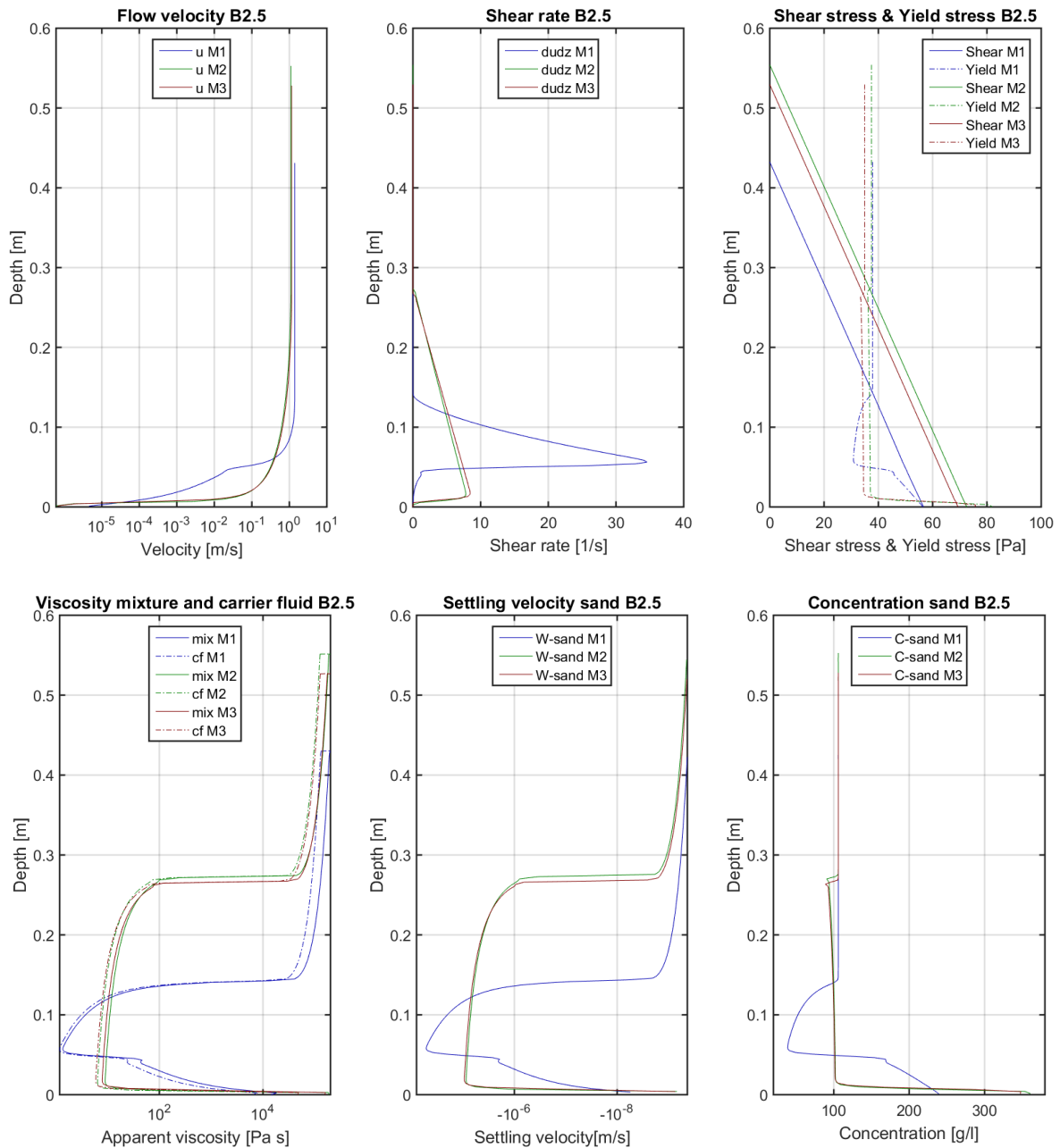
Figure 5-21 Sim. 2.5 increased discharge. Results of all three models after 2000 s.

Figure 5-22 depicts the evolution of the wiggle in time of Model 1. The wiggle is present after 500s and during the computation it is enhanced. The cause of the magnification is twofold. The positive feedback mechanism in the model as explained in Chapter 2 enhances a further decrease in the concentration. It is questionable whether physically the reduction rate is correct. By the best authors knowledge these kinds of belts - with a significant increase and decrease of concentration over small depth - are not measured in experiments. Secondly it is a result of the stiffly coupled processes in the model. The apparent viscosity profile also includes strong variations over depth in the sheared region. These variations are unlikely. The wiggles can be smoothened by averaging the viscosity over several grid cells (depending on the grid size). The apparent viscosity will remain more persistent resulting in smaller deviations in the settling velocity and segregation rate.

Another option is to add (numerical) diffusion in the transport equation. Solely molecular diffusion is present in the model. Shear dispersion is a physical diffusion process which is not accounted for in these simulations. Thereafter it is also common to add artificial diffusion in numerical models.
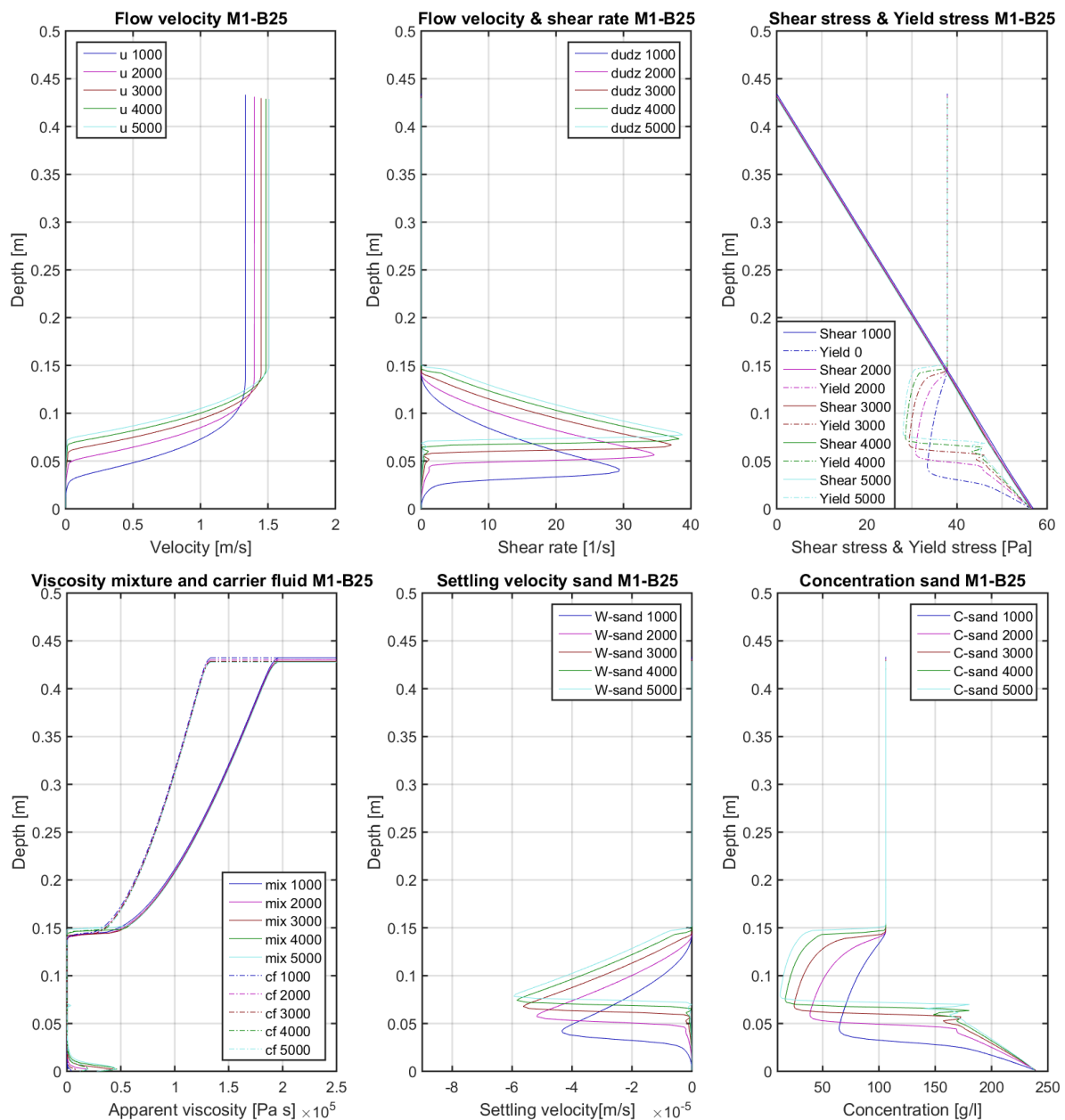
Figure 5-22 Sim B2.5 increased discharge. Evolution of Model 1; 100, 500, 1000, 2000 s.

Practical application

To improve the management of tailings and land reclamation planning it is beneficial to control the segregation of material (Chryss et al., 2012; Kesteren et al., 2015). The operation can be influenced by varying the discharge. Secondly it is influenced by the channel slope. A comparison is made between Simulations B2.1, B2.4 and B2.5 if the mixture in all three simulations would flow along a beach having the same length. A length of 400 m is chosen, an (average) value used in research and numerical simulations before (Blight et al., 1985; Sittoni et al., 2015). The decreased slope results in a lower velocity, hence the mixture requires more time to flow down the beach. While less time is needed if the discharge increases. Table 5-11 presents this required

time per simulation of Model 1 and 2. Figure 5-23 and Figure 5-24 present the results of Model 1 and Model 2 respectively. The increase in concentration (compared to the initial concentration) near the bed is calculated with the graphs and presented in Table 5-11. The area of deposited material is calculated. The results appear to differ per model.

Table 5-11 Average flow velocity, time span and concentration increase of Sim. B2.1, B2.4, B2.5

Model	Simulation	$\bar{u}$ [m/s]	Δt [s]	Concentration increase [kg/m]
1	B2.1	0.26	1538	1.50
1	B2.4 decreased slope	0.075	5333	1.10
1	B2.5 increased discharge	1.16	345	1.14
2	B2.1	0.24	1667	1.06
2	B2.4 decreased slope	0.077	5160	0.98
2	B2.5 increased discharge	0.91	440	0.58

The maximum concentration increase is obtained by Simulation B2.1 for both models. More sand segregates in Model 1; the maximum shear rates in this model are 2.5 times larger compared to Model 2 (also seen in Figure 5-19). The declined slope results in lower shear rates for both models and the shear rates and shear zone are almost even (Figure 5-19). The difference in concentration increase between the two models diminishes near the bottom. The increased discharge results in larger differences in shear stress between the models. Consequently the variation in shear rate between the models is a factor 4-5 and the concentration increase varies a factor 2.

For both models it is more convenient to use a smaller slope or larger discharge to transport the slurry. A smaller slope diminishes the segregation rates. Although more time is required the 'lost' of granular material is reduced. With an increased slope the mixture travels faster. Less time is needed to arrive at the end of the beach. Although the enhanced settling velocities the deposited material is reduced because less time is available to settle. Depending on the type of mixture (Bingham or power law behaviour) one of these two options is preferred, i.e. a reduced slope for Model 1 and an enhanced discharge for Model 2.
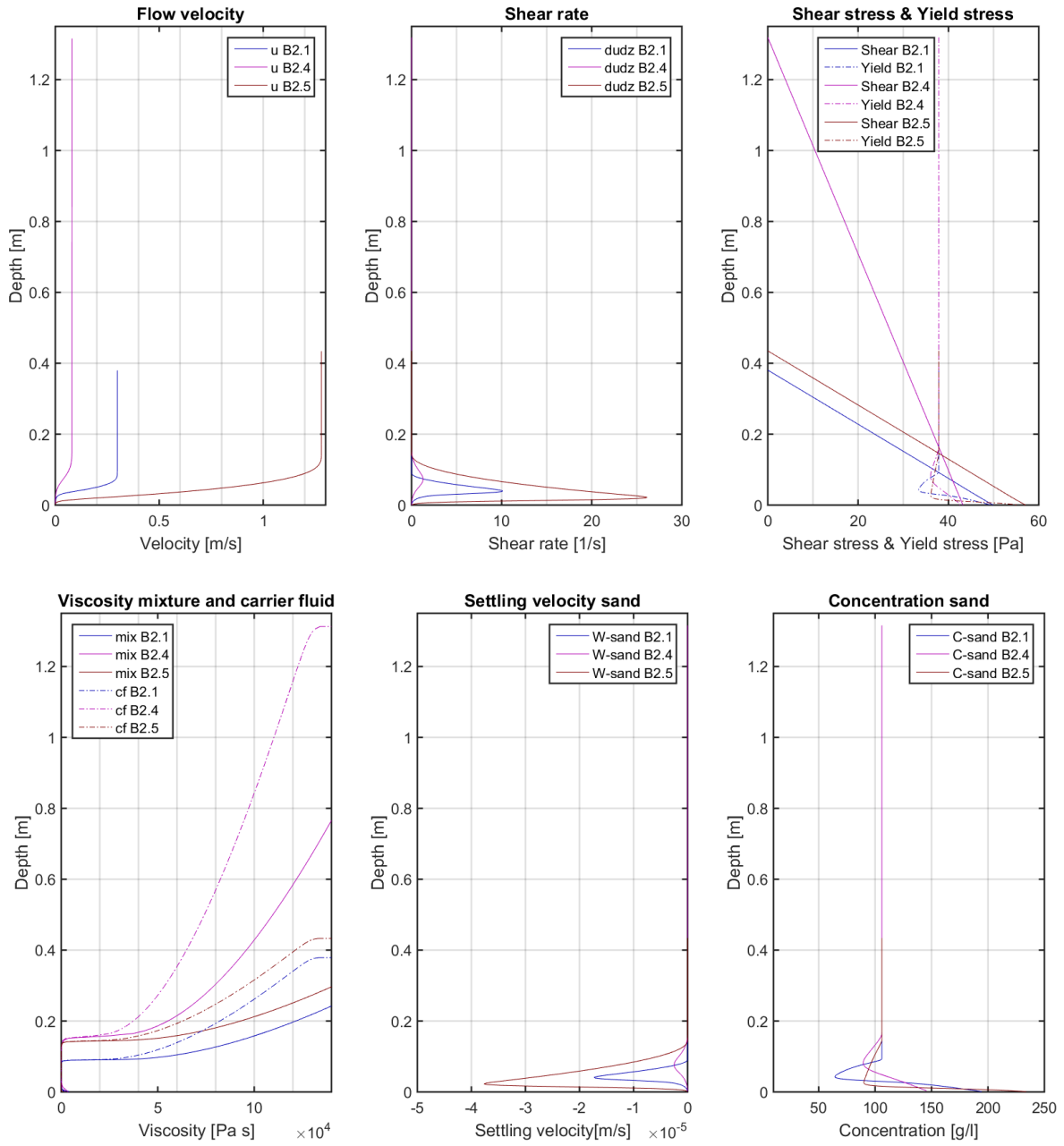
Figure 5-23 Sim. B2.1, B2.4, B2.5. Flow along a beach of 400 m. Comparison of results of Model 1
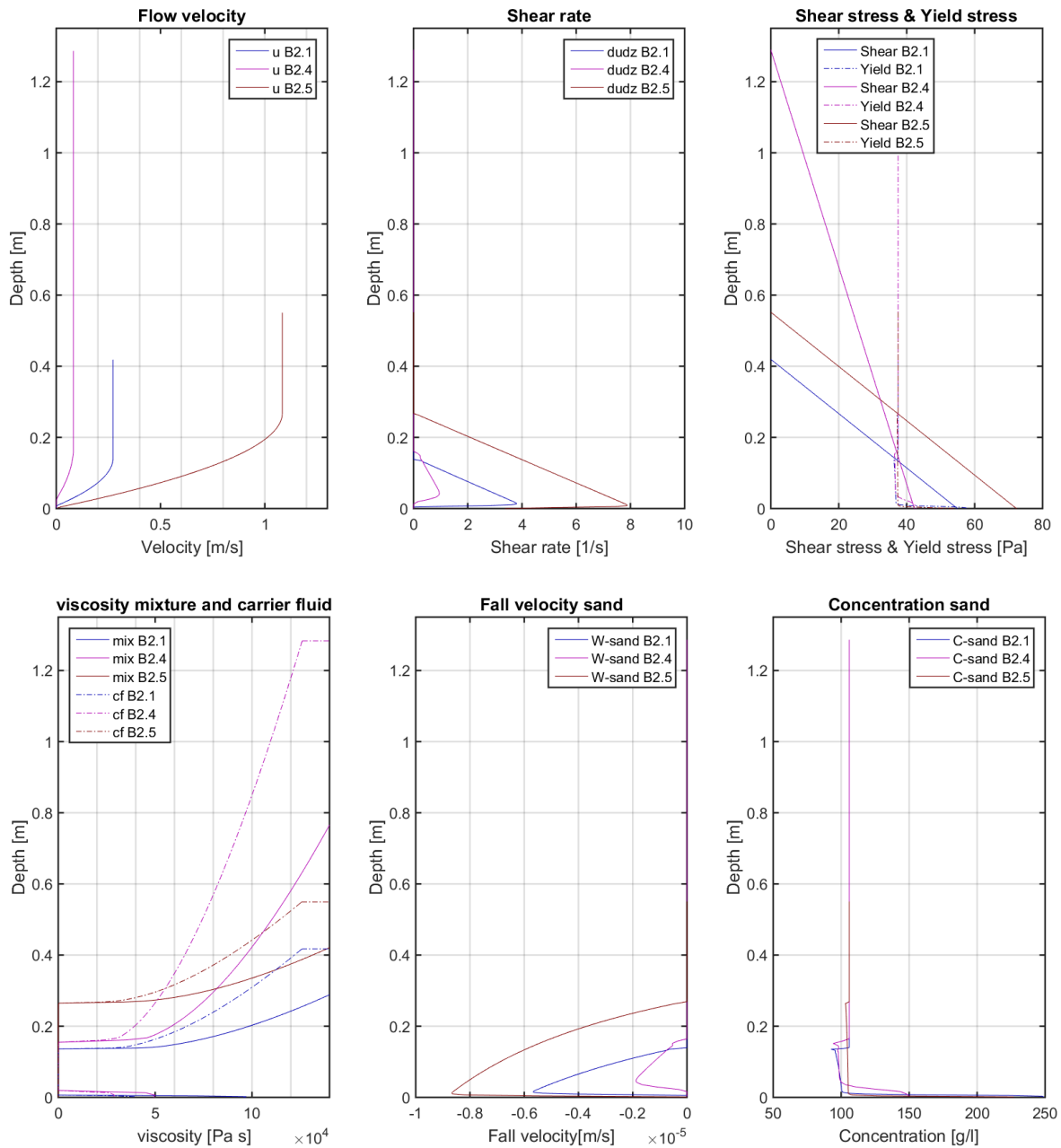
Figure 5-24 Sim. B2.1, B2.4, B2.5. Flow along a beach of 400 m. Comparison of results of Model 2

Prolonged simulations

Simulation B2.1 is used once more to make a long time simulation of 20,000 and 30,000 s (5.5 h and 8.3 h respectively) for all three models. The results are presented in Figure 5-25 and Figure 5-26.

The disturbance of Model 2 and 3 disappeared in the top of the sheared region. A small wiggle is observed in Model 1 above the gelled bed. The disturbance does not significantly increase in time if Figure 5-25 and Figure 5-26 are compared.

The concentrations of the deposited sand range between 106-200 g/l (φ_{sand} = 0.04-0.07) and 200-250 g/l (φ_{sand} = 0.07-0.09) for Model 1 and Model 2 and 3 respectively. Between the sand particles clay is present, hence the maximum concentration of sand might be smaller. Although the value of the simulations is still much less than the $\varphi_{sand, maximum}$ = 0.6. The height of the deposited material does not increase significantly after 20,000 s. Also the concentration of the deposited material of at both times is almost equal.
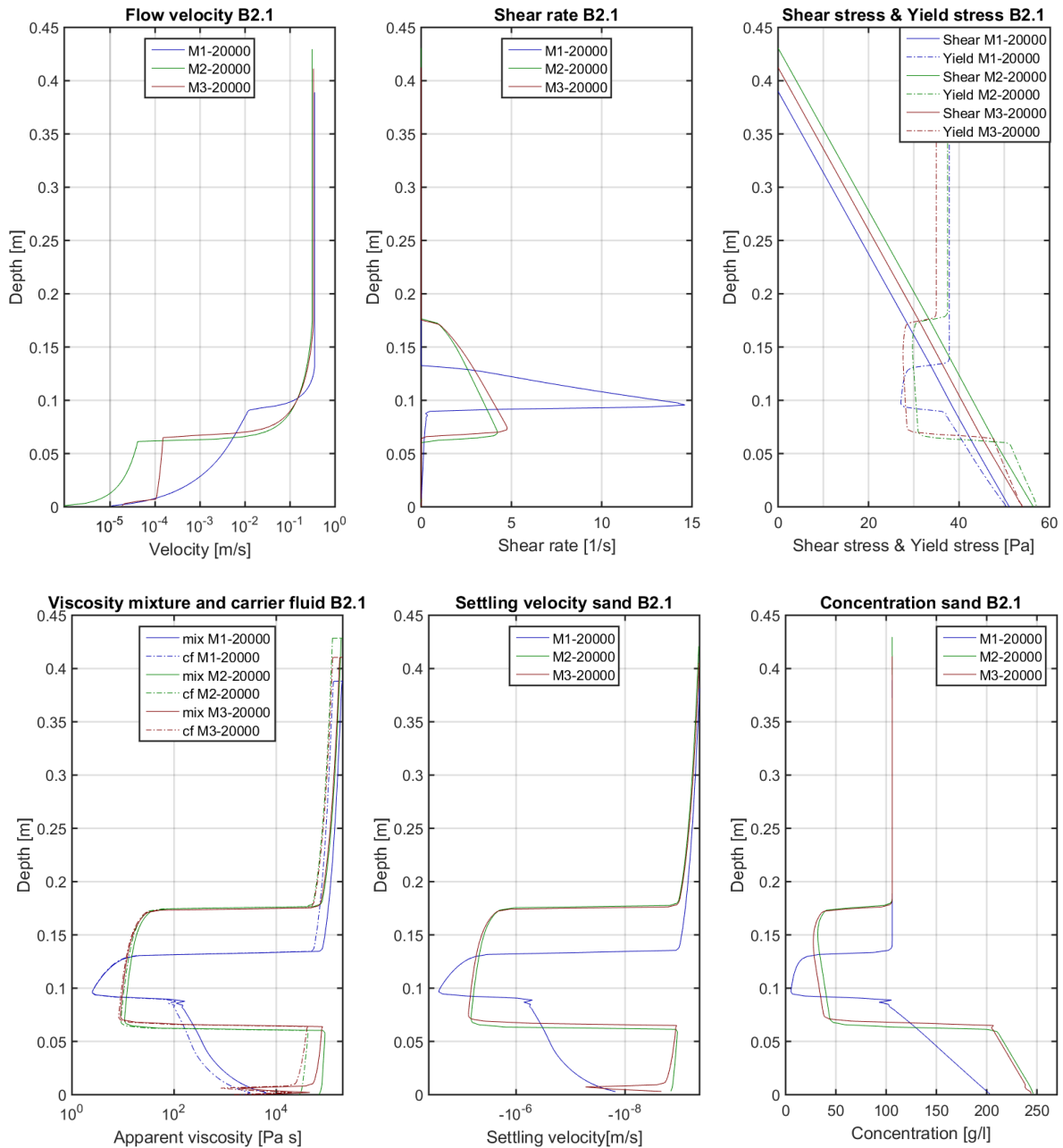
Figure 5-25 Sim B2.1 Prolonged reference simulation – Result of all three models after 20000 s.

The small increase in concentration results in higher yield stresses. These values are relatively sensible because of the high model parameters. The velocity near the bed reduces significantly. Consequently the apparent viscosity increases and a diminished settling velocity is obtained near the bed. The settling of particles in this region is much smaller compared to the region above. Consequently the layer of segregated grows faster in height instead of compacting. The results are compared with observations of (Sanders et al., 2002) presented in Chapter 2. The behaviour of

the experiment and numerical simulation are similar. The measurements depict a strong decrease in velocity if the concentration increases near the bed. However in these experiments the total concentration increase is larger near the bed, 0.1-0.2. Because the rheological properties and flume configuration differ between the experiment and the numerical calculation a satisfactory comparison cannot be made.

Model 3 attains a concerning behaviour. In the concentration profile a small decrease is visible in the gelled bed layer (at 0.01 m). Here the solids concentration increased notably and the reduction is rather unlikely. At the same height a significant change in the segregation rate and apparent viscosity is perceptible. It is unexpected that these disturbances are only the result of the reduction in concentration. A detailed view on the shear stress and yield stress profile tells that these two parameters alternate close to the bottom. Therefore the apparent viscosity alters significantly and as a result the settling velocity as well.

In Figure 5-26 the disturbance is even more pronounced and a new disturbance entered the domain. In an alternating fashion the yield stress and shear stress dominate each other between the bed and 0.05m above. An equal behaviour occurred in the horizontal bed configuration. Although in those simulations the wiggling behaviour started after 500s computation time and also on top of the (thin) gelled bed. In these simulations the disturbance is in the gelled bed. Here the flow velocity is already small (due to the high concentration) and disturbances are minuscule in the shear rate profile.

The disturbances in the viscosity profile are unexpected from nature. These can be diminished by averaging the viscosity over the depth of the gelled bed layer.

The presented long term simulations were performed experimentally to study the model. A tailing would traverse 5.2 km (20,000 s) to 7.8 km (30,000 s) given the mean velocity. To the authors best knowledge this length has never been used in flume experiment and even impossible. For mining operations it is a long distance. Hence the model might still be suitable for the short distances.
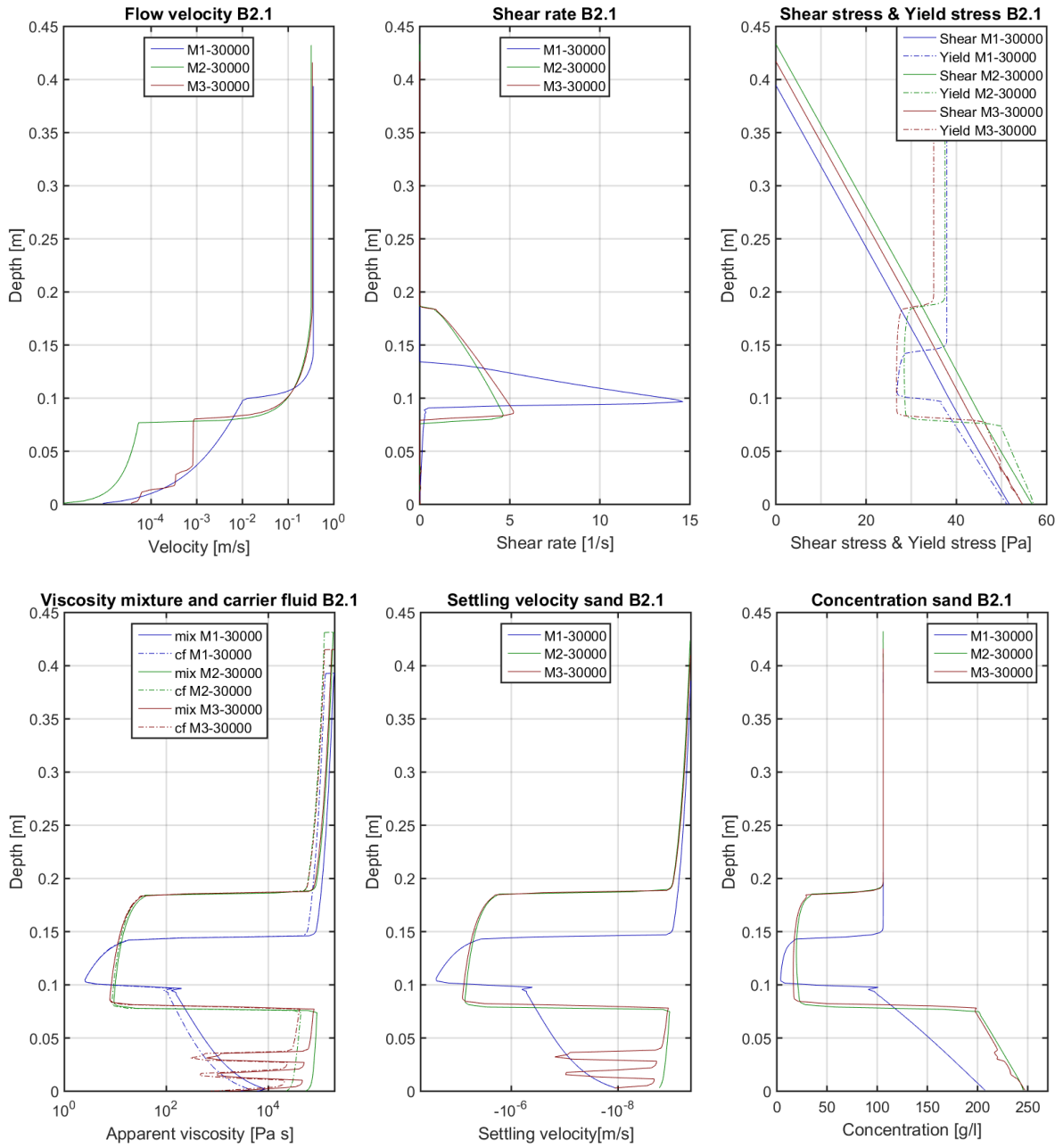
Figure 5-26 Sim. B2.1 Prolonged reference simulation – Result of all three models after 30000 s.

5.4. Verification with physical experiment

In literature different physical studies are found on (segregating) non-Newtonian flow (presented in Chapter 2). The model is verified with the experiment of B. Pirouz (Pirouz et al., 2013). Their paper presents one recorded velocity profile and a relative concentration profile of a certain tailing in a half-pipe channel test. These graphs and corresponding rheological and hydraulic properties (described in the paper) are used for the verification of the model.

The simulation is done with the horizontal bed configuration without settling, i.e. the sheared flow above the segregated material is simulated. Therefor the measured results are used as if these

were static during the experiment. Secondly the slope configuration including settling is used. Both results are compared with the presented velocity profile of the paper.

5.4.1. Experimental set-up

The tilting flume facility is presented in Figure 5-27. A half-pipe was installed in the rectangular flume in the follow-up of the tests. Different pipe diameters were used, 228 mm and 326 mm. The tailings recirculated in the testing facility. In the agitator tank the flume was mixed to obtain a homogeneous concentration distribution over depth prior to the flow through the half-pipe. The pumps drove the flow through transportation pipelines (90 mm). The discharge was adjustable, 2.5-20 l/s. Turbulence within the incoming tailing dissipated in the inlet tank. The flexible hose connected the inlet tank to the half-pipe. The velocity profile was measured at 8 m distance from the pipe entrance.
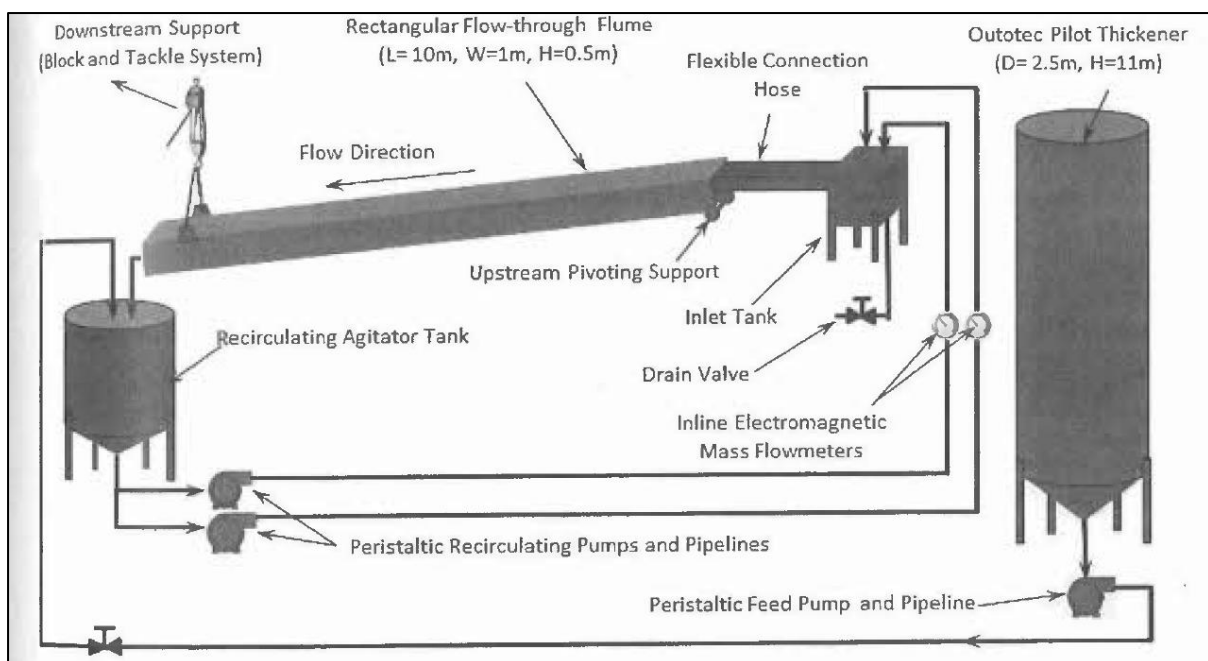
Figure 5-27 Tilting flume facility of (Pirouz et al., 2013).

For every test the solids concentration and flow rate was known. Initially a relative steep slope was installed for which no deposition occurred. Gradually the slope was decreased until material deposited. At this point the flow characteristics were measured.

At the start and end of each test a sample at the end of the flume was taken to determine the rheology. The measurement was done with bob in cup Thermo HAAKE VT550 rheometer. The tailings fitted a Herschel-Bulkley model.

5.4.2. Model input parameters

The (measured) hydraulic properties are presented in Table 5-12.

Table 5-12 Hydraulic parameters of (Pirouz et al., 2013).

Parameter		Value	unit
Diameter pipe	D	326	[mm]
Discharge	Q	13.79	[l/s]
Depth	H	61	[mm]
Width	W	254	[mm]
Flow Area	A_{wet}	0.0108	[m²]
Surface velocity	$u_{surface}$	1.7	[m/s]
Average velocity	$u_{average}$	1.28	[m/s]
Slope	$\sin(\theta)$	0.05	[-]

The rheological properties and concentrations are derived from the paper. The total concentration is given by mass. The exact volume concentrations per fraction are not presented. The value is converted to volume concentrations assuming a density of ρ = 2650 kg/m³ for all the granular material. A figure presenting the sieve curve analysis is used to determine the concentration per solids fraction. 43 % of the material has diameter smaller or equal to 80 μm. In the table of the paper there is no information on fractions smaller than 80 μm. Regarding coarse material the lower bound of the diameter is 44 μm. It is assumed that 40 % of the material is clay and 60% is sand.

Table 5-13 Soil content and rheological parameters of (Pirouz et al., 2013).

Parameter		Value	unit
Solids concentration	φ_{sol}	0.40	[-]
Sand concentration	φ_{sa}	0.24	[-]
Clay concentration	φ_{cl}	0.16	[-]
Yield stress	τ_y	10.1	[Pa]
Surface velocity	μ	0.596	[Pa s]
Flow rate	n	0.573	[-]

The 1DV model has a different geometry therefore some of the parameters demand a conversion. Because the parameters fit a Herschel–Bulkley model, theoretical Model 1 is used to simulate the flow in the 1DV model. The input parameters of Model 1 are adapted to agree with the values of yield stress and viscosity and the sediment concentrations. The corresponding model parameters (Model 1) for the horizontal bed configuration are:

Table 5-14 Parameters of Model 1 to simulate the experiment to simulate the conditions after 6 s as if they were static.

Model 1		unit
n_f	2.5	[-]
a	1.56	[-]
A_y	2403	[-]
A_μ	3.975	[-]
β	2.7	[-]
$\phi_{sasi,max}$	0.6	[-]
μ_w	0.001	[Pa s]

m	5000	[-]
h	0.56	[m]
$\bar{u}$	1.2 – 1.3 – 1.35	[m/s]

For the segregating flow along a slope a conversion of the input parameters was required as well. The weight of the water results in a downward force acting on the bottom of the pipe. This force is equal to the force in the 1DV model. The wall shear stress along the wet area is the ratio of the force and the perimeter. Because the hydraulic radius differs between the circulum flume and 1DV model, the actual wall shear stress in the model is recalculated. The flow depth and mean flow velocity are equal to the ones in the experiment. The required slope for the 1DV model is recalculated with the wall shear stress of the 1DV model. The calculation is presented in Appendix I. Table 5-15 presents the resulting input parameters.

Table 5-15 Parameters Model 1 to simulate segregating flow along a slope of (Pirouz et al., 2013)

Model 1		unit
n_f	2.5	[-]
a	1.56	[-]
A_y	2403	[-]
A_μ	3.975	[-]
β	2.7	[-]
$\phi_{sasi,max}$	0.6	[-]
d_{50}	250	[μm]
μ_w	0.001	[Pa s]
m	5000	[-]
h	0.61	[m]
$\bar{u}$	1.28	[m/s]
D-pipe	326	[mm]
Q	0.0781	[m³/s]
Wet area	0.061	[m2]
Slope: $\sin(\theta)$	0.019	[-]

5.4.3. Result

Horizontal bed – non-segregating

The non-segregating flow on a horizontal bed is compared to the measured velocity profile of the experiment and presented in Figure 5-28. In this experiment the flow circulated in the test facility for an unknown amount of time before the velocity was measured. During this time segregation occurred and a bed layer was formed. The thickness of this layer is estimated from the velocity profile. Every time the fluid passed the mixing tank the mixture was mixed and the initial (homogeneous) concentration was obtained.

In the simulation of the model this effect is not coded. Therefore the velocity profile of the simulation is shifted upward to a point right above the formed bed.

Figure 5-28 presents model simulations of u=1.2; 1.3 and 1.35 m/s. For the latter the model is able to simulate the measured velocity profile.
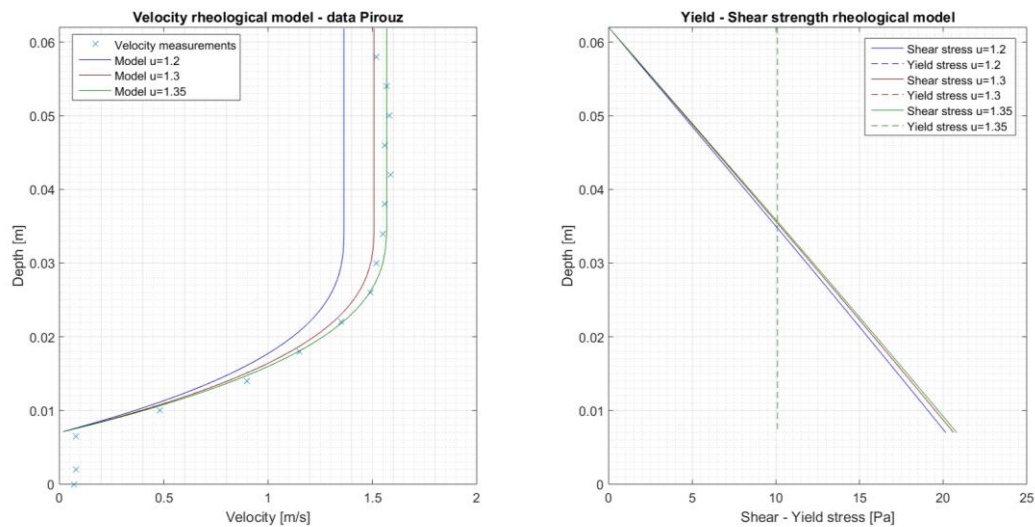
Figure 5-28 Result simulation non-segregating flow with different flow velocities (lines 1.2, 1.3 and 1.35 m/s). Left: velocity including measurements (Pirouz et al., 2013). Right shear stress and shear rate profile.

Slope – segregating

For the slope configuration two simulations were done. For the first simulation the parameters as presented in Table 5-15 were used. The blue line in Figure 5-29 presents the result. The flow velocity is too low and the water level to high compared with the experiment. The calculated slope is not steep enough.

The dissimilarity can have three reasons. First the calculation of the adjusted hydraulic parameters is not detailed enough. In a pipe the downward force cannot be calculated exact using the method as explained above. The modes of water parallel to the centre line of the pipe exhibit a forcing, affecting the downward directed force. Secondly the flume was circulated for a certain amount of time before the velocity profile was obtained. Although the flume was constantly re-mixed, material could segregate. The slope of the deposited material may deviate from the slope of the flume. Lastly because of the short simulation time a numerical artefact due to spin-up may have an influence.

The slope ($\sin(\theta)$) is increased to 0.025 in the second simulation. The result is the red line in Figure 5-29. The curve fits the measured velocity.
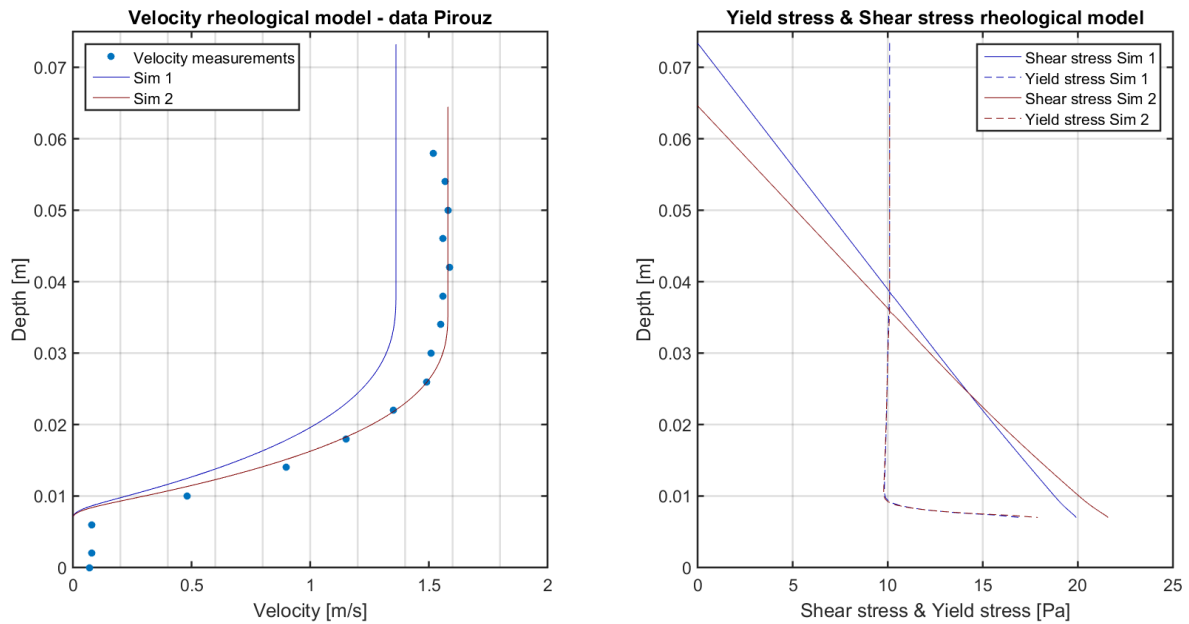
Figure 5-29 Results segregating flow for different slopes. Left: velocity profiles including measurements (Pirouz et al., 2013). Right: Shear stress and yield stress profile.

5.5. Conclusions

5.5.1. Non-Segregating flow

The adjusted 1DV model is able to simulate a laminar non-segregating open channel flow on a horizontal bed (including prescribed water depth and flow velocity) as well as on a slope (with a prescribed discharge).

- The results are compared to the analytical solution of P. Slatter and a good agreement is found if the sheared region is larger than four grid cells. In simulations where the sheared zone covers a small amount of grid cells (1-3) there is a larger difference between the numerical and analytical solution.
- The numerical mutation of the yield stress results in a modification of the velocity profile and shear rate profile. A large value of parameter m (5E3) is required to minimize this effect as seen from the comparison with the analytical solution.

The coupling of the rheological and hydrological processes corresponds to the results of (numerical) experiments found in literature.

- In the plug-zone the velocity profile is a straight line, the shear rate is close to zero, the apparent viscosity has a relative large value.
- In the sheared zone the velocity profile has a parabolic shape for Bingham fluids and power law shape for power law fluids. The shear rate increases linearly and the apparent viscosity decreases drastically with vertical coordinate.
- At the bed the velocity is zero, the shear rate decreases to zero and the apparent viscosity increases.

- If the solids concentration or viscosity increases the differences between the models become larger. A logical result due to the differences in the formulations.

5.5.2. Segregating flow

Regarding the laminar segregating flows the adjusted 1DV model is able to simulate these flows on a sloping bed.

- The numerical mutation of the yield stress results in a modification of the velocity profile and shear rate profile. A large value of parameter m (5E3) is required to minimize this effect.
- If a horizontal bed and a prescribed mean velocity and flow depth are used a wiggling behaviour is found in the simulation. This is a result of the prescribed boundary conditions who force the fluid to flow without the possibility to adapt the mean flow velocity or flow depth. The velocity profile is transformed resulting in a modification of the shear stress, yield stress, viscosity, settling velocity and concentration profile. The yield stress and shear stress profile cross multiple times (in the sheared and unsheared zone) generating disturbances in the system.

- With the use of a sloping model the wiggling behaviour as seen in the horizontal bed simulation does not occur.
- A small single wiggle (non-physical) is observed in the profiles of Model 1, 2 and 3. The cause is a steep gradient in the concentration profile. The wiggle may growth (slightly) or decrease in time. No additional wiggles are introduced.
- If a smaller grid size is used, the accuracy of the computation increases. The wiggle in the models is smoothed.
- A computational time step smaller than 0.1s does not influence the model results significantly.
- If the simulation time is long enough, the area of deposited material does not change significantly. The maximum sand concentration in the simulations is 0.04-0.09 (by volume). The value is below the maximum concentration of sand. Due to the very small settling velocities the concentration increase is minimized in this area.
- The wiggles can be smoothened by averaging the viscosity over several grid cells and/ or adding (numerical) diffusion.
- For a long time simulation along the slope disturbances enter the domain of Model 3. The disturbances are generated by large changes in the apparent viscosity in gelled bed layer. They are non-physical.
- Mutations of the slope and predefined discharge result in changes in the flow velocity and water depth according to the results of physical experiments. Hence the shear stress, apparent viscosity, settling velocity and concentration change compared to the reference simulation.

- Two simulations are performed to model a measured flow of an experiment. These are a first step towards the modelling of existing flows. The preliminary results are promising. Although only a velocity profile of one physical experiment is simulated. More verifications are necessary to quantify the performance of the model. Especially the simulation of flows through a wide rectangular (shaped) channel would give more insight.

6. Conclusions & Recommendations

The objective of this thesis was to study the definition of the rheological properties including segregation of a laminar non-Newtonian flow. Thereafter these formulations are implemented in an existing numerical 1DV model – analogous to Delft3D - to study the coupling between the hydrodynamics, rheology and segregation.

Literature study

The non-Newtonian properties and the coupling of the hydrodynamics, rheology and segregation challenge the research towards these flows. Nonetheless the industry demands to study and simulate these flows to optimize their execution processes.

- Within this thesis the focus was on laminar high concentrated mud-sand flows. However research towards the processes in the transitional regime between laminar and turbulent flow and turbulent flows would enhance the applicability of the model (possibly by extension of the model).
- The study takes into account the segregation of granular material. This segregation induces differences in viscosity affecting the Re. Transitions between the laminar and turbulent regime might occur at different Re.
- The segregation leads to a non-homogenous distribution with layers of different densities. These stratifications may cause instabilities and enhancement of vertical and horizontal processes (e.g. sediment transport).
- This model focusses on the non-Newtonian flows whereas Delft3D includes segregation in Newtonian flows. The transition between these two is described in literature but not implemented in the model to date.

Rheological models

Three rheological models, derived from three different fields of expertise, are calibrated and compared with experimental data. All three models are able to quantify the measured yield stress and plastic viscosity as a function of an-organic material and water content. The sensitivity analysis proves that a profound measurement of a mixture (e.g. maximum solids concentration) improves the model predictions.

If the concentration and/ or Sand to Solids ratio increase the differences between the models and between the model predictions and data become more profound. The variation between the models is also found in the mathematical formulation. The divergence with the data can be caused by the formulation, application range of the model and/ or the accuracy of the measurement.

- The formulations can be improved by incorporating (more) physical properties of the material as parameters instead of determining them empirically.
- An experiment which includes rheological measurements and measurements of the physical properties of the material for different water contents, Sand to Solids ratios and total volume concentrations could contribute to this improvement. The high concentration ranges may hamper an accurate measurement of the physical properties. A

high concentration in a diluted carrier fluid may hinder a correct measurement of the strength. Although the measurement devises are still in development enabling more accurate measurements in future.

- Especially for the high Sand to Solids ratios, where the formation of a granular skeleton is possible, the formulations need an optimization or extension.

Segregation model

In Chapter 3 a segregation model is presented which is analogous to existing models. The model is based on a theory concerning shear induced settling and hindered settling. The two theories are both verified with experiments. To date the new integral model including both physical processes is not compared to data.

- To increase the solidity of the model it is recommended to compare the segregation model with physical experiments. Also these experiments should cover a wide range of water contents, Sand to Solids ratios and total volume concentrations to contribute to this verification and possibly enhancement of the formula.
- The segregation model covers only granular concentrations to 25% by volume. An extension to higher sand concentrations is required.

Numerical model

The three rheological models and the segregation model are implemented in a 1DV model, analogous to Delft3D. The objective is to understand the numerical application of the formulas in a 1DV model before they are implemented and used in a (more complicated) 2D and 3D environment. Besides the implementation of the models, general extensions of the model were necessary.

- The linear concentration theory as explained in Chapter 2 is used in rheological Model 1 and 2. The theory includes the maximum solids content of granular material, $\varphi_{sasi-max}$. This value can be estimated based on the fraction of sand and silt within the mixture. Currently the parameter is a predefined value of the mixture. From the theoretical analysis based on the work of (A. D. Thomas, 1999) it was concluded that an adaption of this value increases the accuracy of the prediction.
  It is expected that the implementation of an exact calculated value of the $\varphi_{sasi-max}$ improves the accuracy of the calculation. Thereafter if the model is able to calculate the value based on the concentrations, it is also possible to program the formula such that the value is updated for changing concentrations due to segregation.
- To model these laminar flows, the k-ε model is not involved in the computations, i.e. the only present viscosity is the molecular viscosity. Delft3D includes the possibility to model the correct flow state (turbulent or laminar) based on the Re and gradient in solids concentration. It would be an interesting study to test whether Delft3D can model laminar and turbulent flows and the transition zone without a predefinition of the user. The theoretical study mentioned above would support this research.

Numerical simulation

The model is able to simulate a laminar non-Newtonian flow along a slope including segregation. The three rheological models are analysed based on three numerical parameters, (i.e. yield stress parameter m, grid spacing and time step) and globally physical parameters (i.e. solids

concentrations, yield stress and viscosity). The flow model is verified based on an experiment of B. Pirouz.

- A profound sensitivity analyses is suggested on all parameters within the rheological model to attain a better understanding of the (limits of the) model. The recommendation also applies to the segregation model.
- The verification of the simulations including segregation is only done analytical and qualitatively based on a single velocity profile. Increasing the amount of verifications with experiments (in rectangular flumes) contributes to a better understanding of the numerical model.
- The 1DV model can be used as an alternative of an analytical model as presented in the work of (Sisson et al., 2012a).
- The two Bingham models including segregation obtain a reduced (nearly) constant concentration in the shear zone. It gives rise to a simplified schematization of the calculation.
- This model only takes into account the one dimensional vertical processes whereas in nature flows have three dimensional structures. Implementation of the formulas in Delft3D would enable to model the three dimensional structures as well. However this also requires more research towards these three dimensional flows.

A new step forward is made in the research towards mud-sand flows by defining and implementing these rheological formulas and segregation formula in a 1DV numerical model. Along with this new challenges are discovered which request further research.

Nomenclature

A	Empirical parameter
A_y	Parameter yield stress Model 1
A_μ	Parameter viscosity Model 1
A_{clay}	Clay activity
a	anisometric parameter
B	Empirical parameter
K_y	Power yield stress Model 2
K_μ	Power viscosity Model 2
C_y	Empirical parameter yield stress Model 3
c_l	Concentration of certain fraction
c_u	Undrained shear stress
d	Particle diameter
D	Empirical parameter viscosity Model 3
D_s	Molecular diffusion
g	Gravitational acceleration
H	Total water depth
h	Mean water depth
h_0	Initial flow depth
k	Layer number in numerical model
K	Consistency index
K_y	Parameter yield stress Model 2
$k_{yield}\varphi_{sandmax}$	Empirical parameter yield Model 3
$k_{visc}\varphi_{sandmax}$	Empirical parameter viscosity Model 3
K_μ	Parameter viscosity Model 2
L	Typical length scale
LI	Liquid Index
LL	Liquid limit
m	Emperical parameter yield stress modification
m_1	Amount of connected particles within the primary aggregate
m_2	Rate of increase of the size of the aggregate
n	Flow index
n_{sand}	Porosity of sand
n_f	Fractal dimension
p	Hydrostatic pressure
PI	Plasticity Index
R_a	Size of the aggregate
R_h	Hydraulic radius
R_p	Size of the primary particle
t	Time
u	velocity x-direction
$\bar{u}$	Average velocity x-direction
v	velocity y-direction
W	Water content

W_{rel}	Relative water content
$w_{sand,0}$	Settling velocity single sand grain
w_{sand}	Settling velocity sand
x	Horizontal coordinate
y	Horizontal coordinate
z	Vertical coordinate

Greek symbols

α	Empirical parameter shear induced hindered settling equation
β	Empirical parameter of linear concentration
Γ_t	Turbulent diffusion
ε	Turbulent eddy dissipation
λ	Linear concentration
ρ	Density
ρ_a	Density of aggregate
ρ_{cl}	Density of clay
ρ_{cf}	Density of carrier fluid
ρ_s	Density of solids
ρ_{sa}	Density of sand
ρ_w	Density of water
$\rho_{w\&f}$	Density of water and fines
ρ_{sol}	Density of solids
ρ_0	Average density
φ_{cl}	Volume concentration of clay
φ_{si}	Volume concentration of silt
φ_{sa}	Volume concentration of sand
$\varphi_{sa,max}$	Maximum volume concentration of sand
φ_{sol}	Volume concentration of all particles
ξ_{clay}	Mass content of clay
ξ_0	Minimum clay content to obtain cohesive behaviour
μ	Viscosity
$\mu_{apparent}$	Apparent viscosity
μ_w	Dynamic viscosity of water
μ_p	Plastic viscosity
μ_{cf}	Viscosity of carrier fluid
μ_{mix}	Viscosity of mixture
σ_y	Yield pressure
τ	Shear stress
τ_y	Yield stress
τ_w	Wall shear stress
θ	Angle of the slope
ν	Kinematic viscosity
ν_h	Eddy viscosity
ν_t	Turbulent kinematic viscosity
ζ	Fluctuation from mean water level
Ψ	Solids fraction
$\dot{\gamma}$	Shear rate
$\dot{\gamma}_c$	Critical shear rate

List of Figures

List of Tables

Bibliography

Alam, N., Ozdemir, O., Hampton, M., & Nguyen, A. (2010). Dewatering of coal plant tailings: Flocculation followed by filtration. *Elsevier*.

Bagnold, R. A. (1954). Experiments on a gravity-free dispersion of large solid spheres in a Newtonian fluid under shear.

Blight, G., Thomson, R., & Vorster, K. (1985). Profiles of hydraulic-fill tailings beaches, and seepage through hydraulically sorted tailings. *J. S. Afr. Inst. Min. Metall.*, *85*(5), 157–161. http://doi.org/10.1016/0148-9062(86)91253-2

Bushell, G., Yan, Y., Woodfield, D., Raper, J., & Amal, R. (2002). On techniques for the measurement of the mass fractal dimension of aggregates. *Elsevier*.

Chryss, A., Fourie, A. B., Mönch, A., Nairn, D., & Seddon, K. D. (2012). Towards an Integrated Approach to Knowledge Management. *The Journal of the Southern African Institute of Mining and Metallurgy*, *112*(NOVEMBER). Retrieved from http://citeseerx.ist.psu.edu/viewdoc/download?doi=10.1.1.199.4255&rep=rep1&type=pdf

Coussot, P. (1997). *Mudflow rheology and dynamics*. Balkema.

Dankers, P. J. T., Sills, G. C., & Winterwerp, J. C. (2008). On the hindered settling of highly concentrated mud-sand mixtures. *Proceedings in Marine Science*, *9*, 255–274.

Dankers, P. J. T., & Winterwerp, J. C. (2007). Hindered settling of mud flocs: Theory and validation. *Continental Shelf Research*, *27*(14), 1893–1907. http://doi.org/10.1016/j.csr.2007.03.005

Deltares. (2014). *Delft3D - 3D/2D modelling suite for integral water solutions*.

Dyer, K., & Manning, A. (1999). Observation of the size, settling velocity and effective density of flocs, and their fractal dimensions. *Journal of Sea Research*, 87–95.

Fitton, T. G., & Slatter, P. T. (2013). A tailings beach slope model featuring plug flow. In *Paste 2013* (pp. 493–503).

Fitton, T., Williams, M., Seddon, K., Bhattacharya, S., & Chryss, A. (2007). Simulation of Thickened Tailings Stacks. In *International seminar on Paste and Tickened Tailings* (p. 305).

Flemming, B. W. (2000). A revised textural classification of gravel-free muddy sediments on the basis of ternary diagrams. *Continental Shelf Research*, *20*(10-11), 1125–1137. http://doi.org/10.1016/S0278-4343(00)00015-7

Haldenwang, R., & Slatter, P. (2006). Experimental procedure and database for non-Newtonian open channel flow. *Journal of Hydraulic Research*, *44*(2), 283–287. http://doi.org/10.1080/00221686.2006.9521682

Haldenwang, R., Slatter, P., & Chhabra, R. (2010). An experimental study of non-Newtonian fl uid fl ow in rectangular fl umes in laminar , transition and turbulent fl ow regimes JOURNAL OF THE SOUTH AFRICAN. *Journal of the South African Institution of Civil Engineering*, *52*(1), 11–19.

Horsley, M. R., Horsley, R. R., Wilson, K. C., & Jones, R. L. (2004). Non-Newtonian effects on fall velocities of pairs of vertically aligned spheres. *Journal of Non-Newtonian Fluid Mechanics*, *124*(1-3 SPEC. ISS.), 147–152. http://doi.org/10.1016/j.jnnfm.2004.09.002

Jacobs, W., Le Hir, P., Van Kesteren, W., & Cann, P. (2011). Erosion threshold of sand-mud mixtures. *Continental Shelf Research*, *31*(10 SUPPL.), S14–S25. http://doi.org/10.1016/j.csr.2010.05.012

Jacobs, W., van Kesteren, W. G. M., & Winterwerp, J. C. (2008). Strength of sediment mixtures as a function of sand content and clay mineralogy. In *INTERCOH 2005* (pp. 91–107).

Kesteren, W. Van, Ree, T. Van De, Talmon, A., Lucas Pardo, D. M., Luger, D., & Sittoni, L. (2015). A LARGE-SCALE EXPERIMENTAL STUDY OF HIGH DENSITY SLURRIES DEPOSITION ON BEACHES. In *TS17: 17th Inernational conference on Transport and Sedimentation of solids*.

Kranenburg, C. (1994). The fractal structure of cohesive sediment aggregates.pdf. *Estuarine, Coastal and Shelf Science*, *39*, 451–460.

Litzenberger, C. G. (2003). *Rheological study of kaolin clay slurries*.

Lourenco, P., & Pina-Henriques, J. (2006). Validation of analytical and continuum numerical methods for estimating the compressive strength of masonry, 1977–1989.

Merckelbach, L. (2000). *Consolidation and strength evolution of soft mud layers*. Retrieved from http://www.narcis.nl/publication/RecordID/oai:tudelft.nl:uuid:0f3a28e2-d652-4162-a980-116a4f616be4

Merckelbach, L. M., & Kranenburg, C. (2004). Determining effective stress and permeability equations for soft mud from simple laboratory experiments. *Géotechnique*, *54*(9), 581–591. http://doi.org/10.1680/geot.2004.54.9.581

Mietta, F., Chassagne, C., Manning, A. J., & Winterwerp, J. C. (2009). Influence of shear rate, organic matter content, pH and salinity on mud flocculation. *Ocean Dynamics*, *59*(5), 751–763. http://doi.org/10.1007/s10236-009-0231-4

Mitsoulis, E., & Zisis, T. (2001). Flow of Bingham plastics in a lid-driven square cavity. *Journal of Non-Newtonian Fluid Mechanics*, *101*(1-3), 173–180. http://doi.org/10.1016/S0377-0257(01)00147-1

Mueller, S., Llewellin, E., & Mader, H. (2010). The rheology of suspensions of solid particles. *Proc. R. Soc. A*, *466*(4), 1201–1228. http://doi.org/10.1007/BF01432034

Papanastasiou, T. C. (1987). Flows of Materials with Yield. *Journal of Rheology*, *31*(5), 385. http://doi.org/10.1122/1.549926

Pennekamp, J. G. S., Talmon, A. M., & van Kesteren, W. G. M. (2010). Determination of Non-

Segregating Tailings Conditions. In *19th World dredging congress* (pp. 848–858).

Pirouz, B., Seddon, K., Pavissich, C., Williams, P., & Echevarria, J. (2013). Flow through tilt flume testing for beach slope evaluation at. In *Paste 2013* (pp. 457–472).

Richardson, J. F., & Zaki, W. N. (1954). The sedimentation of a suspension of uniform spheres under conditions of viscous flow. *Chemical Engineering Science*, *3*(2), 65–73.

Sanders, R. S., Giffies, R. G., Mckibben, M. J., Sun, R., & Flow, P. (2002). Solids transport in laminar , open-channel flow of non- Newtonian slurries. In *Hydrotransport 15* (pp. 596–611).

Scott, K. J. (1984). *Hindered settling of a suspension of spheres*.

Shook, C. A., Gillies, R. G., & Sanders, R. S. S. (2002). *Pipeline Hydrotransport: With Applications in the Oil Sand Industry*. SRC Pipe Flow Technology Centre.

Sisson, R., Lacoste-bouchet, P., Natural, C., Costello, M., Hedblom, E., Sheets, B., … Sittoni, L. (2012a). An analytical model for tailings deposition developed from pilot scale testing. In *3rd International oil Sand Tailings Conference* (pp. 1–10).

Sisson, R., Lacoste-bouchet, P., Natural, C., Costello, M., Hedblom, E., Sheets, B., … Sittoni, L. (2012b). An analytical model for tailings deposition developed from pilot scale testing. In *3rd International oil Sand Tailings Conference*.

Sittoni, L., Talmon, A., Kester, J. Van, & Uittenbogaard, R. (2015). LATEST NUMERICAL DEVELOPMENTS FOR THE PREDICTION OF BEACHING FLOW AND SEGREGATING BEHAVIOR OF THICK NON-NEWTONIAN MIXTURES.

Skvortsov, A. V, & Sarychev, D. S. (2002). Modeling of Pipeline Sections. *Russian Physics Journal*, *45*(2), 155–162. http://doi.org/10.1023/A:1019651931035

Slatter, P. (2011). The Engineering Hydrodynamics of Viscoplastic Suspensions. *Particulate Science and Technology*, *29*(2), 139–150. http://doi.org/10.1080/02726351.2010.527429

Slatter, P. T., & Williams, A. T. C. (2013). Analysis and flow behaviour prediction of paste material in sheet flow. In *Paste 2013* (pp. 473–480).

Spelay, R. B. R. (2006). Laminair open channel flow of kaolin clay slurries coating sand - 2006.pdf. In *Transport and sedimentation of solid particles* (pp. 301–313).

Spelay, R. B. R. (2007). *Solids transport in laminar, open channel flow of non-newtonian slurries*. Retrieved from http://library.usask.ca/theses/available/etd-01252007-205230/

Talmon, A. M. (2015). Lecture notes OE4625 - SEGREGATING NON-NEWTONIAN SLURRIES.

Talmon, A. M., & Huisman, M. (2005). Fall velocity of particles in shear flow of drilling fluids. *Tunnelling and Underground Space Technology*, *20*(2), 193–201. http://doi.org/10.1016/j.tust.2004.07.001

Talmon, A. M., van Kesteren, W. G. M., Mastbergen, D. R., Pennekamp, J. G. S., & Sheets, B. (2014). Calculation methodology for segregation of solids in non-Newtonian carrier fluids. In *Paste 2014* (pp. 1–15).

Talmon, A. M., van Kesteren, W. G. M., Sittoni, L., & Hedblom, E. P. (2014). Shear cell tests for quantification of tailings segregation. *Canadian Journal of Chemical Engineering*, *92*(2), 362–373. http://doi.org/10.1002/cjce.21856

Talmon, A., & Mastbergen. (2004). Talmon Mastbergen 2004 Solids transport by drilling fluids concentrated bentonite sand slurries.pdf. In *12th International conference on transport and seimentation of solid particles*.

Thomas A, F. T. (2011). Analysis of tailings beach slopes based on slurry pipeline experience. *Paste 2011*, 295–306.

Thomas, A. D. (1999). Thomas, 1999 The Influence of Coarse Particles on the Rheology of Fine Particle Slurries.pdf.

Thomas, D. G. (1965). Transport characteristics of suspension: VIII. A note on the viscosity of Newtonian suspensions of uniform spherical particles. *Journal of Colloid Science*, *20*(3), 267–277. http://doi.org/10.1016/0095-8522(65)90016-4

Treinen, M., Cooke, R., & Znidarcic, D. (2014). A discussion of the critical drivers for tailings beach flows Background - Beach Slope Prediction Models. In *Paste 2014*.

Uijttewaal, W. (n.d.). *CIE5312-Turbulence*.

Winterwerp, J. C. (1998). A simple model for turbulence induced flocculation of cohesive sediment. *Journal of Hydraulic Research*, *36*(3), 309–326.

Winterwerp, J. C., Uittenbogaard, R. E., van Maren, B., & Vanlede, J. (2007). An integral model for high-concentrated mud suspensions in estuaries: part 2. Calibration, validation, and application. *9th International Conference on Nearshore and Estuarine Cohesive Sediment Transport Processes (INTERCOH '07), Brest, France, September 25-28, 2007. Book of Abstracts*, 132–133.

Winterwerp, J. C., & van Kesteren, W. G. M. (2004). *Introduction to the physics of cohesive sediment in the marine environment*.

Zhenhua, M., Merkus, H., Smet, J., Heffels, C., & Scarlett, B. (2000). Nnew developments in particle characterization by laser diffraction: size and shape.